NASA TECHNICAL NOTE

INTERFERENCE EFFECTS OF CANARD CONTROLS ON THE LONGITUDINAL AERODYNAMIC CHARACTERISTICS OF A WINGED BODY AT MACH 10

by Cuyler W. Brooks, Jr.
Langley Research Center
Langley Station, Hampton, Va.

NATIONAL AERONAUTICS AND SPACE ADMINISTRATION • WASHINGTON, D. C. • APRIL 1968

NASA TN D-4436

INTERFERENCE EFFECTS OF CANARD CONTROLS ON THE LONGITUDINAL AERODYNAMIC CHARACTERISTICS OF A WINGED BODY AT MACH 10

By Cuyler W. Brooks, Jr.

Langley Research Center
Langley Station, Hampton, Va.

NATIONAL AERONAUTICS AND SPACE ADMINISTRATION

For sale by the Clearinghouse for Federal Scientific and Technical Information
Springfield, Virginia 22151 – CFSTI price $3.00

INTERFERENCE EFFECTS OF CANARD CONTROLS ON THE LONGITUDINAL AERODYNAMIC CHARACTERISTICS OF A WINGED BODY AT MACH 10*

By Cuyler W. Brooks, Jr.
Langley Research Center

SUMMARY

An experimental investigation of the interference effects of canard controls on two hypersonic winged configurations was made at a Mach number of 10 in the Langley 15-inch hypersonic flow apparatus. The effect of variations in canard size and shape, body length, wing planform, and wing vertical position was determined.

The results indicate that the canard control induces a broad pattern of interference in which the average flow angle over the wing and body surfaces downstream of the canard varies significantly from the free-stream value. The magnitude of the interference increases with increasing canard deflection and, in general, with increasing angle of attack.

The most significant configuration parameters (aside from canard deflection) are wing position and canard size. The low-wing configurations are affected considerably less by interference than the high-wing configurations, especially at higher angles of attack. As would be expected, the larger canard causes larger disturbances in the flow than does the smaller canard.

INTRODUCTION

An important problem encountered in the design of hypersonic aircraft configurations is that of the loss of effectiveness of aft-mounted aerodynamic pitch controls located within the hypersonic shadow region. (See ref. 1.) However, the effectiveness of such controls is maintained in both the subsonic and low supersonic speed ranges. Since the canard control is placed near the nose of the vehicle, it is not subject to the blanketing effect of a shadow region and thus maintains its effectiveness at hypersonic speeds. (See refs. 2 and 3.)

---

*The information herein was offered as a thesis in partial fulfillment of the requirements for the degree of Master of Aerospace Engineering, University of Virginia, Charlottesville, Virginia, June 1967.

Although experimental investigations at hypersonic speeds (refs. 2 and 3) have indicated that the canard does not lose effectiveness even for large control deflections and large angles of attack, the presence of this forward-mounted control creates disturbances in the flow field which directly affect the aerodynamic characteristics of both the wing and the afterbody.

The present investigation was undertaken to determine the magnitude of the canard-induced interference at hypersonic speeds. The canard interference and its variation with angle of attack, with canard deflection, size, and planform shape, as well as with body length, wing planform, and wing vertical position are determined by use of data in references 2 and 3 in conjunction with wing-off data obtained in the present tests. All data were obtained in the Langley 15-inch hypersonic flow apparatus at a Reynolds number of 1.50×10^6 per foot (4.92×10^6 per meter).

SYMBOLS

The longitudinal force and moment coefficients are referenced to the stability axis system with origin 4.8 inches (12.19 cm) from the model base. The wing area and mean aerodynamic chord used to nondimensionalize the forces and moments are always those of the wing (delta or trapezoidal) in question.

Measurements for this investigation were taken in U.S. Customary Units. Equivalent values are indicated herein parenthetically in the International System of Units.

c local chord (wing or canard)

$\bar{c}$ wing mean aerodynamic chord

C general longitudinal coefficient: C_L, C_D, or C_m

C' general coefficient for complete configuration without interference, equation (2)

C_L lift coefficient, $\frac{\text{Lift}}{q_\infty S}$

C_D drag coefficient, $\frac{\text{Drag}}{q_\infty S}$

C_m pitching-moment coefficient, $\frac{\text{Pitching moment}}{q_\infty S\bar{c}}$

d maximum model body diameter

q_∞	free-stream dynamic pressure
r	radial coordinate for body surface
S	wing planform area (reference area)
S_C	canard planform area (including that portion inside fuselage)
t	maximum thickness of airfoil section
t/c	section thickness ratio
x	longitudinal coordinate measured rearward from model nose
x_{cg}	longitudinal distance of moment reference center from model nose
α	geometric angle of attack (referenced to fuselage center line)
δ	canard deflection angle (relative to fuselage center line) positive in the same sense as α
$\Delta_I C$	increment in general coefficients due to canard-wing interference
ϵ	effective induced downwash

Subscripts:

W	wing
B	body (fuselage and nose)
C	canard
L	lift
D	drag

m	pitching moment
WB	wing-body configuration
I	denotes a quantity calculated for the wing-body with interference by equation 3

Model components:

D	delta planform wing
T	trapezoidal planform wing
W_1	wing mounted in high position
W_2	wing mounted in low position
B_1	short body
B_2	long body
C_1	small delta planform canard
C_2	large delta planform canard
C_3	small trapezoidal planform canard

Thus, $DW_1B_2C_1$ denotes the configuration with a high delta wing, long body, and small delta canard.

MODELS

Drawings of the models, showing dimensions and component arrangement, are presented in figure 1. Figure 2 presents the dimensions of the canard control surfaces which were used. Photographs of typical configurations and of the model components are shown in figure 3. Table I presents the model reference dimensions.

TABLE I. - MODEL REFERENCE DIMENSIONS

Delta-wing configuration:		
Reference area, S, in^2 (cm^2)	17.815	(114.935)
Mean aerodynamic chord, $\bar{c}$, in. (cm)	4.667	(11.854)
Canard-wing area ratio, S_c/S –		
Small delta canard, C_1	0.145	
Large delta canard, C_2	0.194	
Trapezoidal canard, C_3	0.145	
Trapezoidal-wing configuration:		
Reference area, S, in^2 (cm^2)	18.216	(117.522)
Mean aerodynamic chord, $\bar{c}$, in. (cm)	4.006	(10.175)
Canard-wing area ratio, S_c/S –		
Small delta canard, C_1	0.142	
Large delta canard, C_2	0.190	
Trapezoidal canard, C_3	0.142	

The delta-wing model of reference 2 had a 70° swept-leading-edge delta planform, and the trapezoidal-wing model of reference 3 had a 45° swept-leading-edge trapezoidal planform. (Trapezoidal refers to the shape of the outboard portion of the wing.) Both wings employed a diamond airfoil section with a thickness ratio t/c of 0.05. The wings were tested in both high (W_1) and low (W_2) positions with respect to the fuselage. (See fig. 1.)

The fuselage for the wing-off configurations of the present investigation consisted basically of a circular, cylindrical afterbody, combined with a sharp 2/3-power nose. The fuselage cylinder for the winged models of references 2 and 3 was modified in the wing-attachment region to intersect the wing with essentially flat sides normal to the planform plane. The forward portion of the fuselage could be varied in length by insertion of a 1.20-inch (3.05-cm) cylindrical spacer just ahead of the wing. Figures 1(a), 1(c), 3(a), and 3(d) show the model with the spacer included (B_2), and figures 1(b), 1(d), and 3(b) show the model with the spacer removed (B_1).

Two canard-surface planforms were studied: a delta planform with 45° leading-edge sweep, and a trapezoidal planform with 22.5° leading-edge sweep (midchord line unswept). The airfoils for both planforms had diamond sections with a maximum thickness of 5 percent of the local chord. Two sizes of delta planforms having total planform areas of 14.5 and 19.4 percent of the delta-wing reference area were tested. The trapezoidal canard had essentially the same canard-wing area ratio as the small delta canard. (See table I.) The canard hinge line (fig. 1) was maintained at the same fixed distance from the model nose in all tests.

The vertical tails (of trapezoidal planform) had 45° swept leading edges and were mounted on the delta wing 2.00 inches (5.08 cm) (approximately 80 percent of the wing semispan) from the body center line. The vertical tails for the trapezoidal wings had 45° swept leading edges and were mounted at the wing tips. Both sets of vertical tails had diamond airfoil sections with a maximum thickness of 5 percent of the local chord.

TESTS

The tests were made in the Langley 15-inch hypersonic flow apparatus at a Mach number of 10. The details of the basic tunnel characteristics appear in reference 4. For tests of the wing-off configurations, the nominal stagnation pressure and temperature were 800 psia (5510 kN/m^2) and 1100° F (866° K), respectively. The dynamic pressure was 1.3 psia (8.96 kN/m^2) and the Reynolds number per foot (1.5×10^6) (4.92×10^2 per meter) was the same as for the winged configuration tests. (See refs. 2 and 3.)

The tests were conducted through an angle-of-attack range of -4° to 20°. For each of the two fuselage lengths, the models were tested without the canard and with each of the three canard surfaces at deflection angles of 0°, 5°, 10°, and 20°.

The models were sting-mounted through the fuselage base, and normal- and axial-force and pitching-moment measurements were made with an internally mounted, water-cooled, six-component strain-gage balance. Base pressure measurements were not made. The angle of attack was corrected for sting and balance deflections caused by aerodynamic loads.

The calculation of the interference increments requires the addition and subtraction of force- and moment-coefficient data obtained on two different balances and under two sets of tunnel test conditions. In order to provide an estimate of the accuracy of the basic force data, a series of repeat runs were made on two of the test configurations, one with a canard control at 10° deflection, and the other with no canard. Each of these configurations was tested through the angle-of-attack range three times. The configuration with the canard control was tested once on one balance at the $q_\infty = 1.7$ psia (11.72 kN/m^2) test conditions, then twice on the other balance, first at the $q_\infty = 1.7$ psia test conditions and then at the $q_\infty = 1.3$ psia (8.96 kN/m^2) test conditions. The canard-off configuration was tested once on the first balance at the $q_\infty = 1.7$ psia (11.72 kN/m^2) test conditions and twice on the second balance at the $q_\infty = 1.3$ psia (8.96 kN/m^2) test conditions. The maximum differences found in the measured coefficients from these data for either configuration were 0.02 in C_L, 0.006 in C_D, and 0.004 in C_m.

The angle of attack is estimated to be accurate to within ±0.1°. The Mach number is constant and is not measured for each test. The Mach number distribution through the test section (ref. 4) shows a maximum deviation of ±0.2 from the average (over the test core) Mach number of 10.03.

METHOD OF DATA ANALYSIS

The canard-induced interference is defined herein as the increment in the longitudinal coefficient C_L, C_D, or C_m of the wing-body caused by the presence of the canard (exclusive of the force or moment due directly to the canard). The interference increments are assumed to be caused by the generation of a wake behind the canard which changes the angle of flow to which the wing and rearward part of the fuselage are subjected. An expression is derived relating this change in flow angle to the lift coefficients with and without interference.

Coefficient Increments

The increment in any longitudinal force or moment coefficient $(C_L, C_D, \text{or } C_m)$ due to the interference effect of the canard $\Delta_I C$ is defined as the amount by which the coefficient (C representing the general coefficient) due to the canard and its interference $(C_{WBC} - C_{WB})$ differs from the coefficient due to the canard alone $(C_{BC} - C_B)$. That is,

$$\Delta_I C = (C_{WBC} - C_{WB}) - (C_{BC} - C_B) \tag{1}$$

where the four coefficients on the right in equation (1) are measured values. This equation requires that the coefficients involved be determined for a common reference area, a common moment reference center, the same canard deflection, and the same angle of attack.

The general coefficient for the complete configuration (WBC) with the canard interference subtracted may be calculated for comparison with the measured coefficient C_{WBC};

$$C' = C_{WBC} - \Delta_I C = C_{WB} + C_{BC} - C_B \tag{2}$$

Effective Downwash Angle

The effective downwash angle ϵ is defined herein as the average (over the wing and aft body surface) change in effective angle of attack or flow direction which will account for the observed lift coefficient increment $\Delta_I C_L$. Lift coefficient was selected to calculate the effective downwash because it is more sensitive to flow angle than drag coefficient, and pitching-moment coefficient cannot be used because the change in center-of-pressure location due to canard interference is not known. The coefficient for the wing-body configuration without the canard C_{WB} has been determined experimentally. The coefficient for the wing-body with the canard interference (but without the direct effect of the canard) is defined as:

$$C_I = C_{WBC} - (C_{BC} - C_B) \tag{3}$$

In functional notation, the effective downwash ϵ can now be written implicitly (see fig. 4):

$$C_{WB}(\alpha + \epsilon) = C_I(\alpha) \tag{4}$$

where it must be assumed that C_{WB} and C_I vary linearly with α over the range ϵ. This expression is considered a reasonable approximation, despite the fact that variation in the coefficient is nonlinear, because in general ϵ is small. Because downwash cannot be calculated directly from this functional relationship, figure 4 shows how ϵ would be determined graphically. The actual calculation of the effective downwash was made by using finite differences.

PRESENTATION OF RESULTS

Figure 5 presents C_L, C_D, and C_m plotted against angle of attack for the wing-off configurations of the present tests. The wing-off coefficients of figure 5 are referenced to the delta-wing reference constants. When used in conjunction with trapezoidal-wing data to obtain interference increments, however, the coefficients were referenced to the trapezoidal-wing reference constants.

Figures 6 and 7 present the longitudinal aerodynamic coefficients from some of the wing-body and wing-body-canard tests of references 2 and 3. These data are replotted herein as a function of α to provide a reference for the calculated interference increments.

In addition to the measured data in figure 7, dashed lines indicate the coefficients without interference (C'), as calculated from the wing-off, canard-off, and body-alone data. The interference increments ($\Delta_I C$), which are the differences between the dashed and solid curves of figure 7, are presented separately in figure 8. Figure 9 presents the calculated effective downwash for each configuration; note that ϵ is positive in the same direction as angle of attack, so that "downwash" is shown as a negative angle.

RESULTS AND DISCUSSION

Interference Terms

Figure 8 shows that the canard-wing interference is strongly dependent on angle of attack and on canard deflection angle. However, the interference is generally small near zero angle of attack, even for the largest canard deflection angles. The variation in interference with increasing angle of attack depends significantly on the configuration and canard deflection angle, and the interference usually increases with canard deflection angle. Since the curves in figure 7 show both the magnitude of the interference and a

comparison of the interference with the corresponding coefficients, the effects of varying the geometric parameters of the configurations are discussed in terms of these figures.

Effects of Wing Position

The effect of wing vertical position on the canard-wing interference is the largest of any of the effects of configuration component variation. A comparison of any high-wing configuration (figs. 7(a) to 7(d) and 7(i) to 7(l)) with the corresponding low-wing configuration (figs. 7(e) to 7(h), and 7(m) to 7(p)) shows that, not only are the interferences larger for the high-wing configuration, but the variation of the interference increment with angle of attack is markedly different. This result is not entirely unexpected, however, since a compression surface (such as the lower surface of the high wing) at supersonic and hypersonic speeds is generally subjected to much larger forces than a surface at or near an expansion region (such as the upper surface of the low wing). Thus, since the interference of the canard tends to affect the lower surface of the high wing and the upper surface of the low wing, the changes in the flow caused by interference have a greater effect on the forces experienced by the high wing.

For the high-wing configurations (W_1) the interference generally causes a decrease in C_L and C_D and an increase in C_m, and the effect generally increases with both angle of attack and canard deflection. The pattern of the effects of interference for the high-wing configurations is consistent for the delta and trapezoidal wings. For the low-wing configurations (W_2) the increments in the coefficients caused by the interference vary between positive and negative, both with angle of attack and with canard deflection. The effects of wing position on C_L, C_D, and C_m for the delta wing (D) differ considerably from those for the trapezoidal wing (T).

Effects of Canard Size

The interference from the canard would be expected to increase with an increase in the ratio of the canard area to the wing area. For both the high-delta wing and the high-trapezoidal wing configurations, such an increase in interference is noted, especially at the higher angles of attack and canard deflections, that is, for conditions where the interferences are greatest. (See figs. 7(b), (c), (j), and (k).) Also, the data for the low-trapezoidal-wing configurations (figs. 7(n) and (o)) show an increase in interference effect with the increase in canard-wing area ratio. In the case of the low-delta-wing configurations (figs. 7(f) and (g)), however, the canard-wing area ratio has little effect on the interference, probably because the leading edge of the inboard portion of the delta wing is far enough forward (compared with that of the trapezoidal wing) that the wake of the canard cannot affect the compression surface of the wing, as the effects of interference are small for both the large and small canard configurations.

Effects of Canard Planform

The effects of canard planform on the canard-wing interference are small and inconsistent. For the long-body high-delta wing configuration (DW_1B_2), the trapezoidal canard (C_3, fig. 7(d)) has somewhat greater interference effects, especially at the lower canard deflections, than the delta canard C_1 (fig. 7(b)). No data obtained on other configurations showed any significant effect of canard shape.

Effective Downwash

The effective downwash (fig. 9) generally increases with canard deflection. For a given configuration, the variation of effective downwash with angle of attack tends to be similar for the four canard deflections of this investigation. This result is consistent with the variation of the coefficient interference $\Delta_I C$ with angle of attack (fig. 8) in indicating that the canard "wake" or interference pattern is similar for all canard deflections. The configurations generally have downwash curves with a definite peak that indicates the center of the disturbance caused by the canard. (See figs. 9(b), (c), (d), (e), (f), (g), (h), (j), and (l). Typically the location of this peak is not dependent on canard deflection. In general, the downwash effect is greater on the high-wing configurations. For the long-body, delta-wing configurations, the peak downwash occurs at an angle of attack about 5^o to 10^o lower for the low-wing configurations than for the high-wing configurations. The 10^o difference in α for the interference peak correlates roughly with the angle (Arctan $1/5 = 11^o$) subtended by the distance (1 inch) (2.54 cm) between the positions of the high and low wings at their distance (about 5 inches (12.70 cm)) from the canard. That is, the low wing tends to encounter the center of the canard interference pattern at a lower angle of attack than the high wing. For example, at $\alpha = 20^o$, a line from the canard to the high wing (on the long body, B_2) is at an angle to the flow of roughly 15^o ($\alpha - (1/2) \times 11^o$). For the line from the canard to the low wing to be at the same angle to the flow of 15^o ($\alpha + (1/2) \times 10^o$), the angle of attack must be roughly 10^o, or 10^o less than for the high-wing configuration. For the trapezoidal-wing configurations (figs. 9(i) to (p)), the downwash pattern for the high wing position is similar to that of the delta-wing configurations, but for the low wing position, the downwash is smaller and more irregular than that of the delta-wing configurations.

CONCLUDING REMARKS

An experimental investigation of the interference effects of canard controls on two hypersonic winged configurations was made at a Mach number of 10 in the Langley 15-inch hypersonic flow apparatus. The effect of variations in canard size and shape, body length, wing planform, and wing vertical position was determined.

The use of canard controls at hypersonic speeds eliminates the problem of loss of control due to the hypersonic shadow region that has been encountered with some aft-mounted controls. However, the canard induces a broad pattern of interference wherein the average flow angle over the wing and body surfaces behind the canard varies significantly from the free-stream value. The maximum angle of attack in these tests was 20°, and at that angle, the interference was still significant for most configurations. Thus, it appears likely that the interference pattern behind the canard will produce significant variations in flow angle in the region of flow bounded by the canard shock wave beneath the vehicle and the Mach line from the canard leading edge above. The magnitude of the interference increases with increasing canard deflection, but the variation of the interference with angle of attack for a given configuration is generally similar for all canard deflections tested.

Of the configuration parameters investigated (aside from canard deflection), wing position and canard size are the most significant. The effects of interference on the low-wing configurations were considerably less than on the high-wing configurations, especially at the higher angles of attack. As would be expected, the canard with the larger canard-wing area ratio causes larger disturbances in the flow than that with the smaller area ratio.

Langley Research Center,
National Aeronautics and Space Administration,
Langley Station, Hampton, Va., September 21, 1967,
126-13-03-09-23.

REFERENCES

1. Putnam, Lawrence E.; and Trescot, Charles D., Jr.: Hypersonic Aerodynamic Characteristics of Plain and Ported Elevon Controls on a 75° Swept Modified Delta-Wing Configuration. NASA TM X-987, 1964.

2. Brooks, Cuyler W., Jr.; and Cone, Clarence D., Jr.: Hypersonic Aerodynamic Characteristics of Aircraft Configurations With Canard Controls. NASA TN D-3374, 1966.

3. Putnam, Lawrence E.; and Brooks, Cuyler W., Jr.: Hypersonic Aerodynamic Characteristics of Wing-Body Configurations With Canard Controls. NASA TN D-3728, 1966.

4. Putnam, Lawrence E.; and Brooks, Cuyler W., Jr.: Static Longitudinal Aerodynamic Characteristics at a Mach Number of 10.03 of Low-Aspect-Ratio Wing-Body Configurations Suitable for Reentry. NASA TM X-733, 1962.

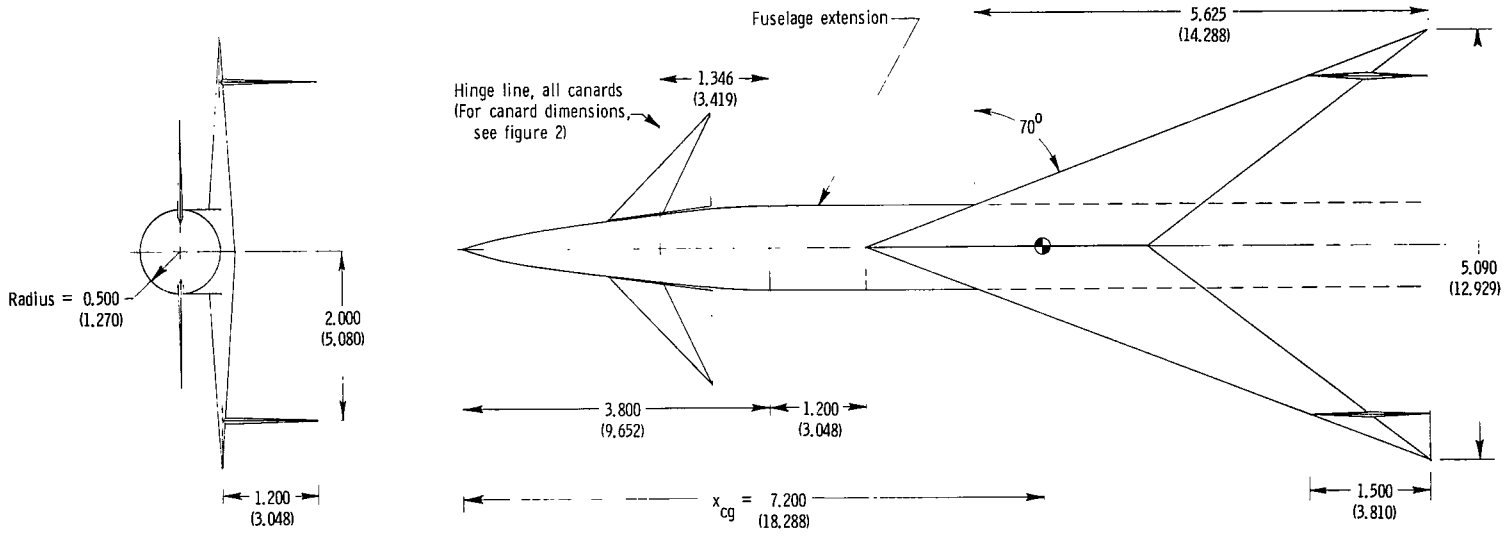

Nose profile	
x/d	r/d
0	0
.5	.1397
1.0	.2218
1.5	.2907
2.0	.3520
2.5	.4085
3.0	.4610
3.1	.4710
3.2	.4800
3.3	.4860
3.4	.4915
3.5	.4960
3.6	.4980
3.7	.5000
3.8	.5000

d = 1.000
(2.540)

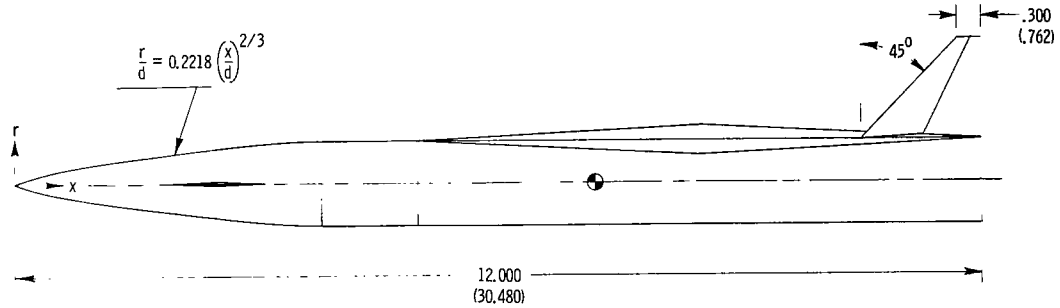

(a) High-wing long-body delta-wing configuration, $DW_1B_2C_1$.

Figure 1.- Model drawings. All dimensions are in inches (and parenthetically in cm). All airfoil sections are diamond sections of t/c = 0.05.

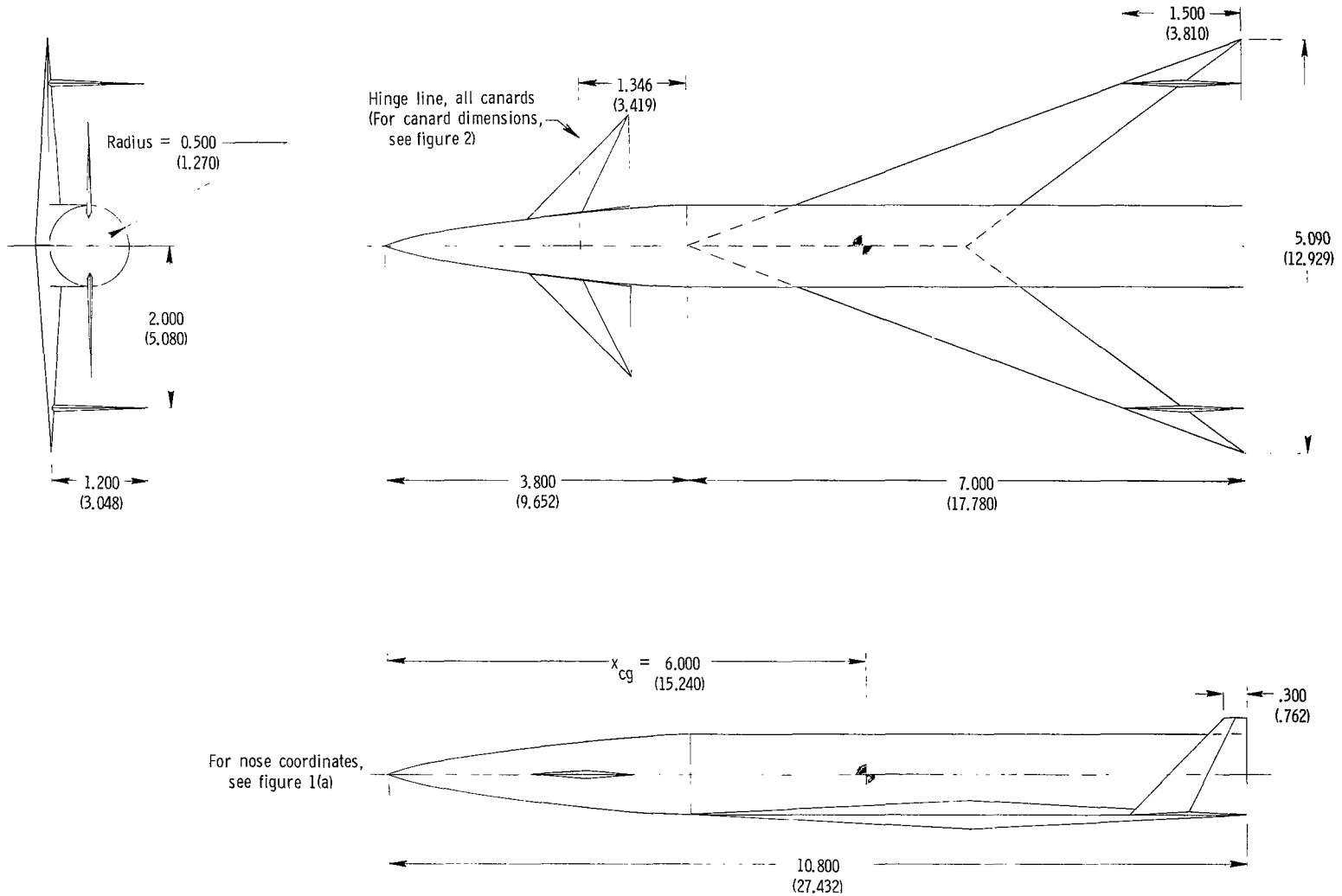

(b) Low-wing short-body delta-wing configuration, $DW_2B_1C_1$.

Figure 1.- Continued.

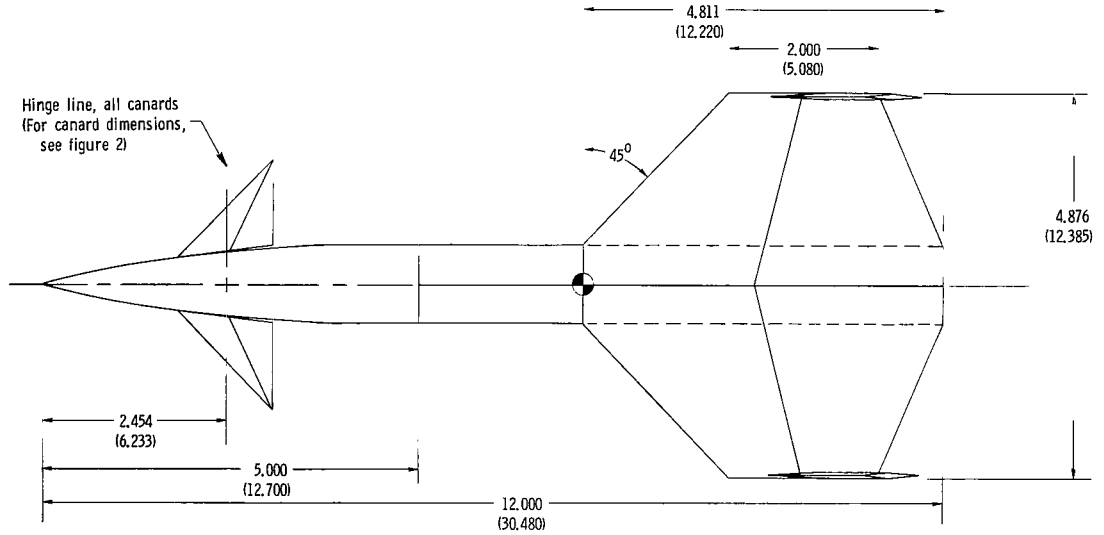

x/d	r/d
0	0
.5	.1397
1.0	.2218
1.5	.2907
2.0	.3520
2.5	.4085
3.0	.4610
3.1	.4710
3.2	.4800
3.3	.4860
3.4	.4915
3.5	.4960
3.6	.4980
3.7	.5000
3.8	.5000

d = 1.000 (2.54)

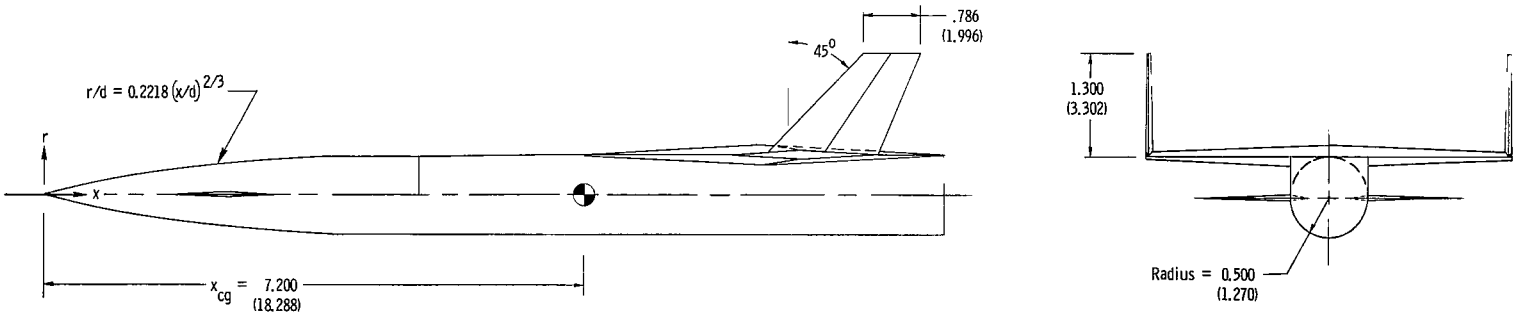

(c) High-wing long-body trapezoidal-wing configuration, $TW_1B_2C_2$.

Figure 1.- Continued.

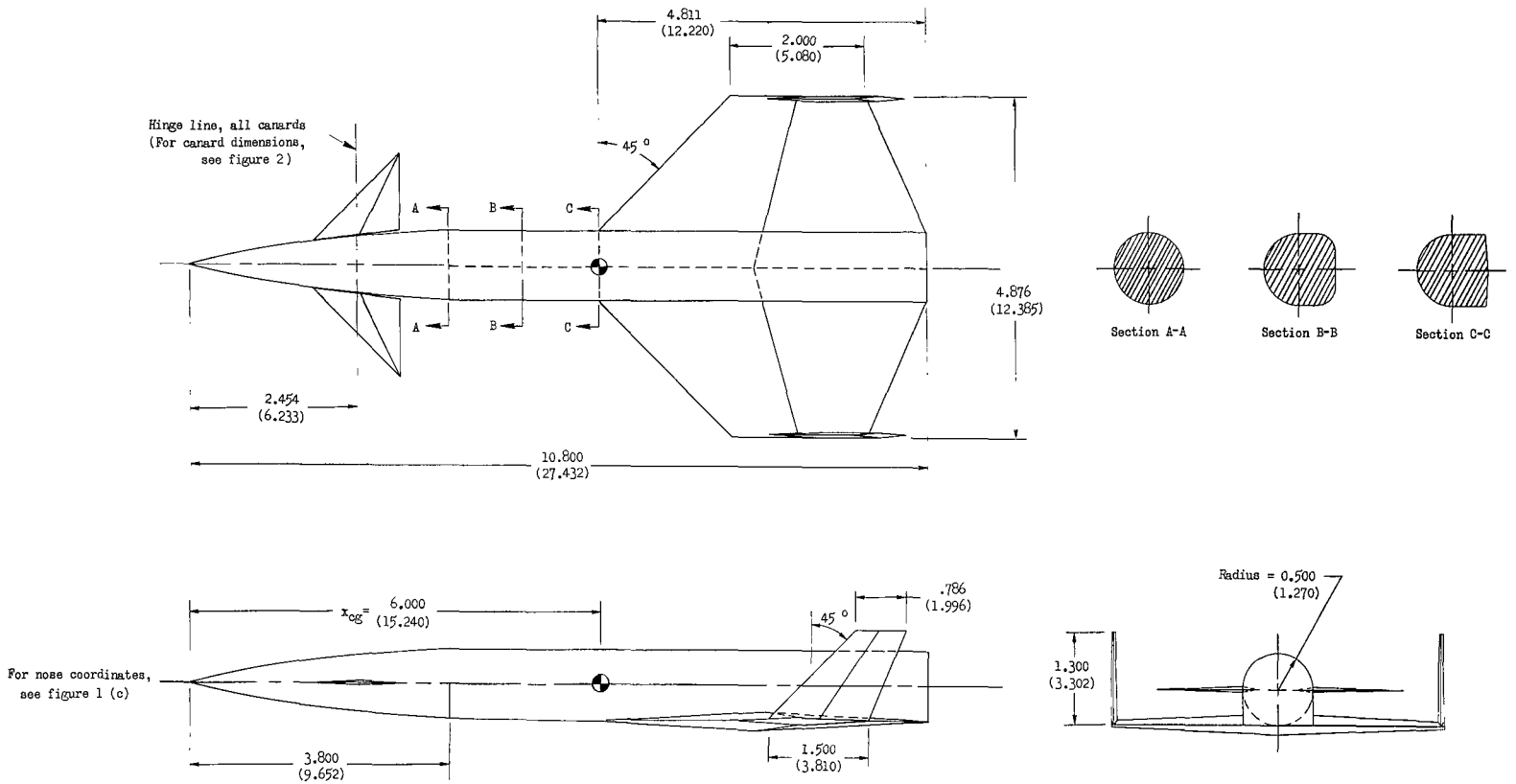

(d) Low-wing short-body trapezoidal-wing configuration, $TW_2B_1C_2$.

Figure 1.- Concluded.

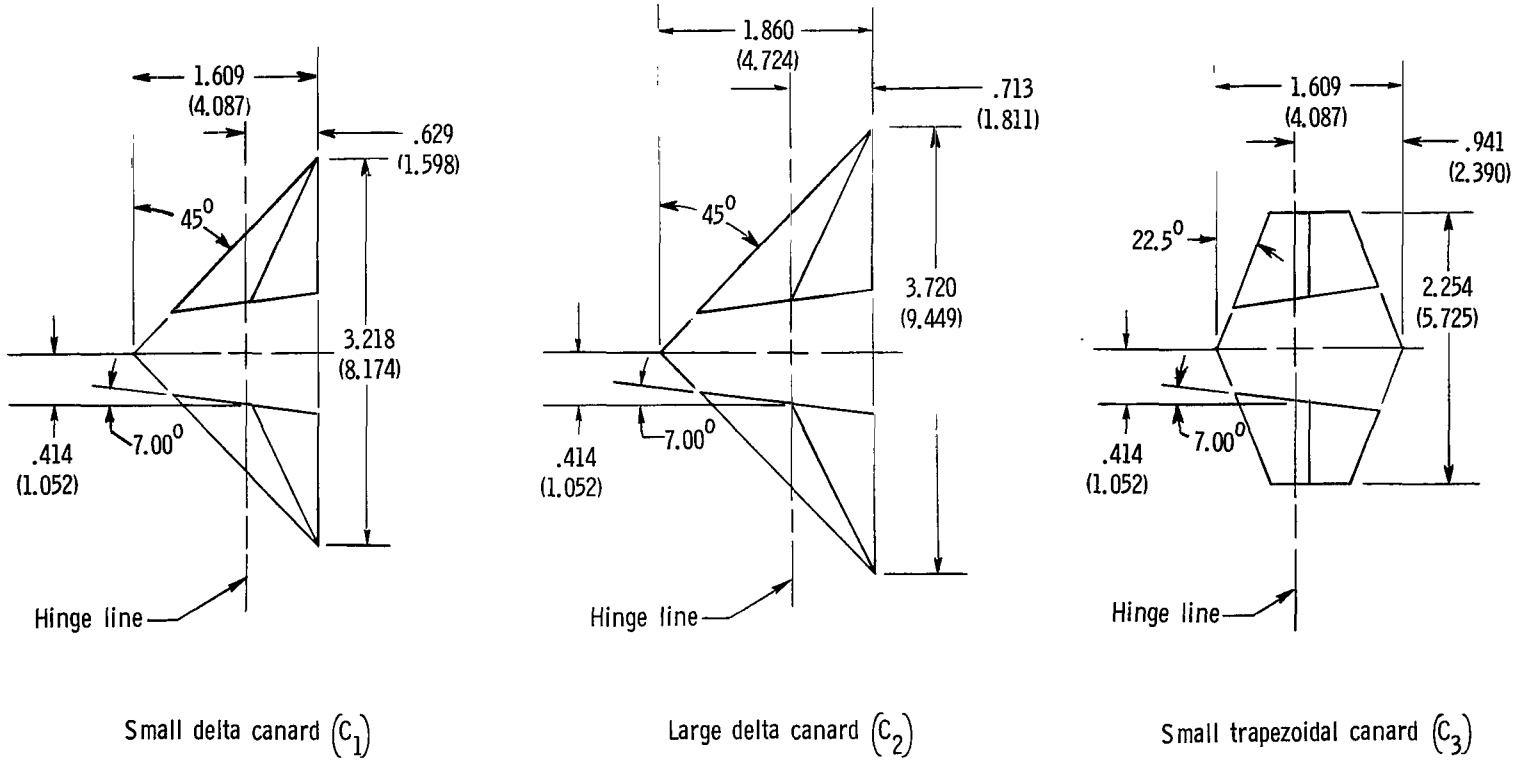

Figure 2.- Planform details of canard control surfaces. All dimensions are in inches (and parenthetically in cm).

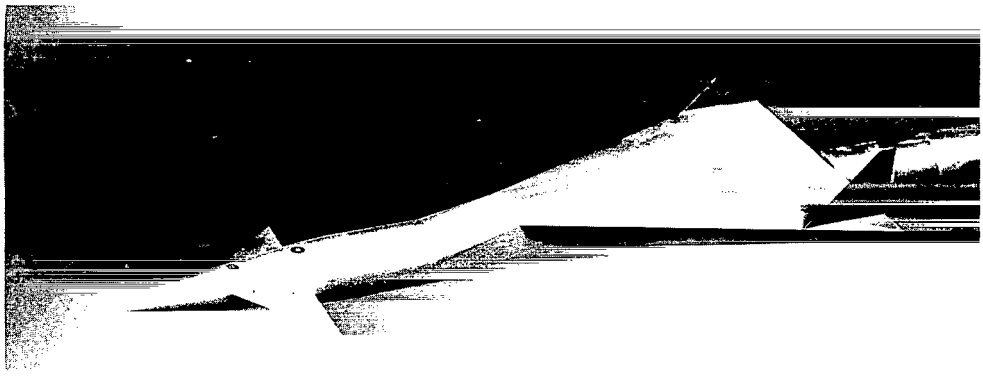

(a) Configuration $DW_1B_2C_1$; $\delta = 10^0$. L-63-9746

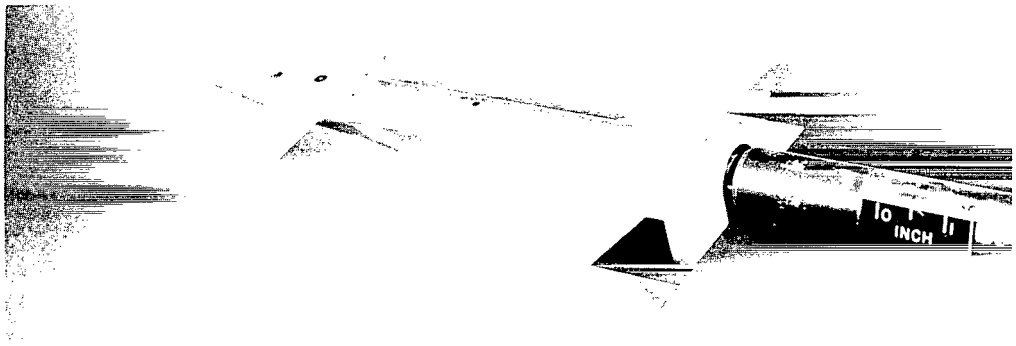

(b) Configuration $DW_2B_1C_1$; $\delta = 10^0$. L-63-9743

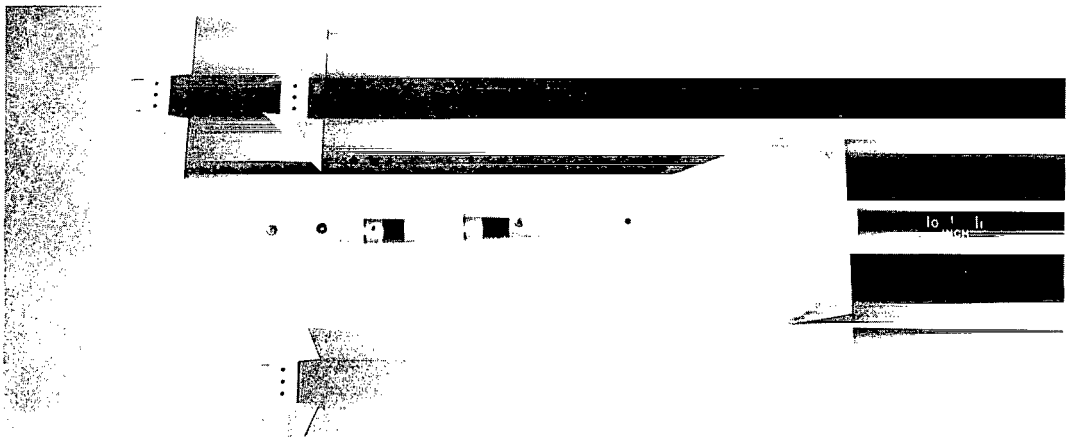

(c) Planform view of all delta-wing model components. L-63-9744.1

Figure 3.- Selected model photographs.

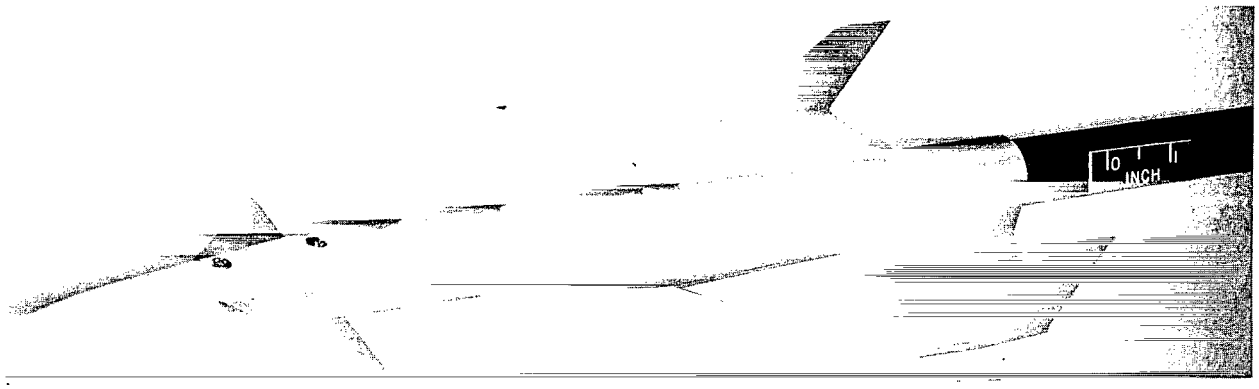

(d) Configuration $TW_2B_2C_2$; $\delta = 10^0$. L-64-6880

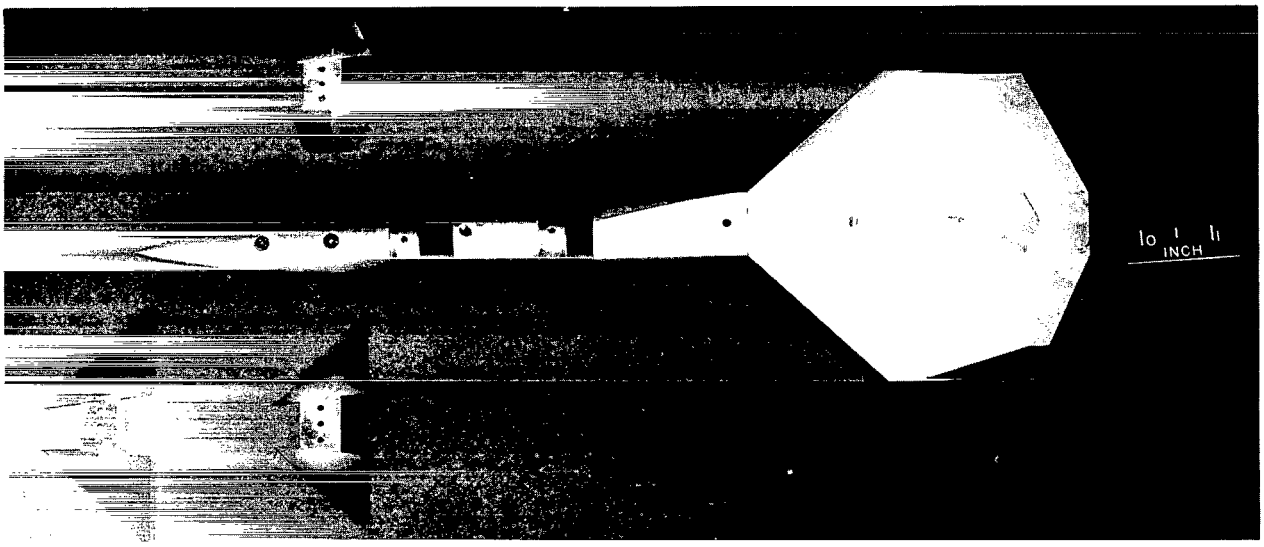

(e) Planform view of all trapezoidal-wing model components. L-64-6879.1

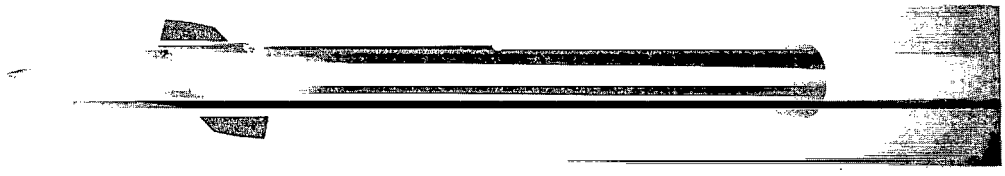

(f) Configuration B_1C_3; $\delta = 10^0$. L-64-7695

Figure 3.- Concluded.

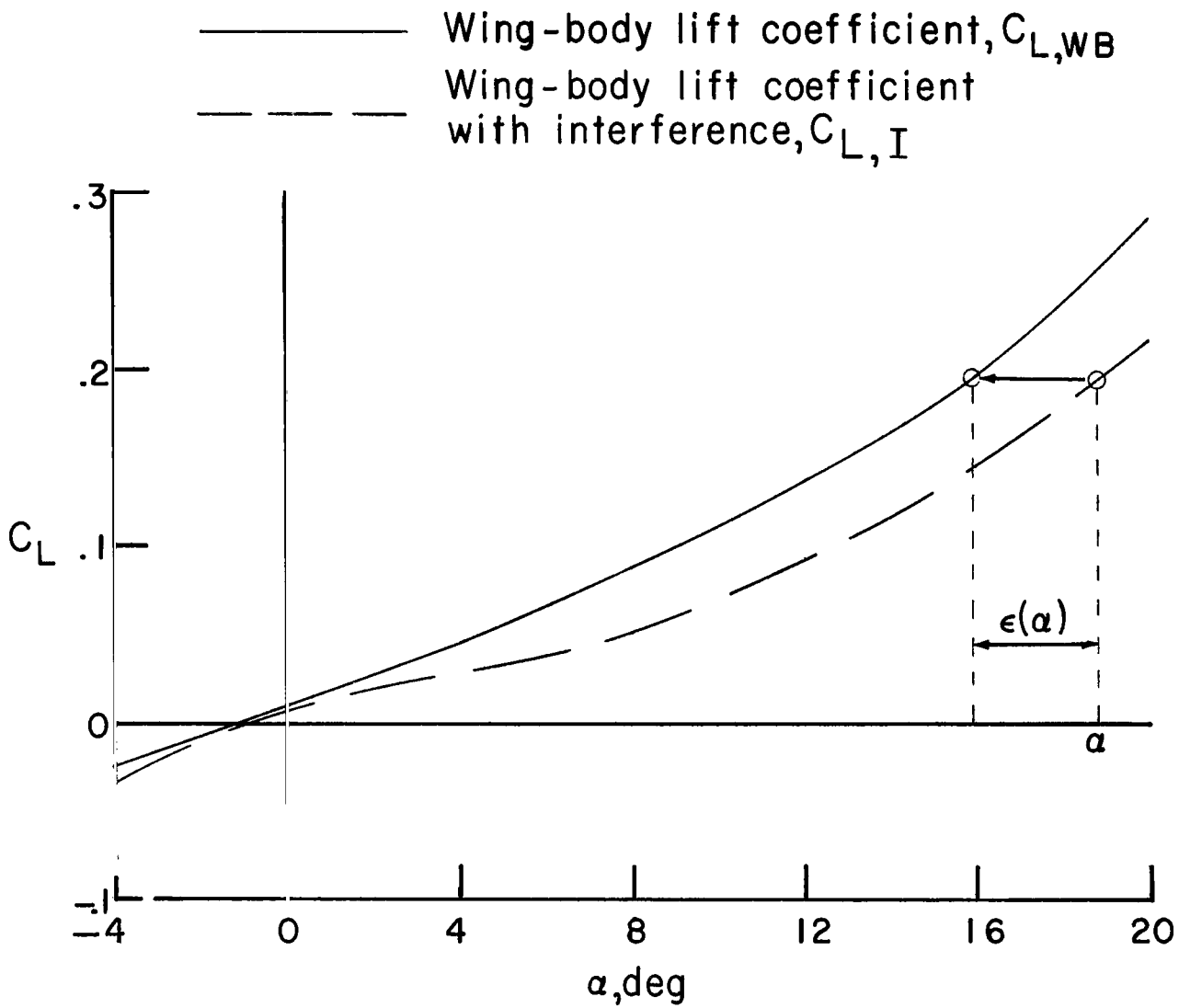

Figure 4.- Sample graphical determination of the effective downwash angle, $\overline{\Delta\alpha}$.

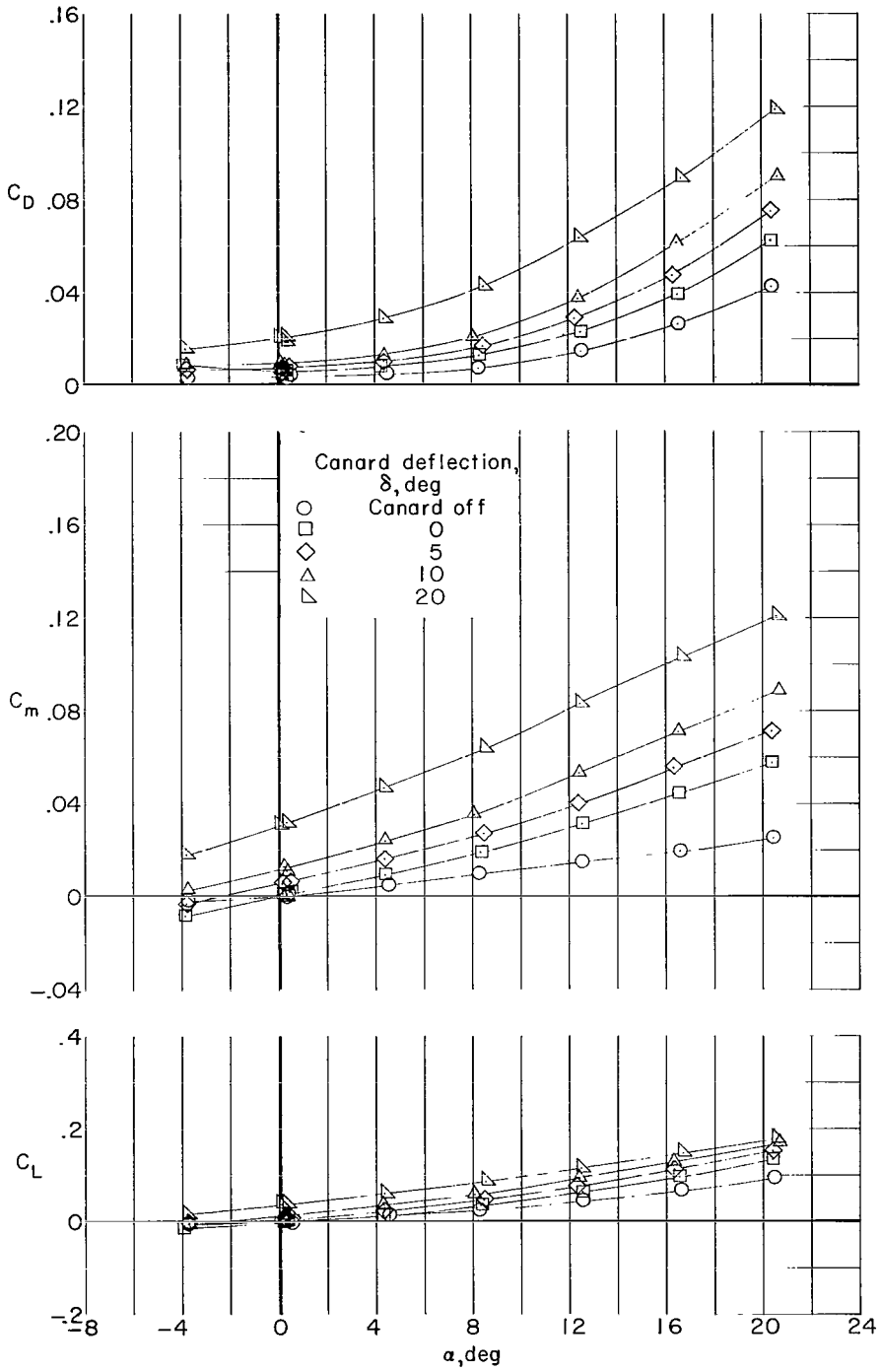

(a) Configuration B_1C_1.

Figure 5.- Longitudinal aerodynamic characteristics of wing-off canard configurations. Coefficients based on delta-wing configuration reference dimensions.

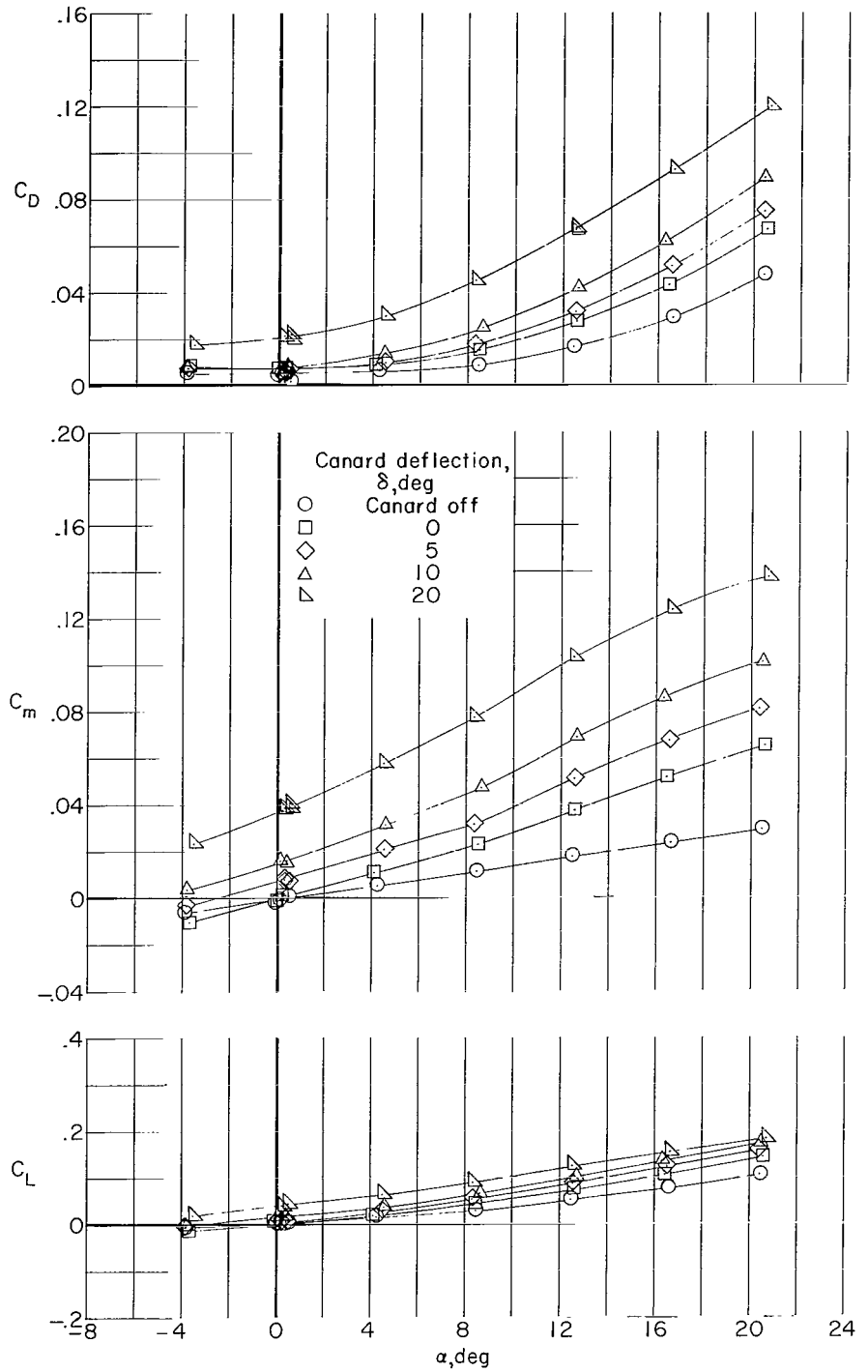

(b) Configuration B_2C_1.

Figure 5.- Continued.

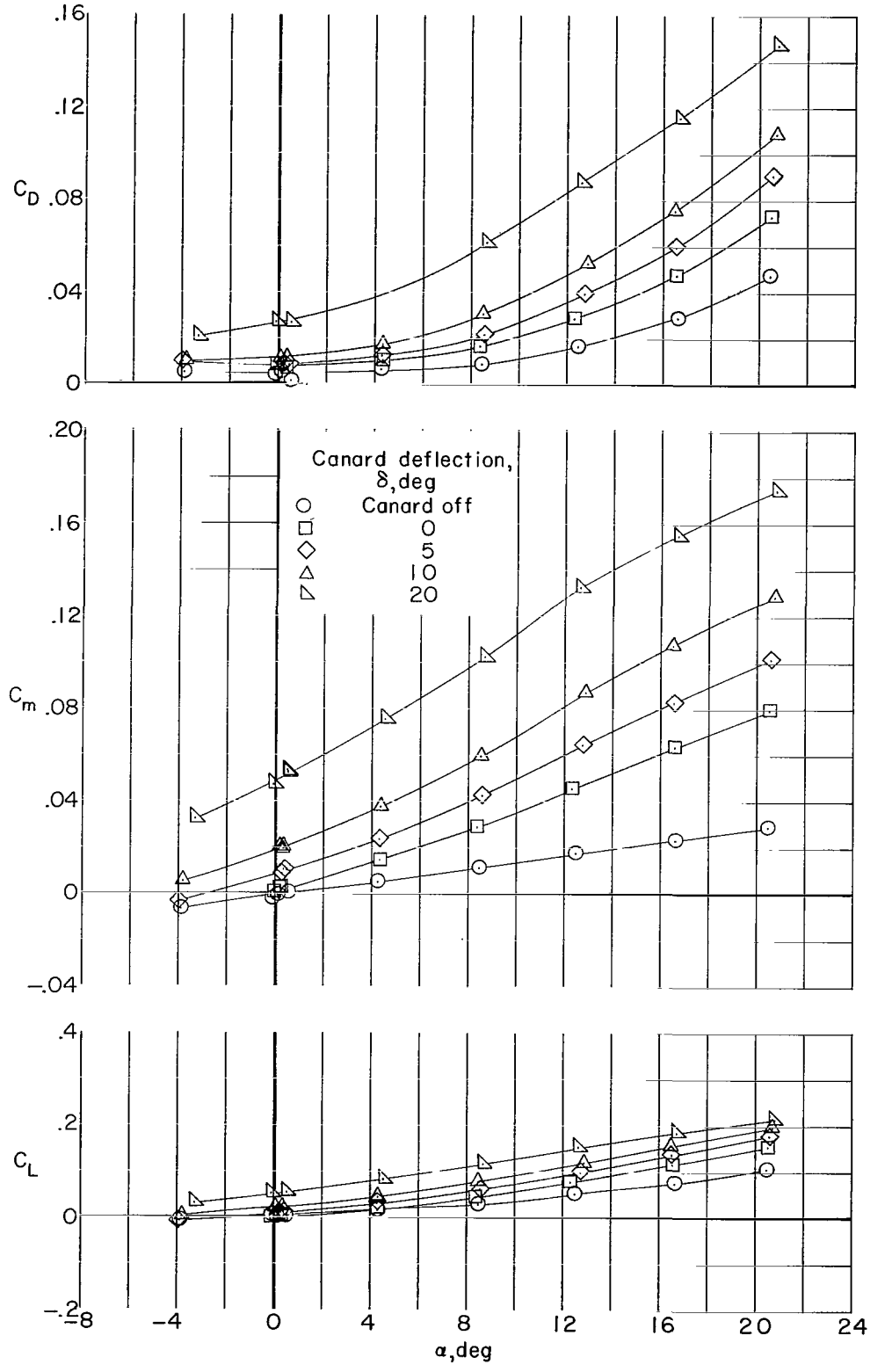

(c) Configuration B_2C_2.

Figure 5.- Continued.

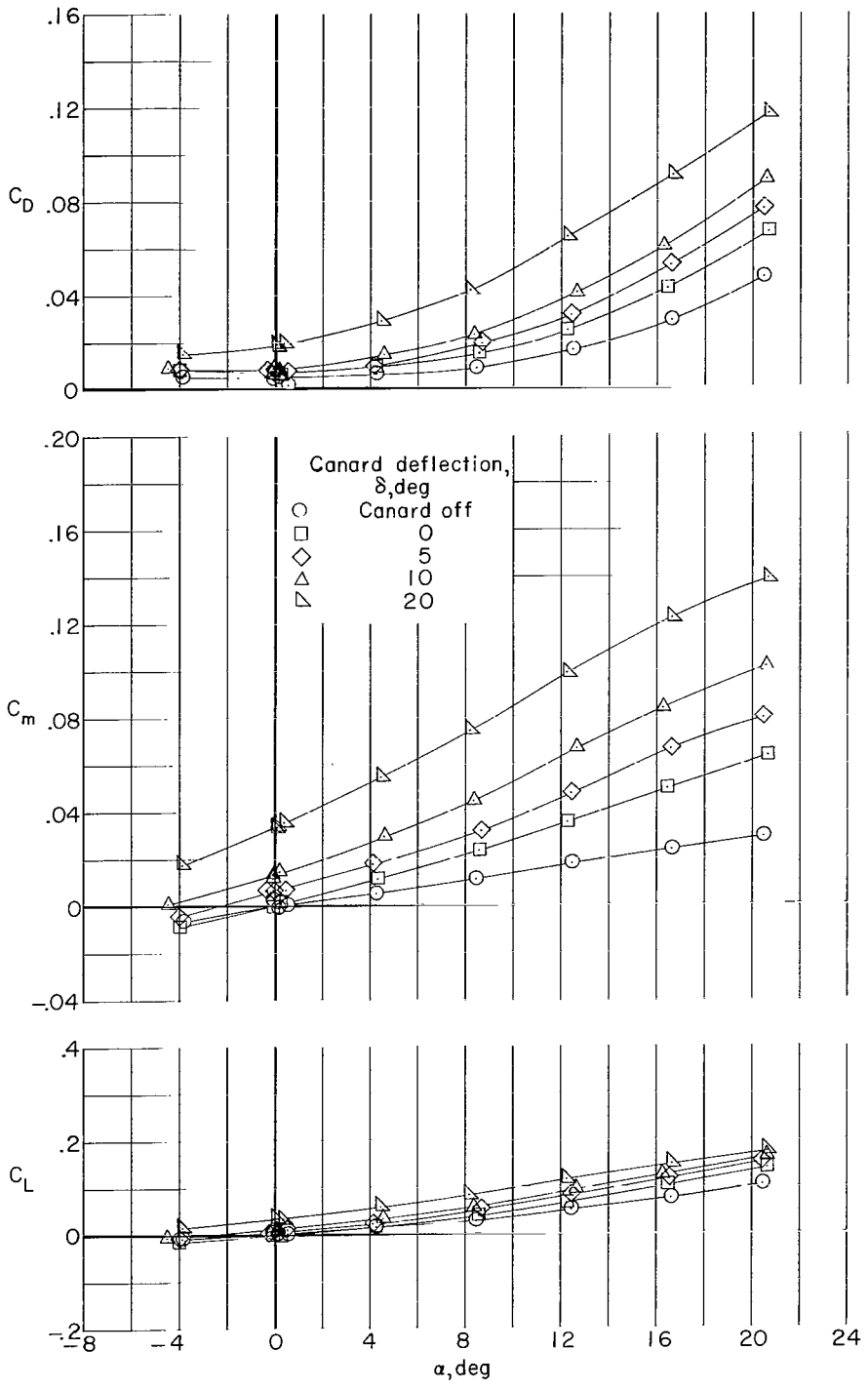

(d) Configuration B_2C_3.

Figure 5.- Concluded.

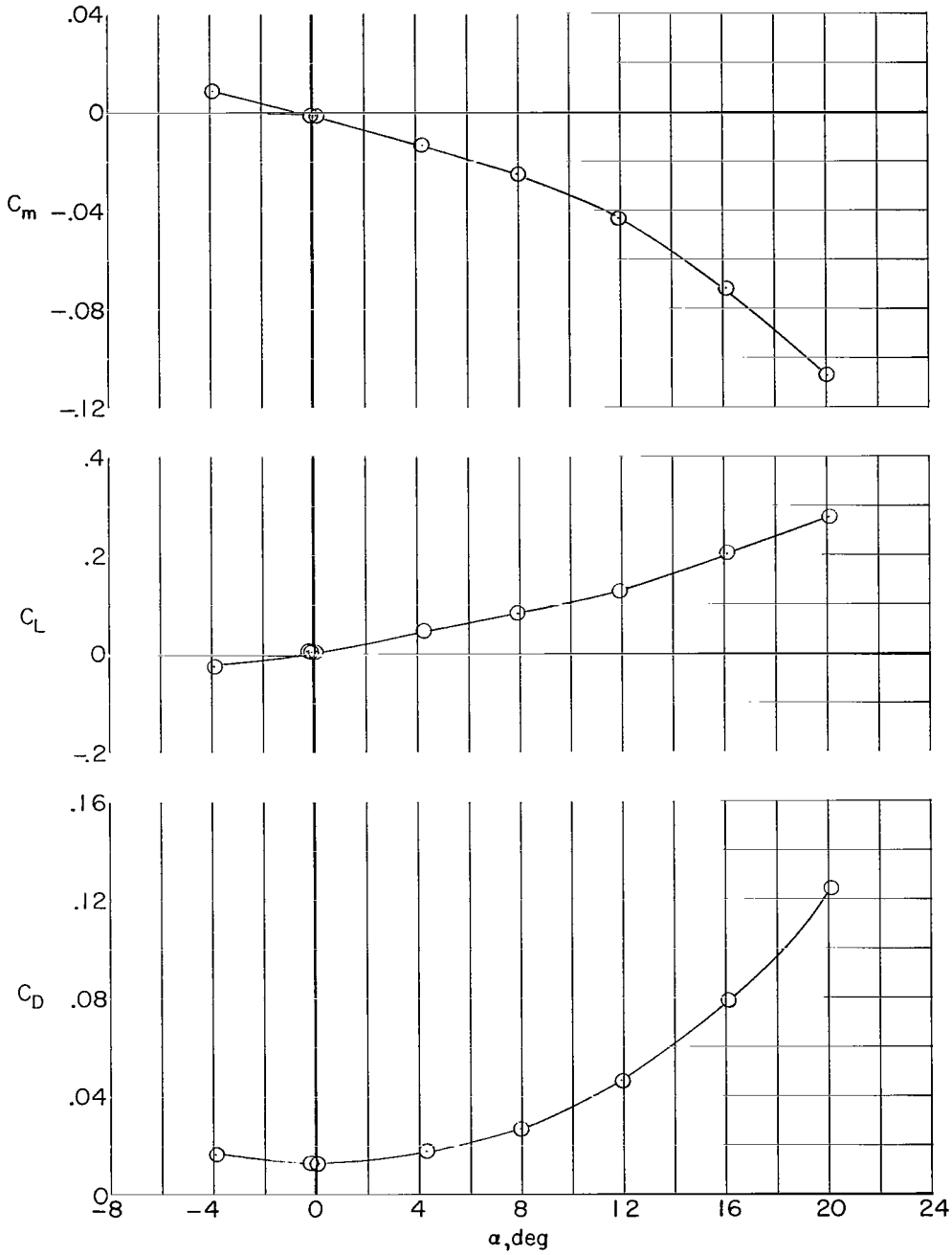

(a) Configuration DW_1B_1.

Figure 6.- Longitudinal aerodynamic characteristics of the canard-off (wing-body) configurations from references 2 and 3.

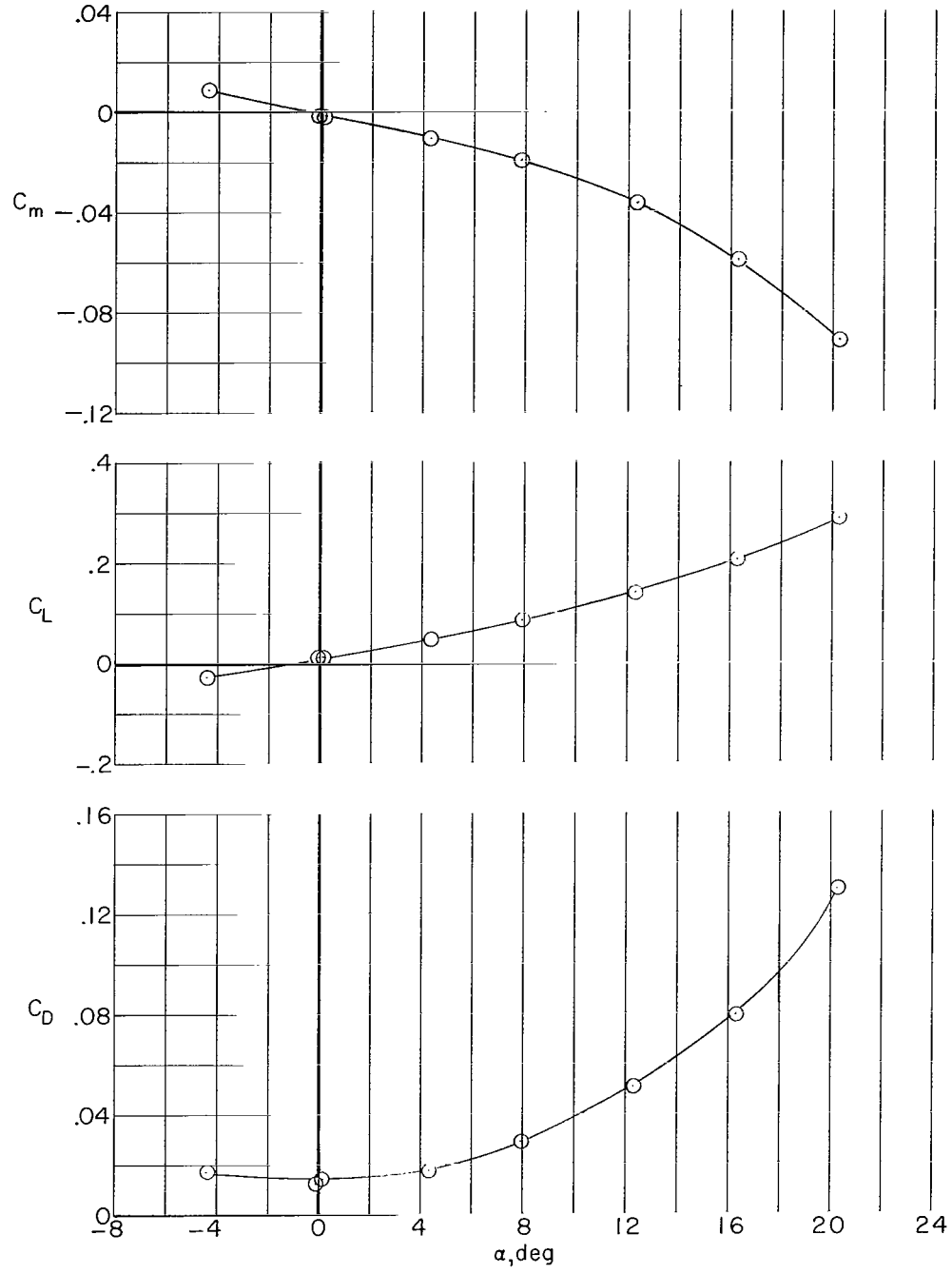

(b) Configuration DW_1B_2.

Figure 6.- Continued.

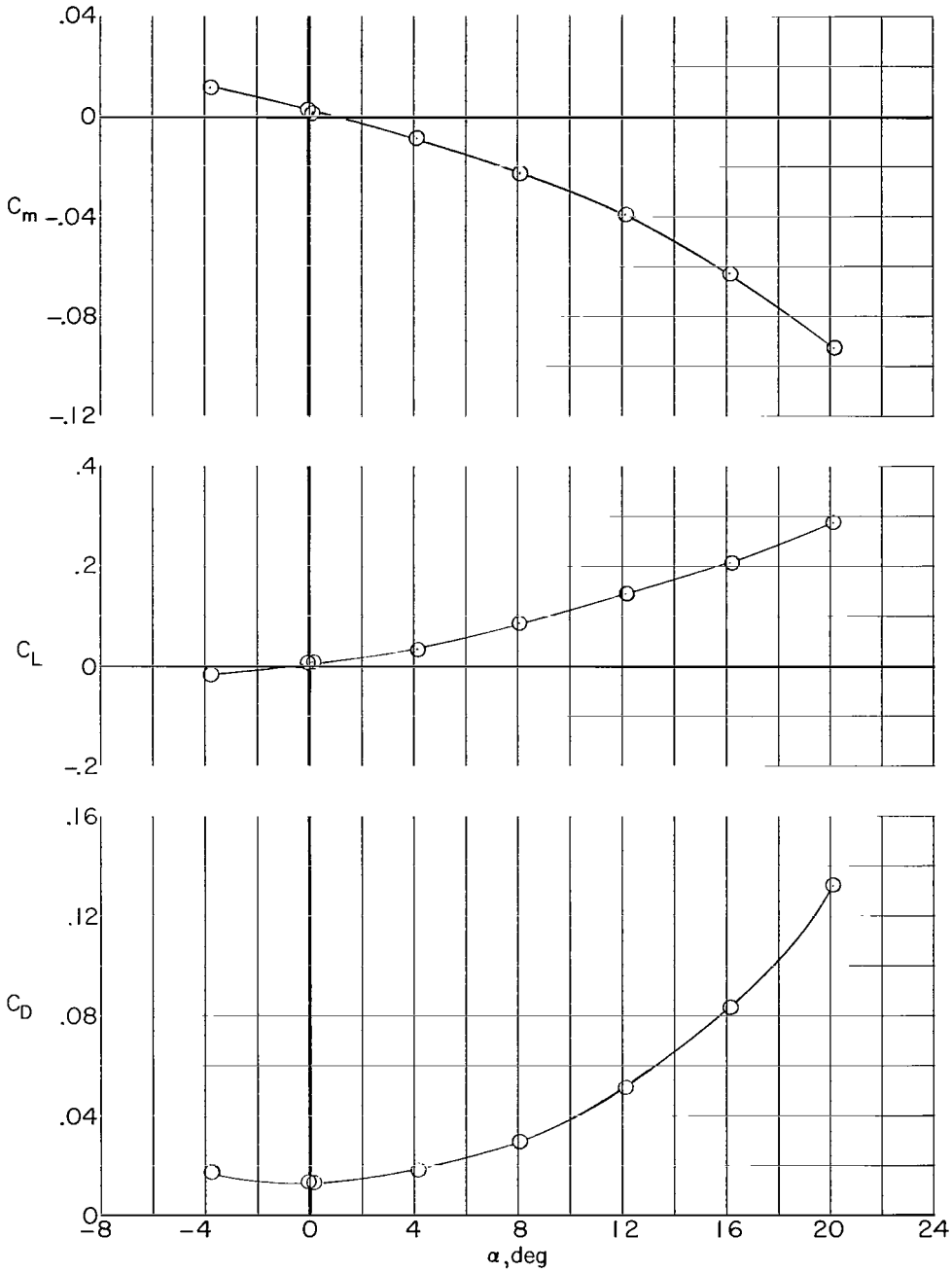

(c) Configuration DW_2B_1.

Figure 6.- Continued.

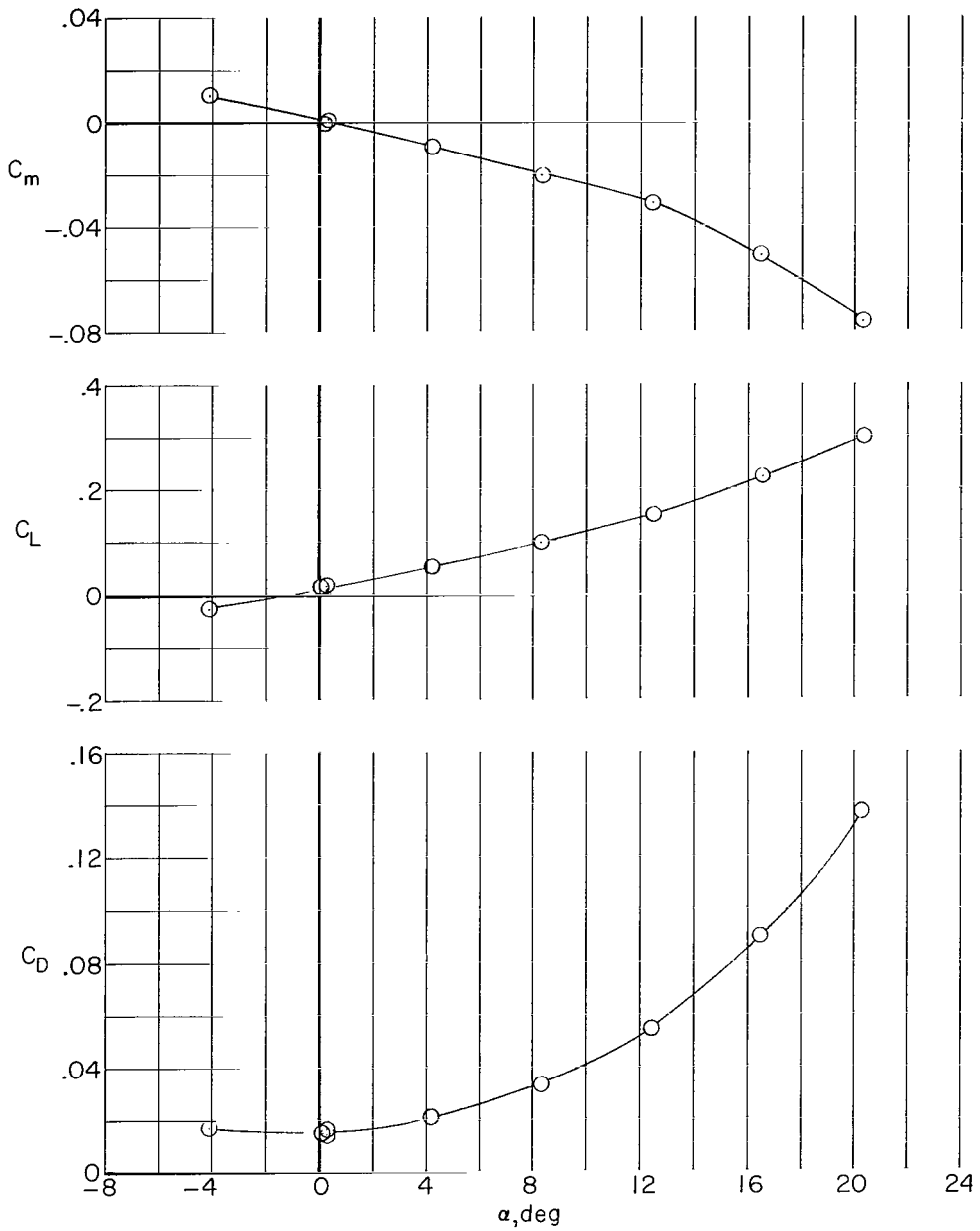

(d) Configuration DW_2B_2.

Figure 6.- Continued.

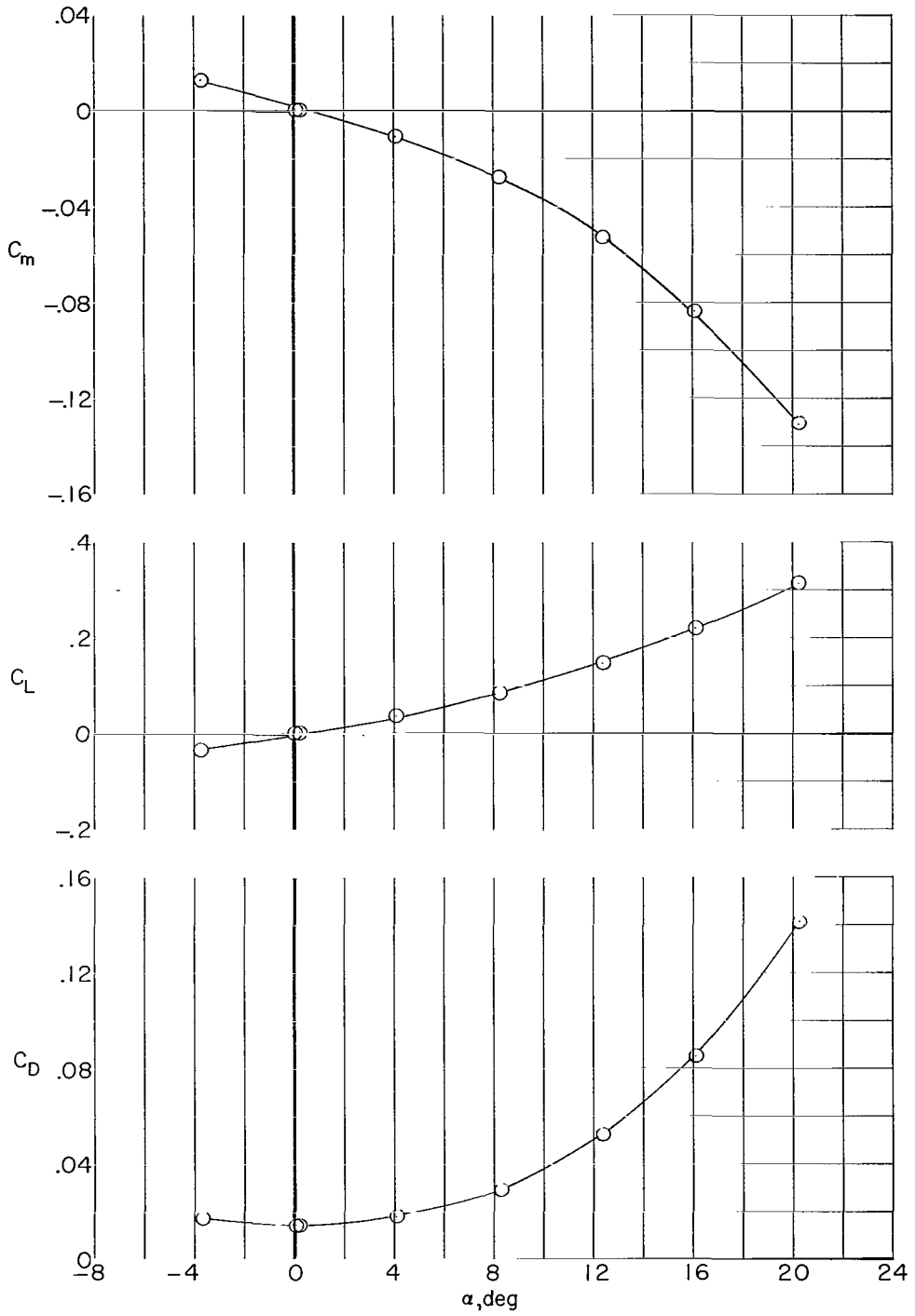

(e) Configuration TW_1B_1.

Figure 6.- Continued.

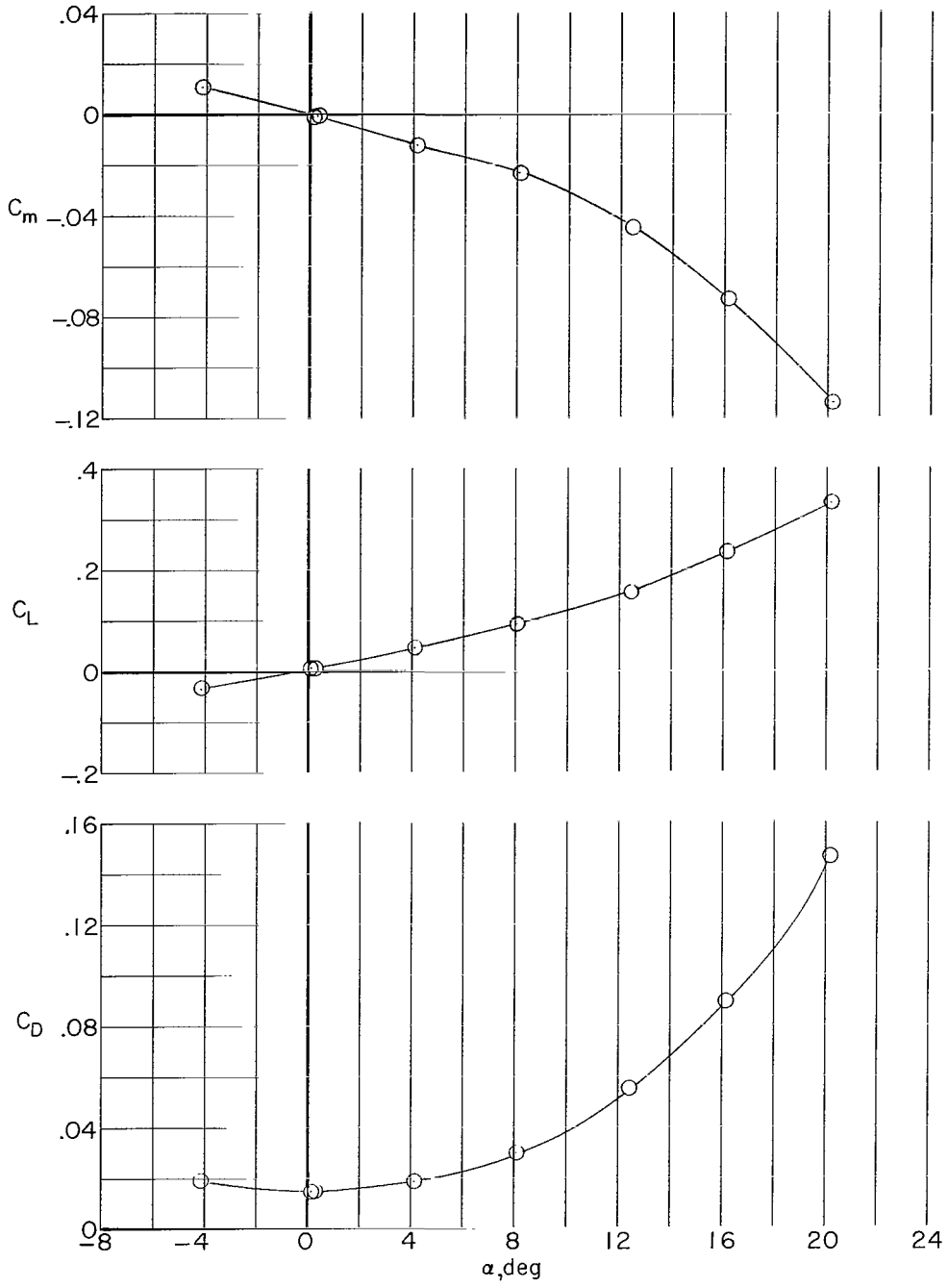

(f) Configuration TW_1B_2.

Figure 6.- Continued.

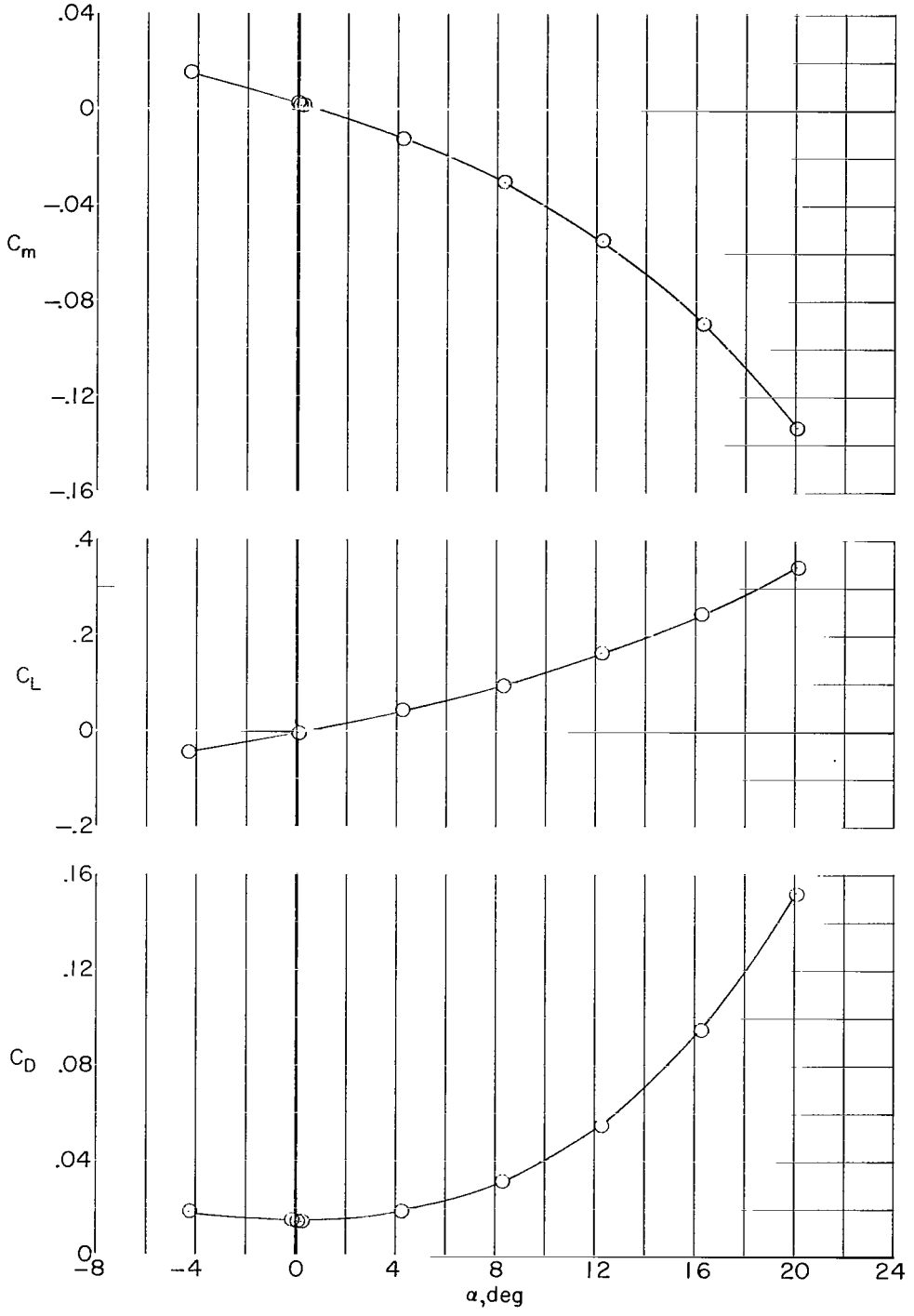

(g) Configuration TW_2B_1.

Figure 6.- Continued.

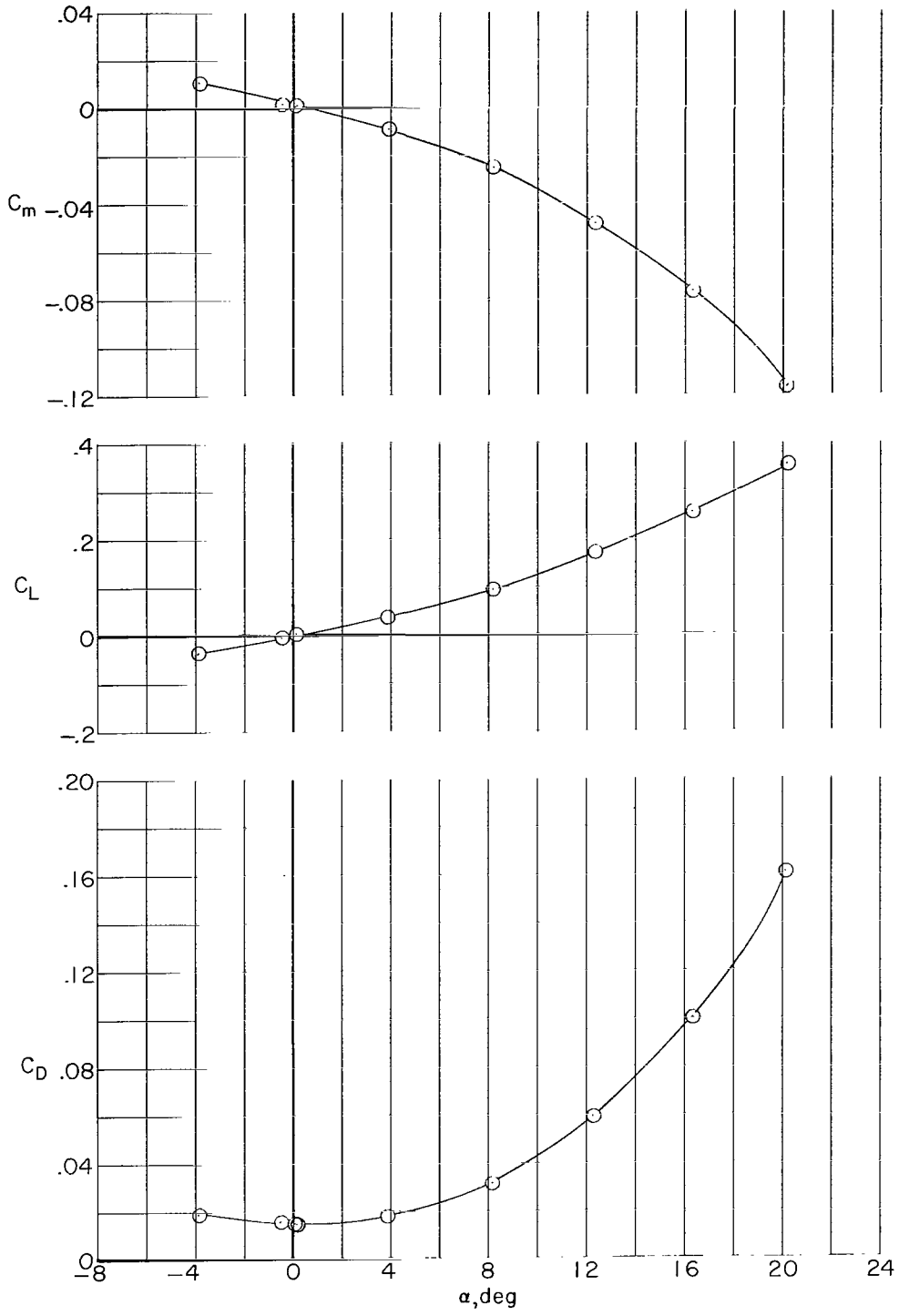

(h) Configuration TW_2B_2.

Figure 6.- Concluded.

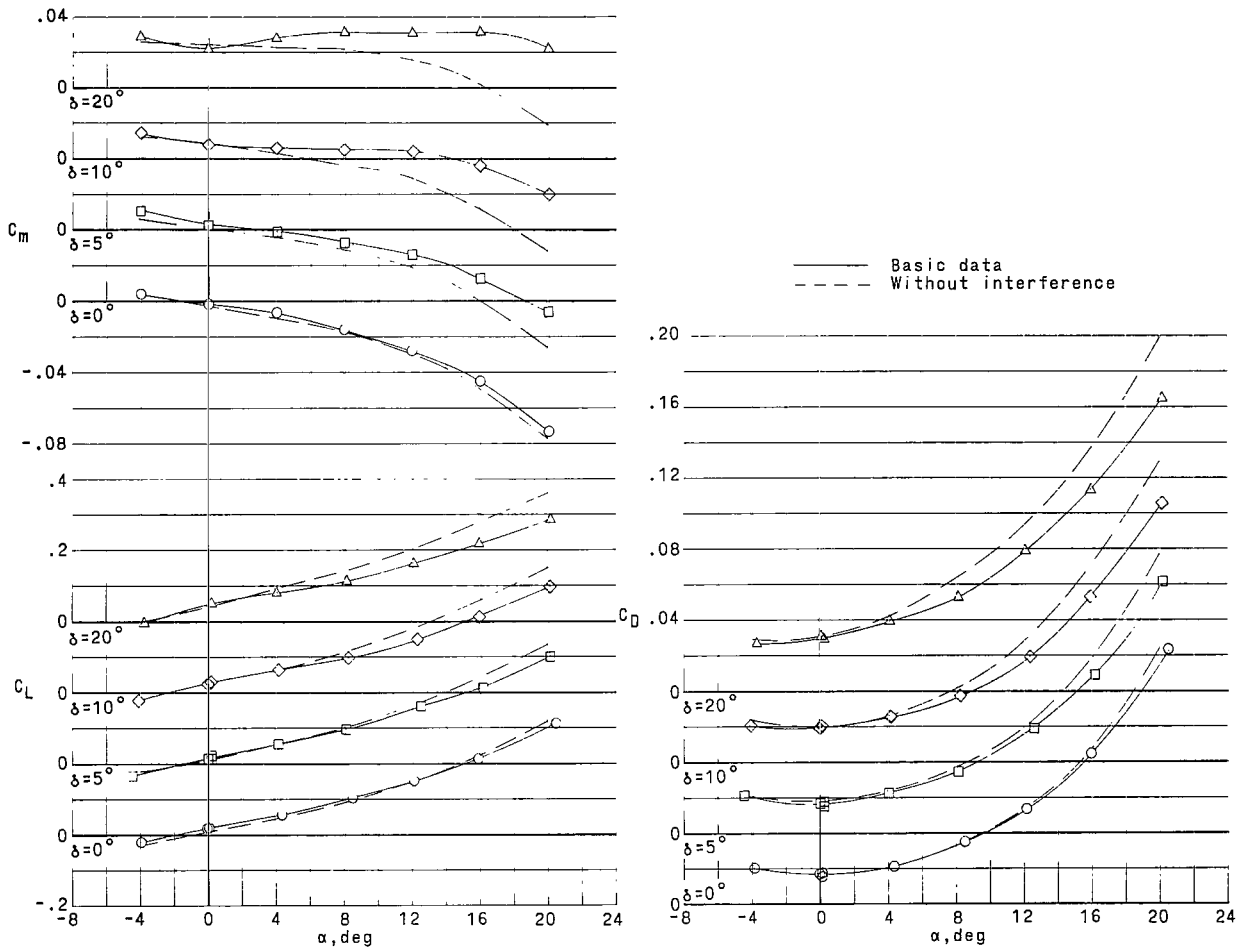

(a) Configuration $DW_1B_1C_1$.

Figure 7.- Comparison of canard control configuration longitudinal data (symbols) with interference-free characteristics (broken lines).

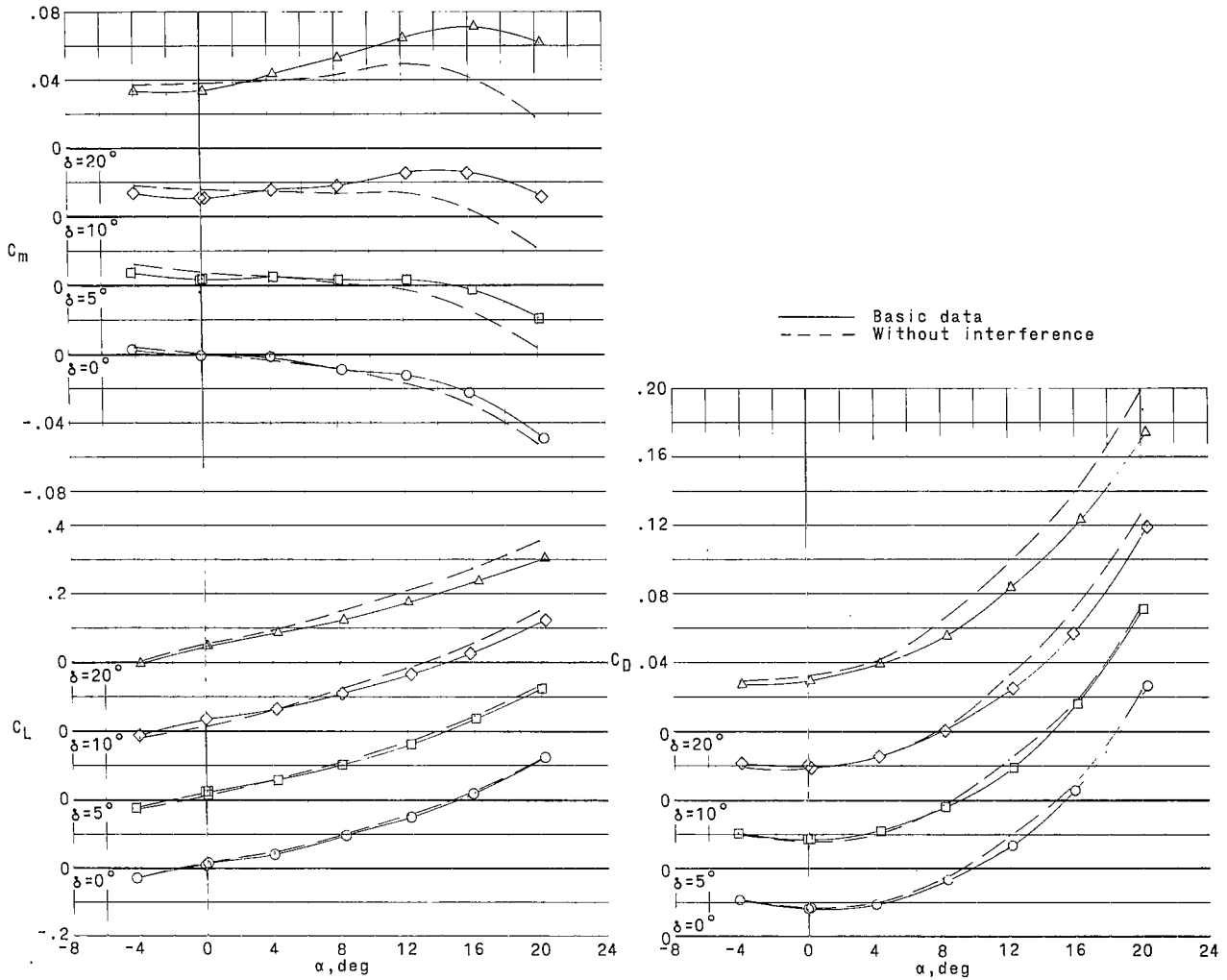

(b) Configuration $DW_1B_2C_1$.

Figure 7.- Continued.

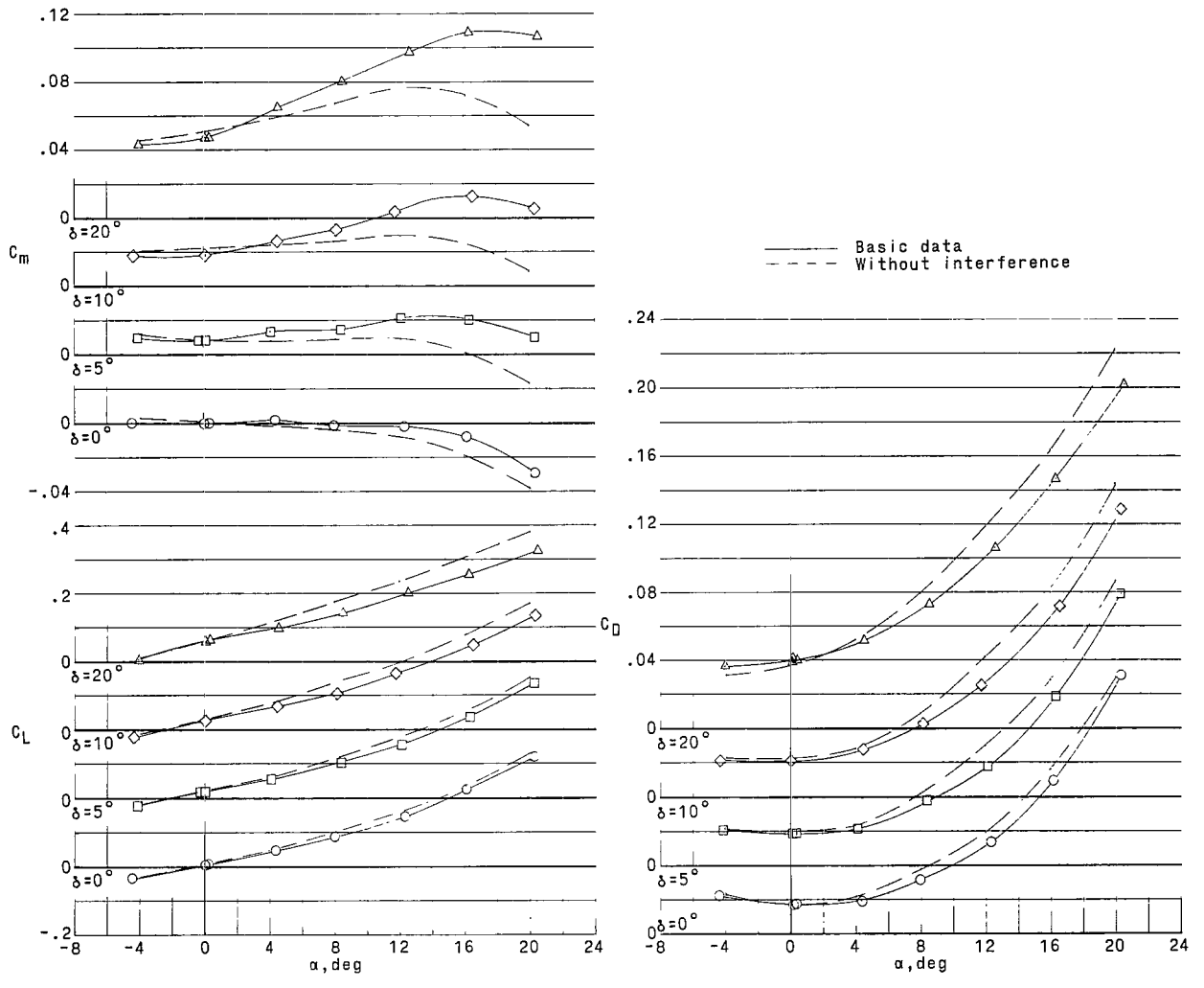

(c) Configuration $DW_1B_2C_2$.

Figure 7.- Continued.

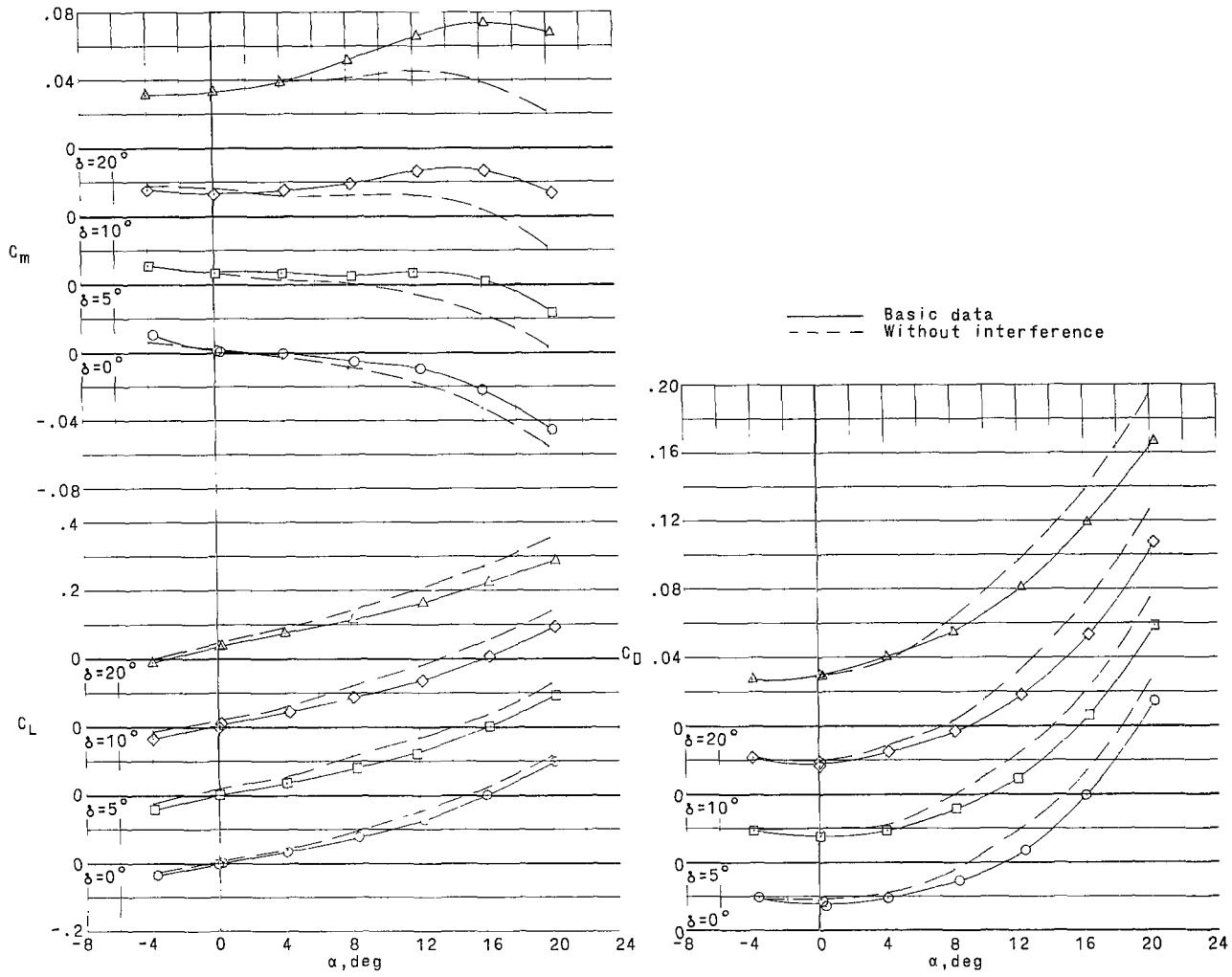

(d) Configuration $DW_1B_2C_3$.

Figure 7.- Continued.

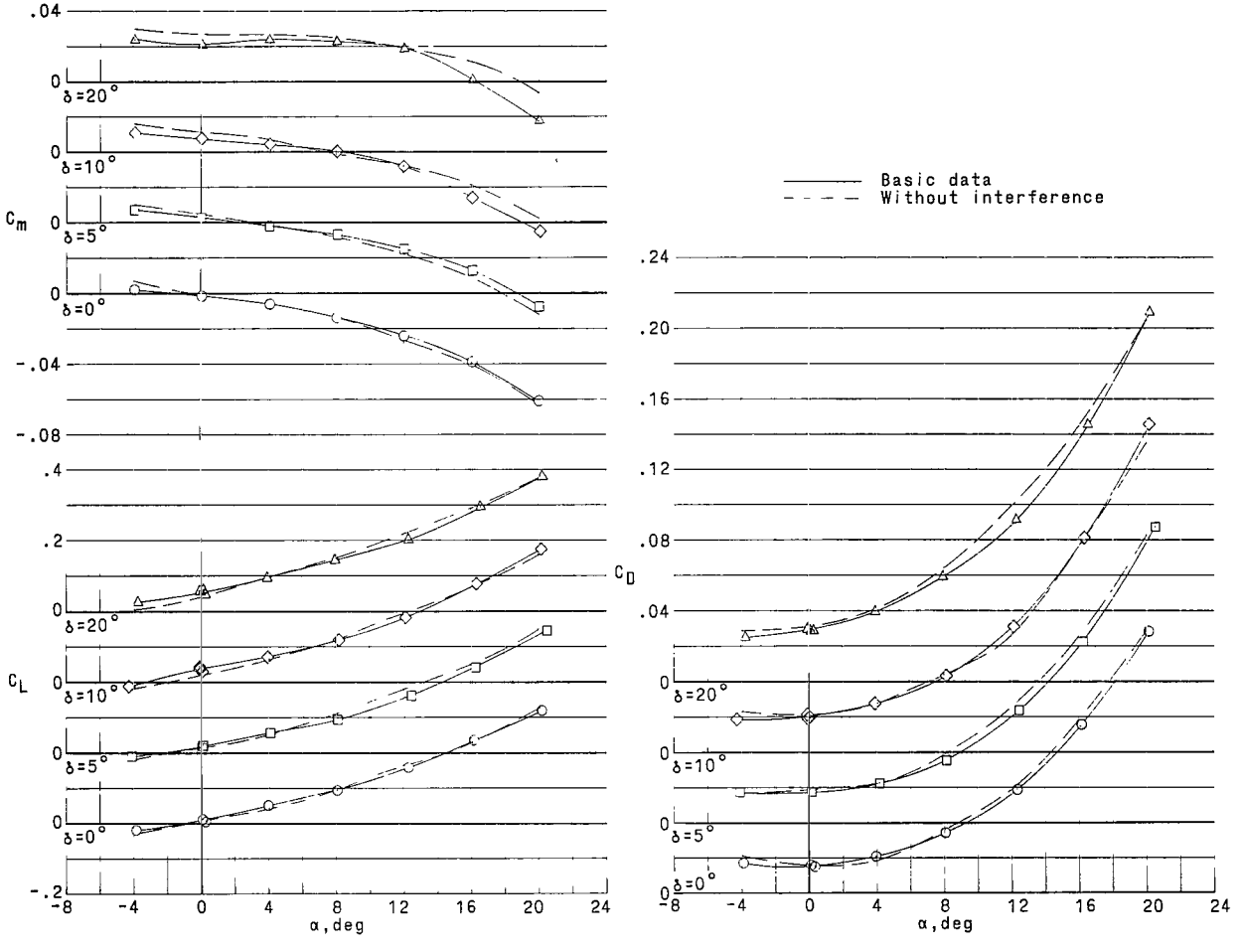

(e) Configuration $DW_2B_1C_1$.

Figure 7.- Continued.

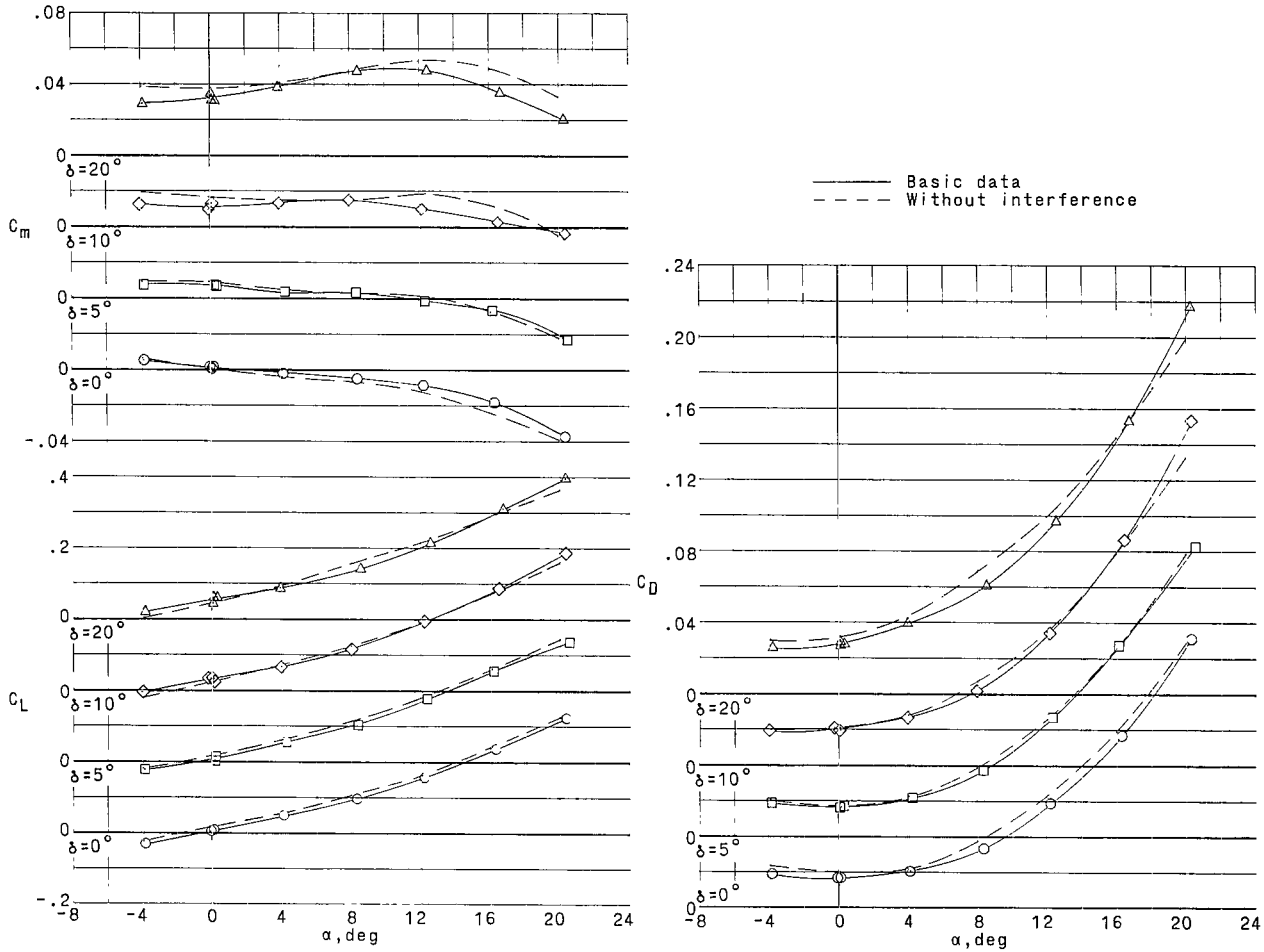

(f) Configuration $DW_2B_2C_1$.

Figure 7.- Continued.

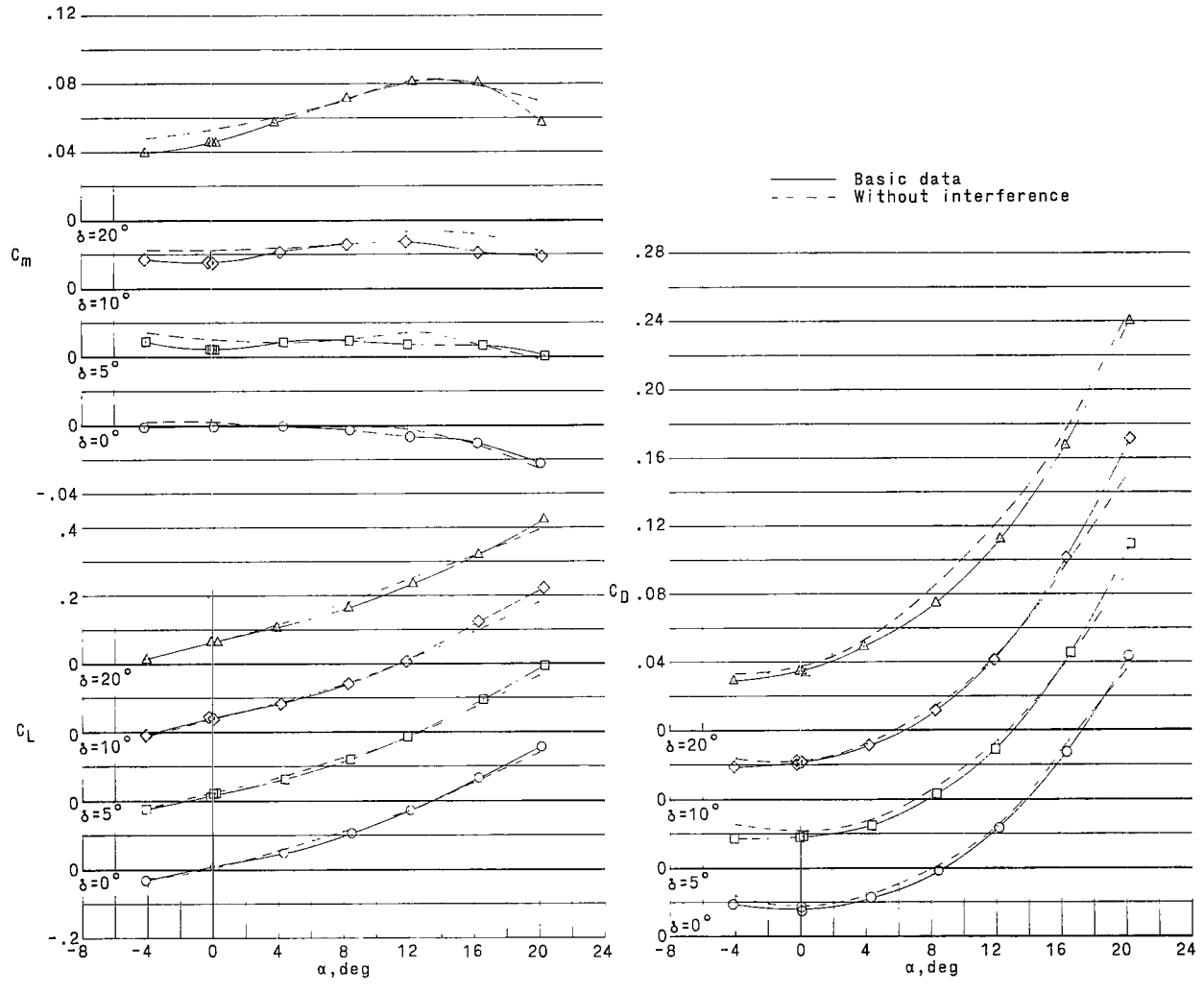

(g) Configuration $DW_2B_2C_2$.

Figure 7.- Continued.

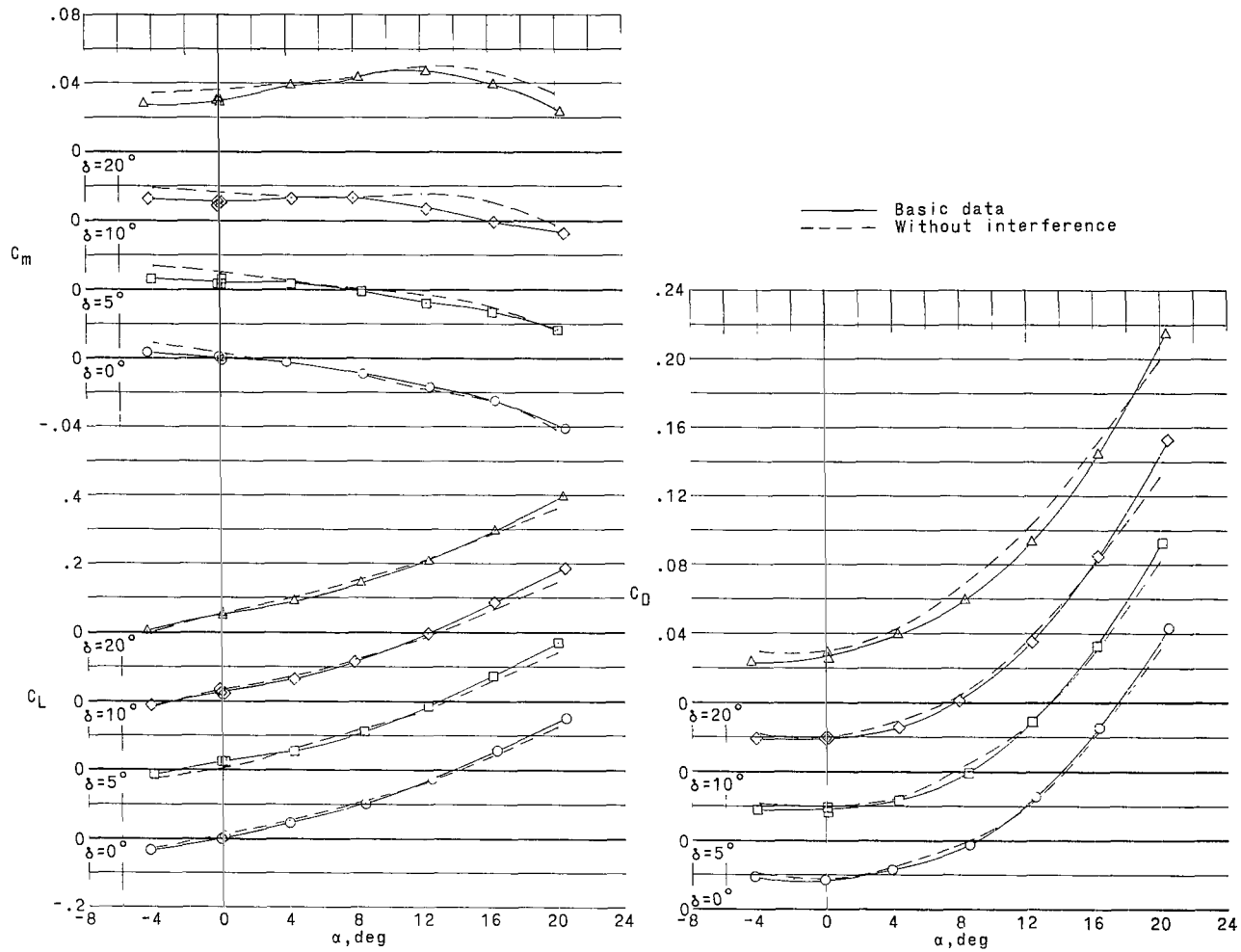

(h) Configuration $DW_2B_2C_3$.

Figure 7.- Continued.

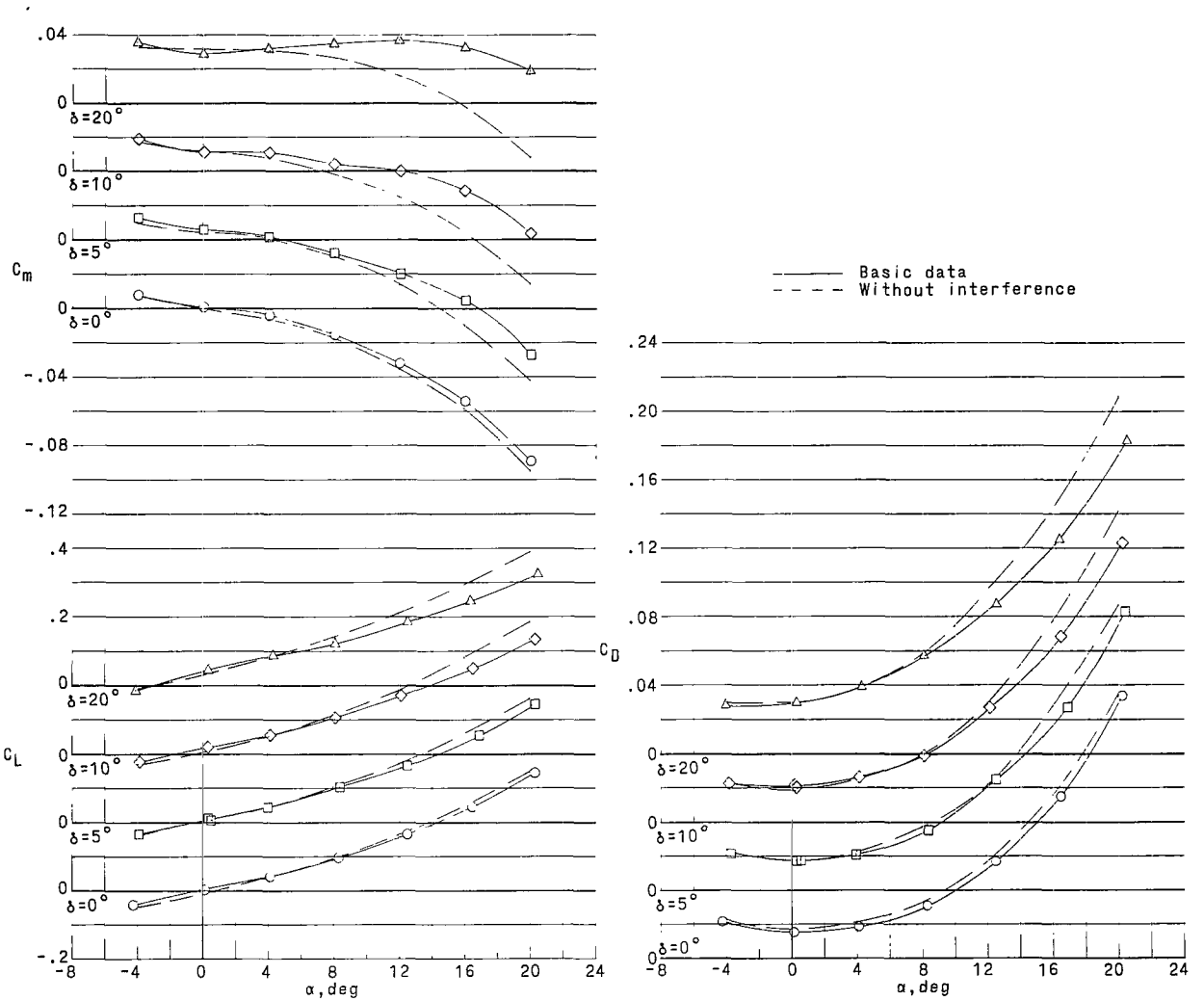

(i) Configuration $TW_1B_1C_1$.

Figure 7.- Continued.

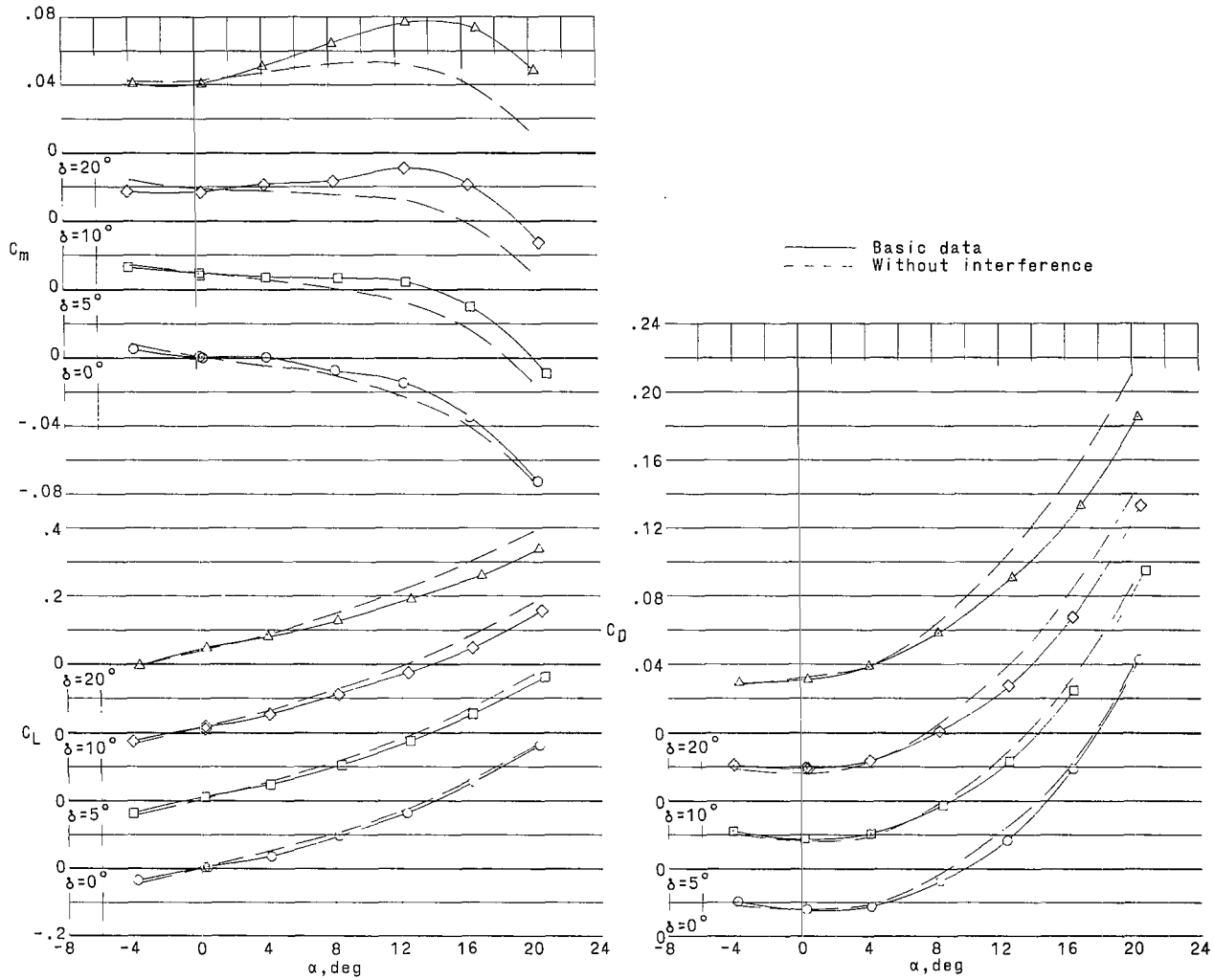

(j) Configuration $TW_1B_2C_1$.

Figure 7.- Continued.

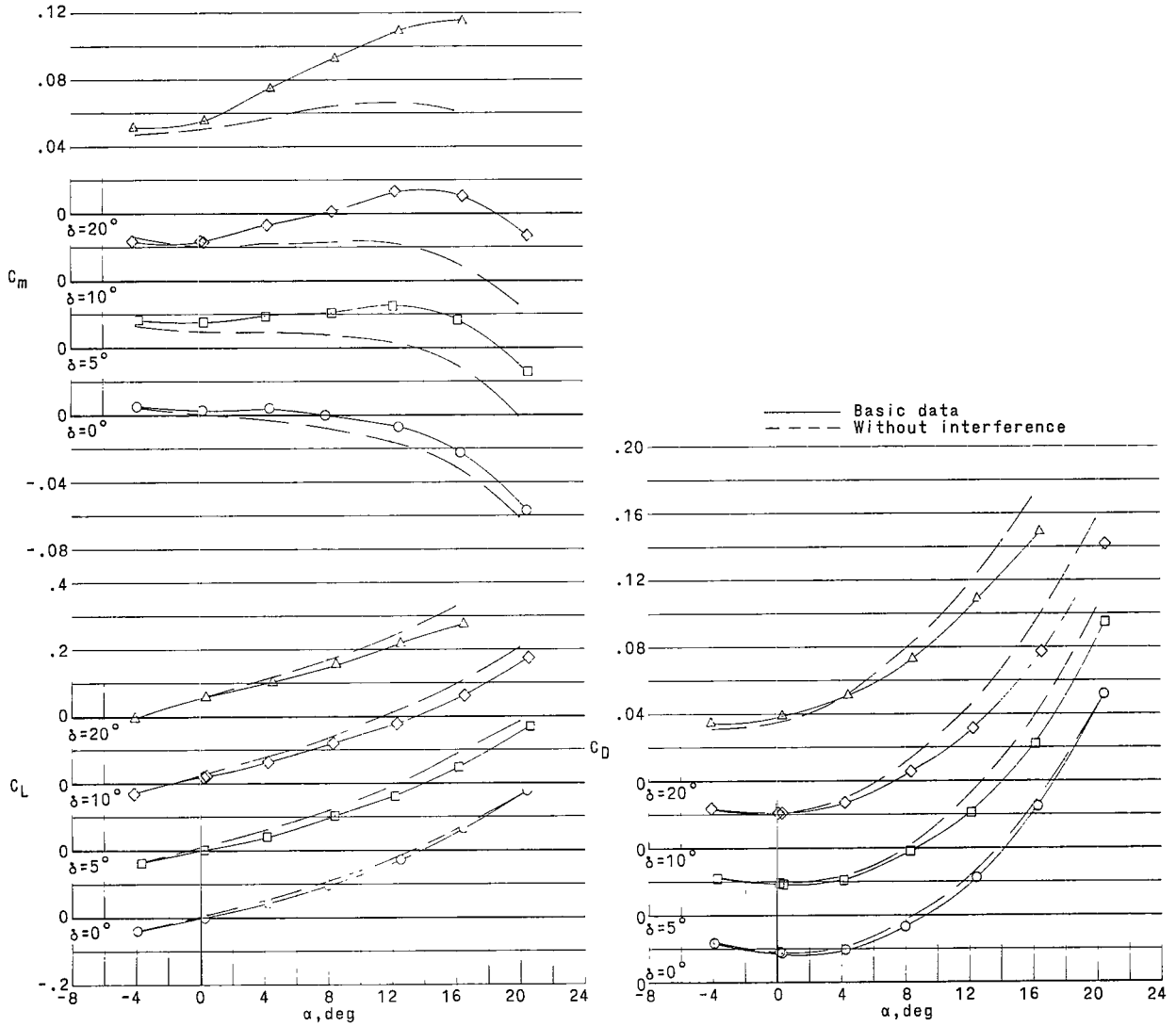

(k) Configuration $TW_1B_2C_2$.

Figure 7.- Continued.

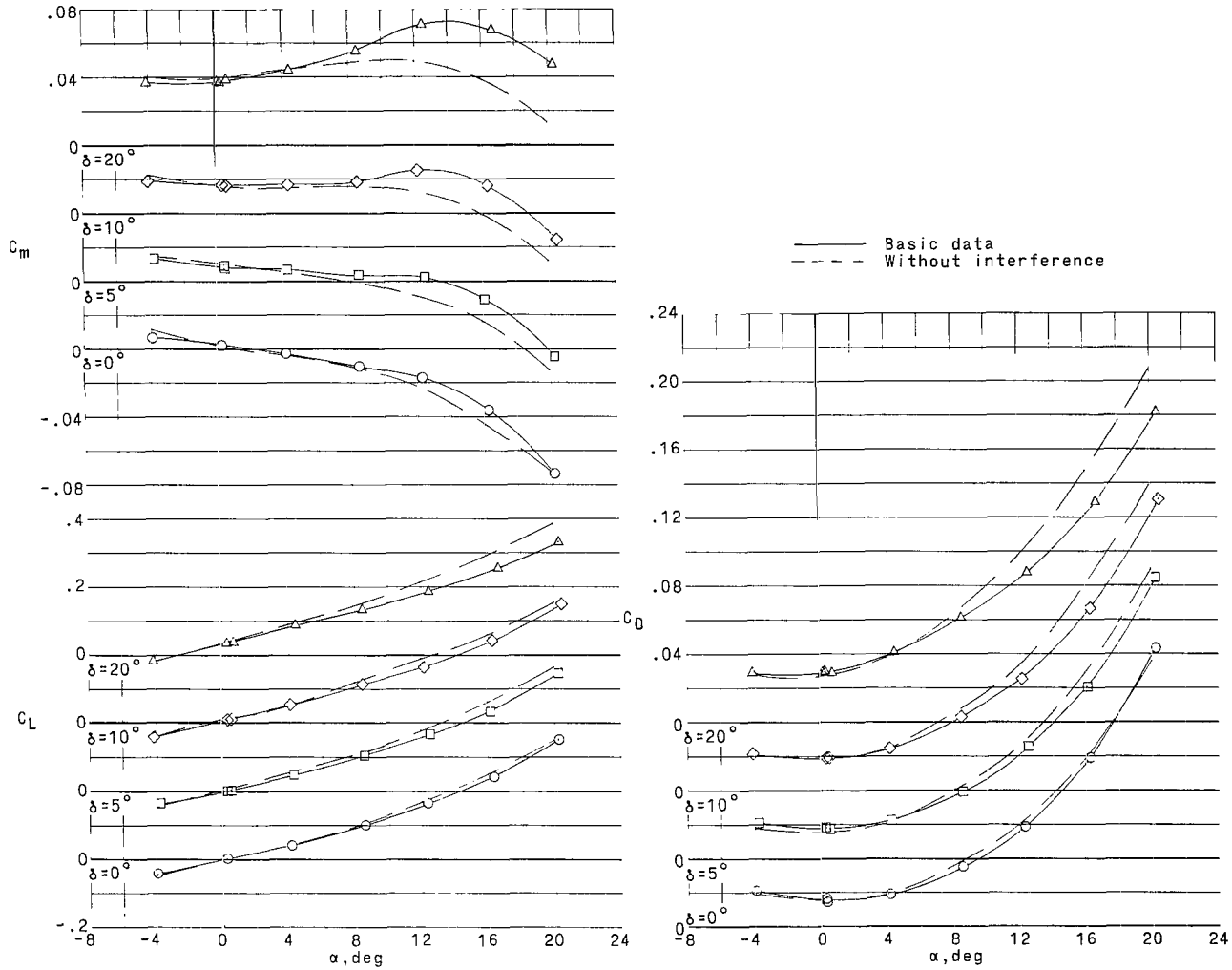

(l) Configuration $TW_1B_2C_3$.

Figure 7.- Continued.

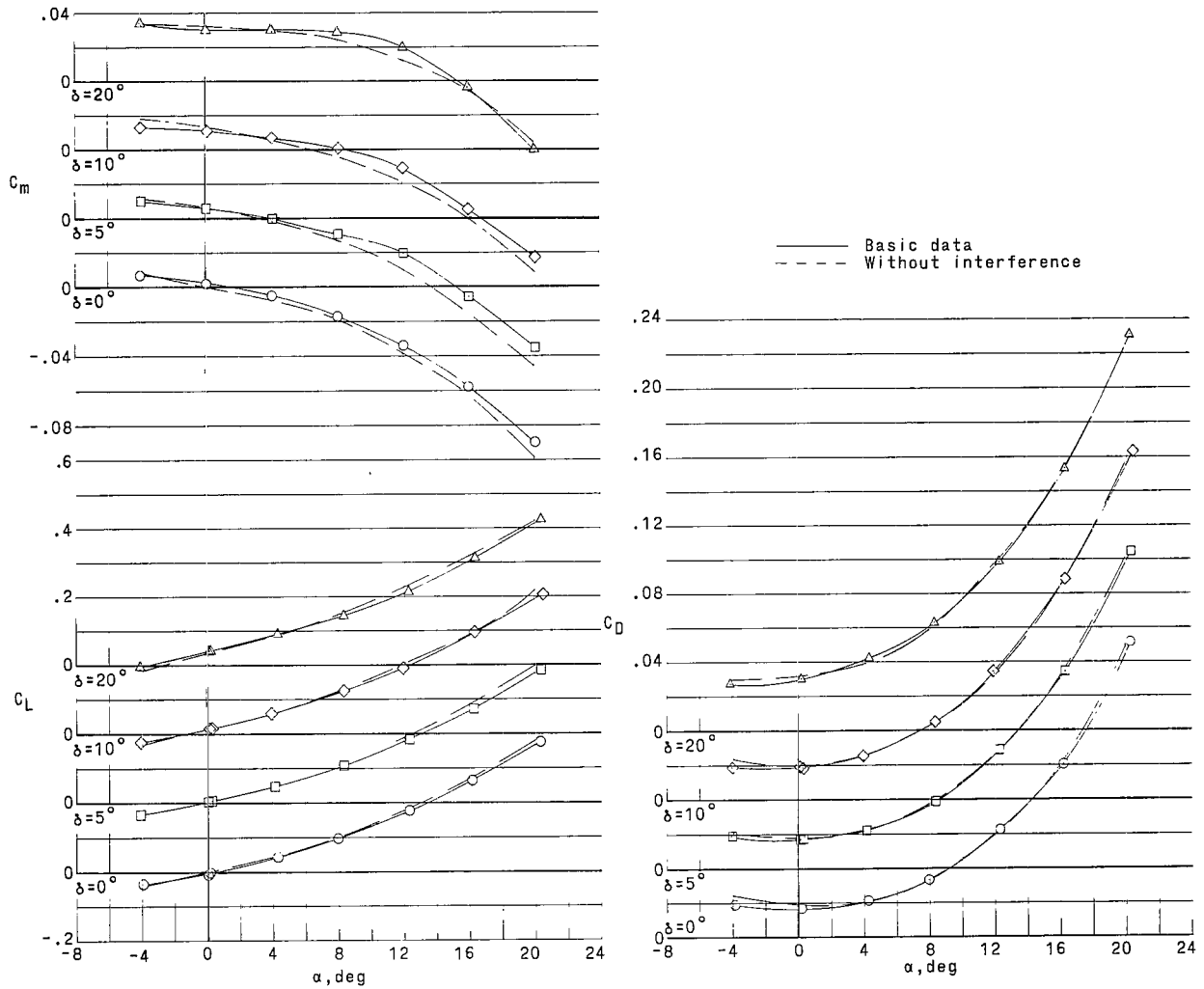

(m) Configuration $TW_2B_1C_1$.

Figure 7.- Continued.

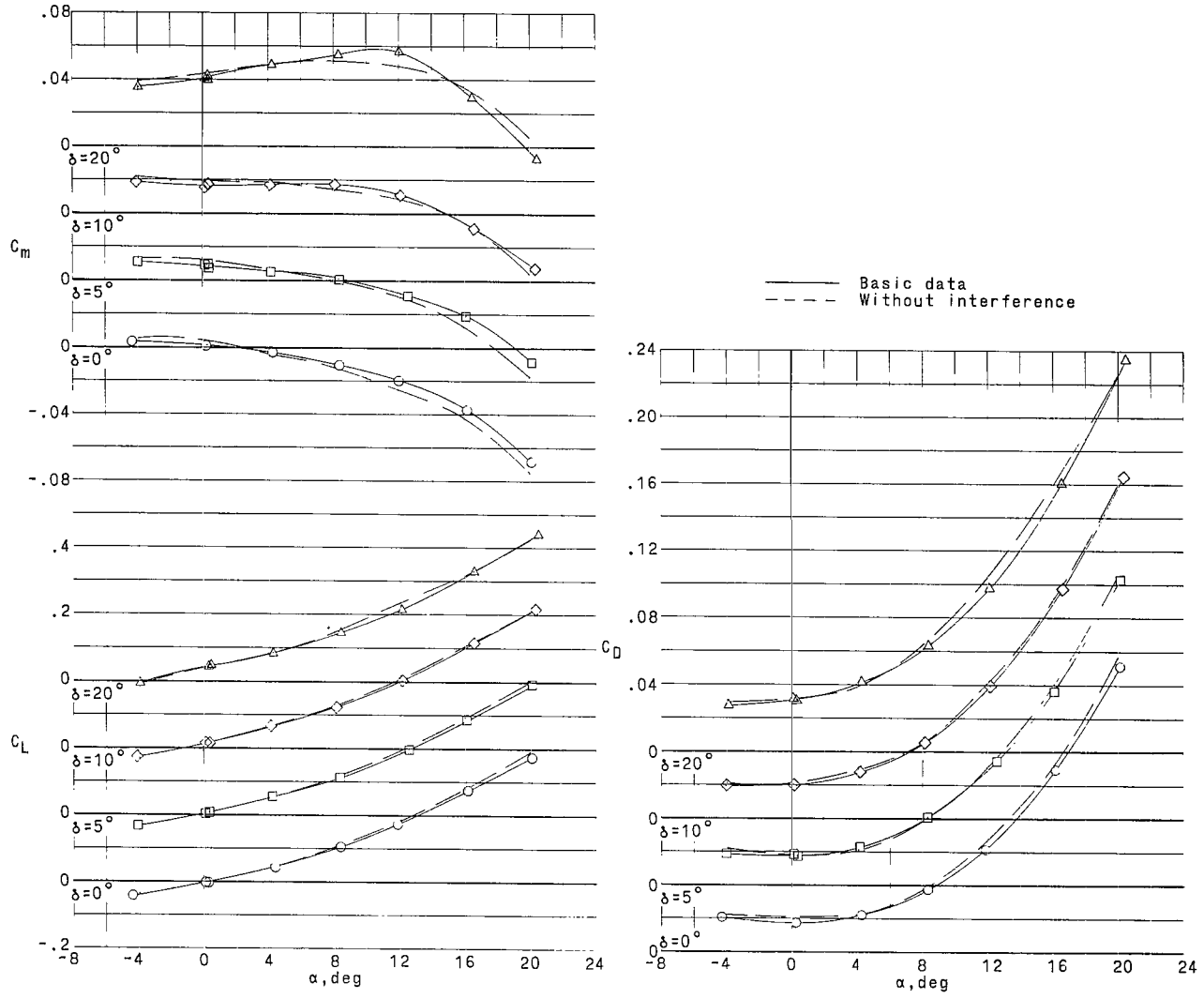

(n) Configuration $TW_2B_2C_1$.

Figure 7.- Continued.

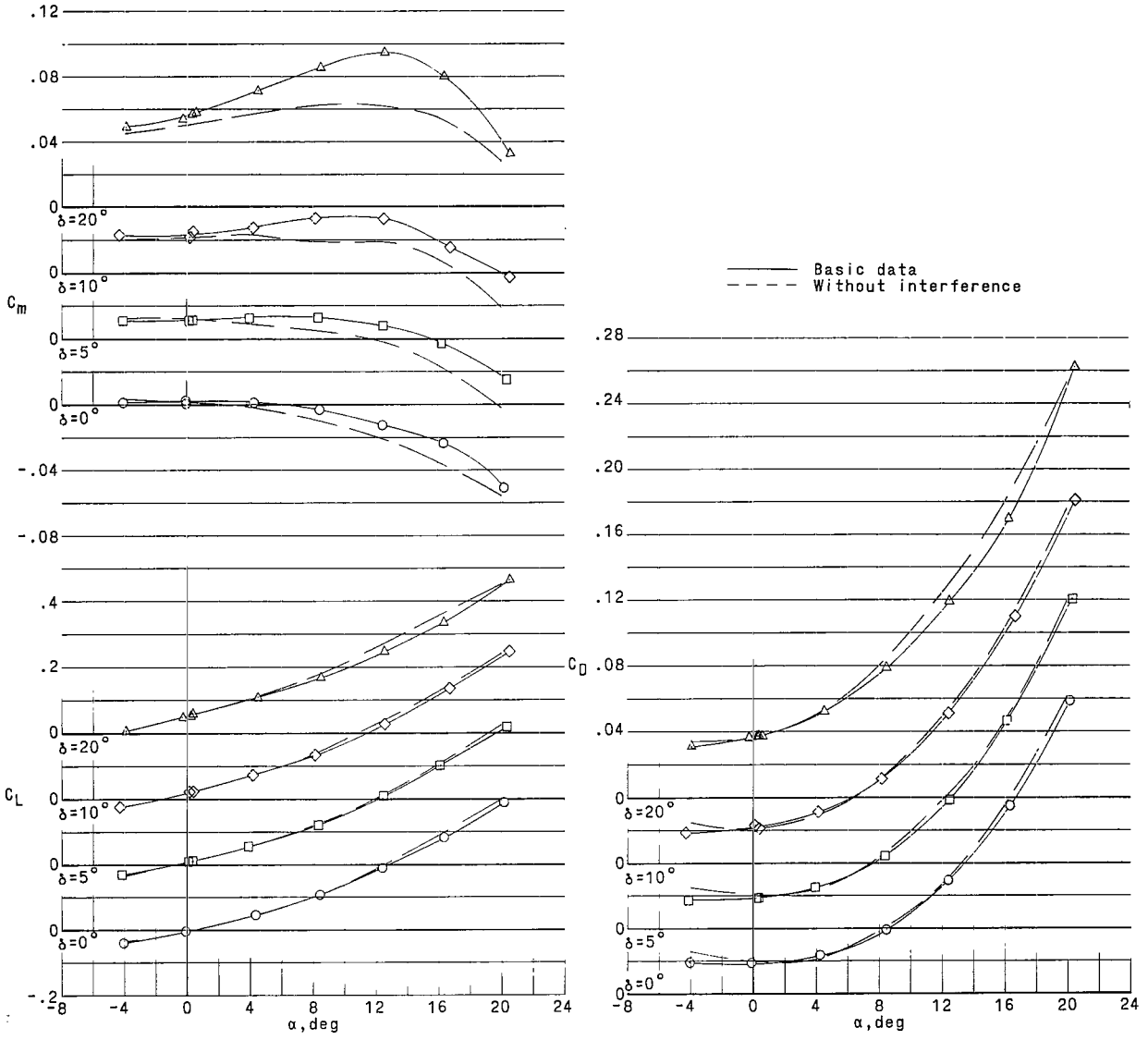

(o) Configuration $TW_2B_2C_2$.

Figure 7.- Continued.

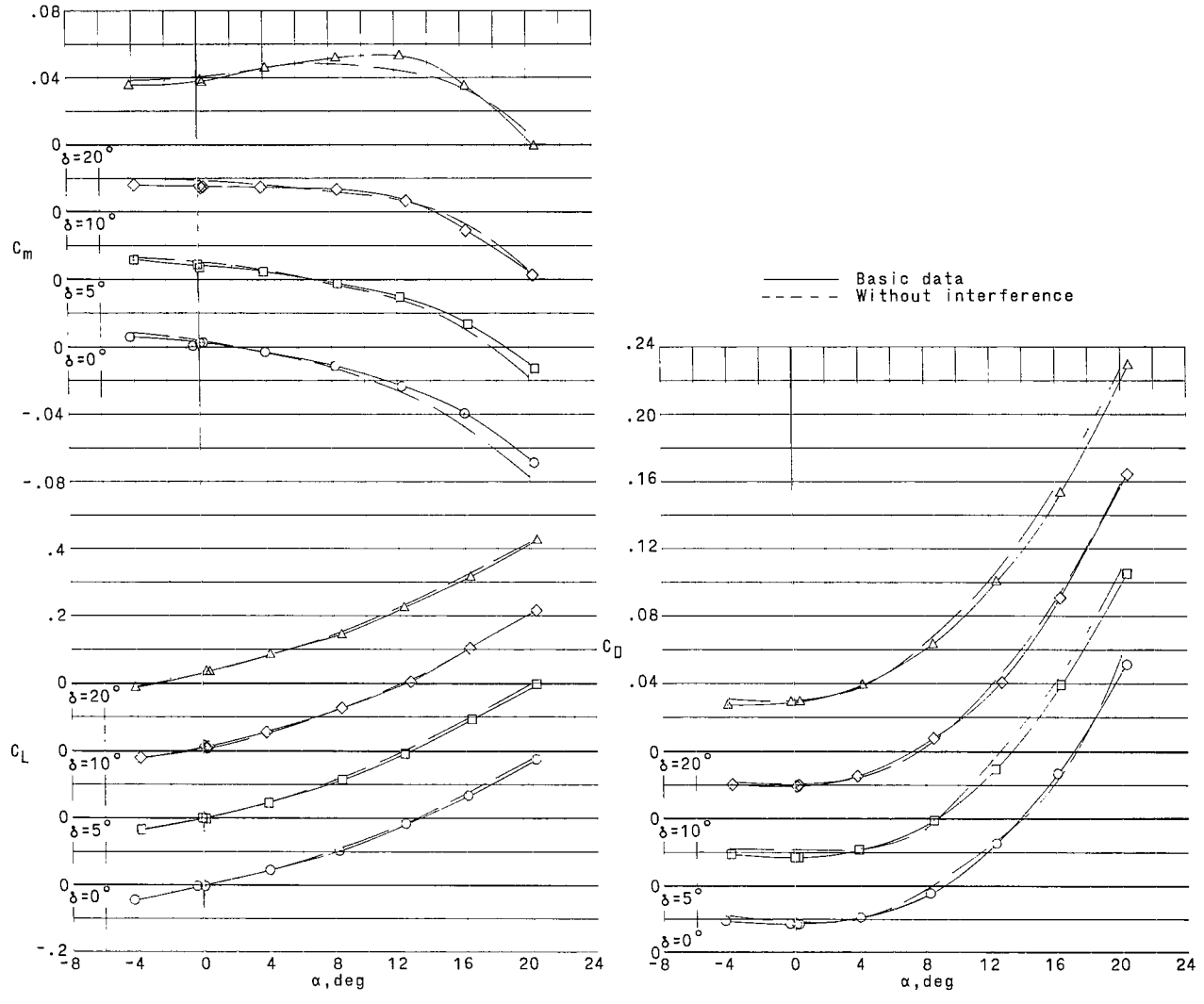

(p) Configuration $TW_2B_2C_3$.

Figure 7.- Concluded.

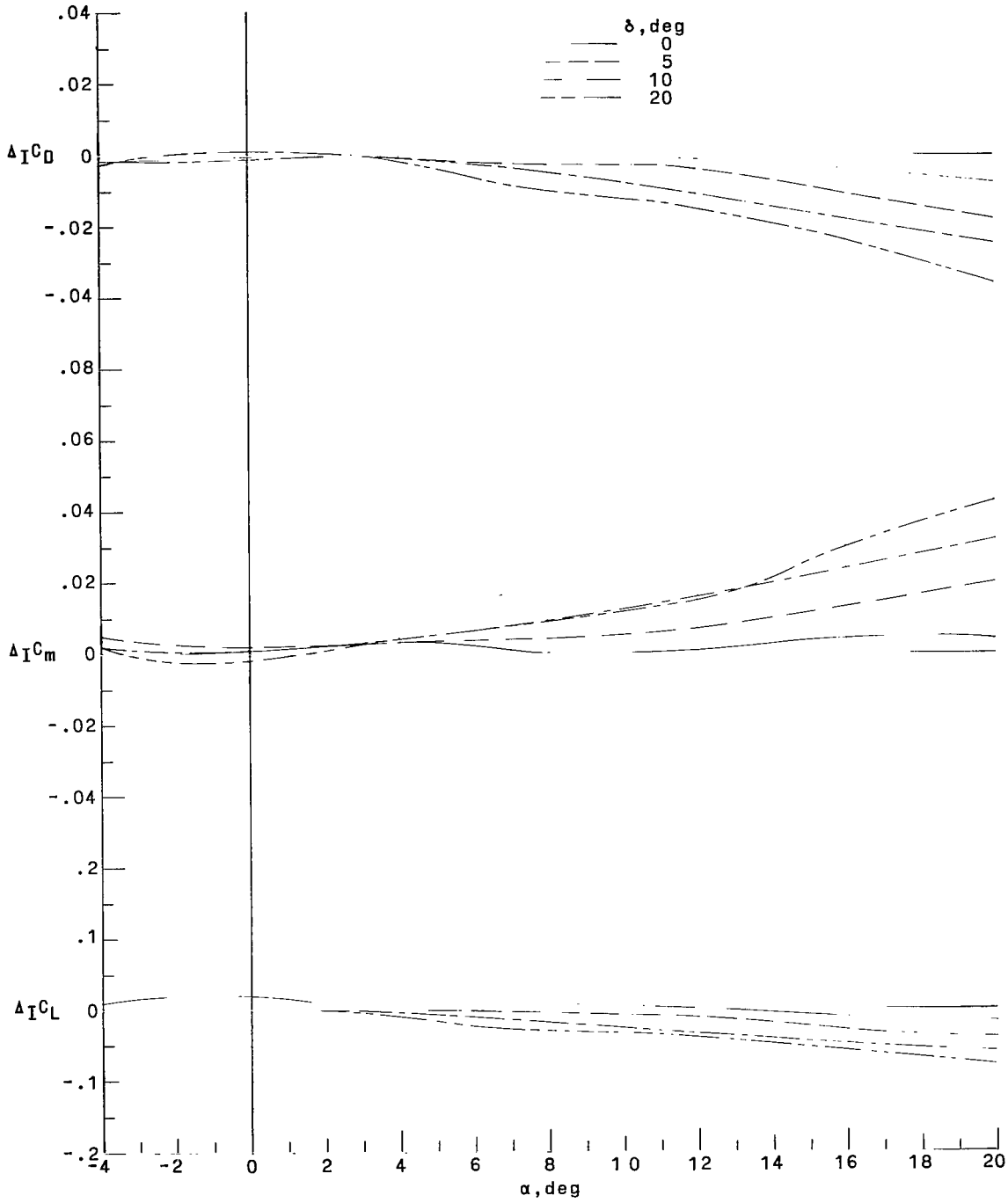

(a) Configuration $DW_1B_1C_1$.

Figure 8.- Variation of interference terms with angle of attack and canard deflection angle.

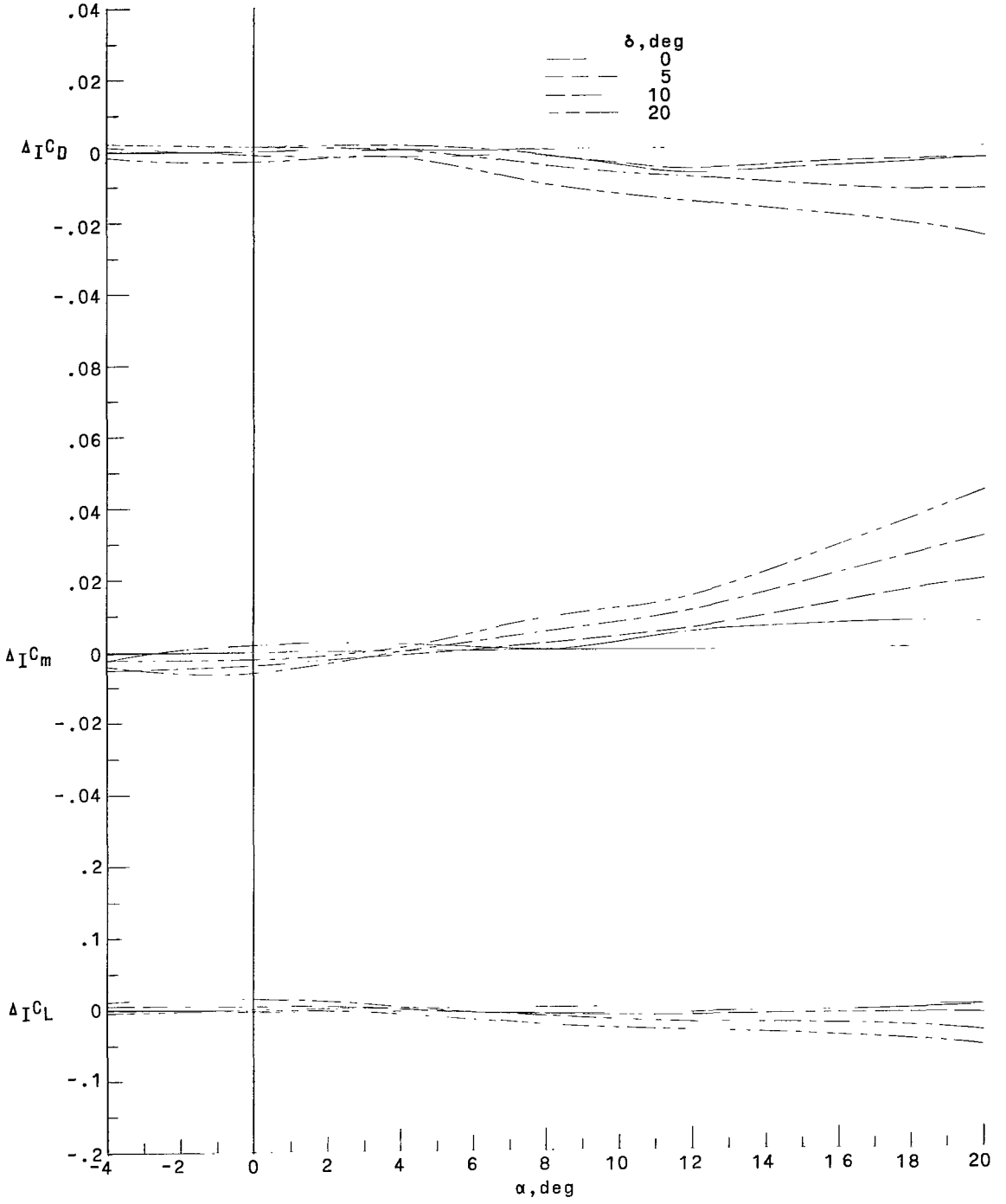

(b) Configuration $DW_1B_2C_1$.

Figure 8.- Continued.

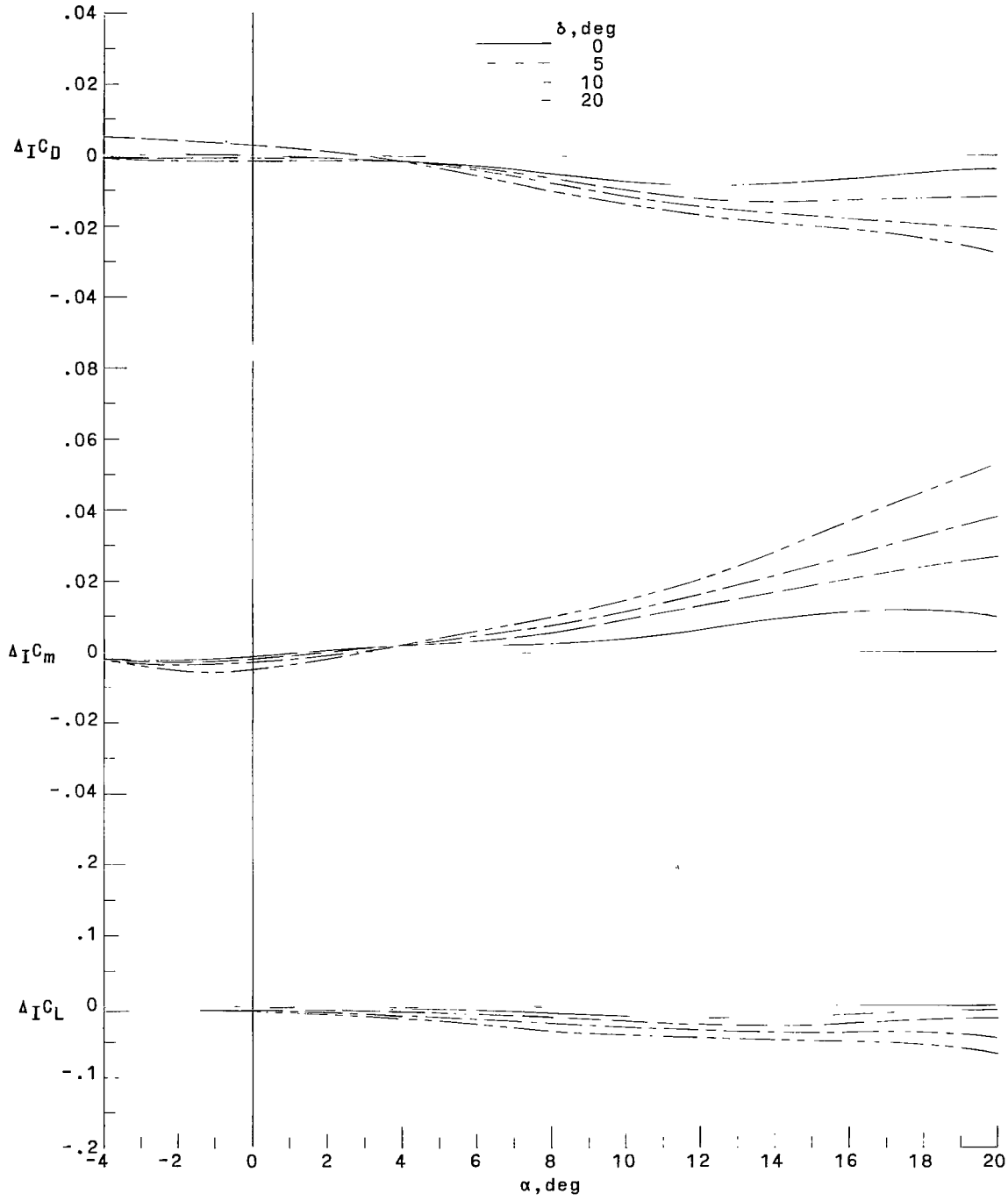

(c) Configuration $DW_1B_2C_2$.

Figure 8.- Continued.

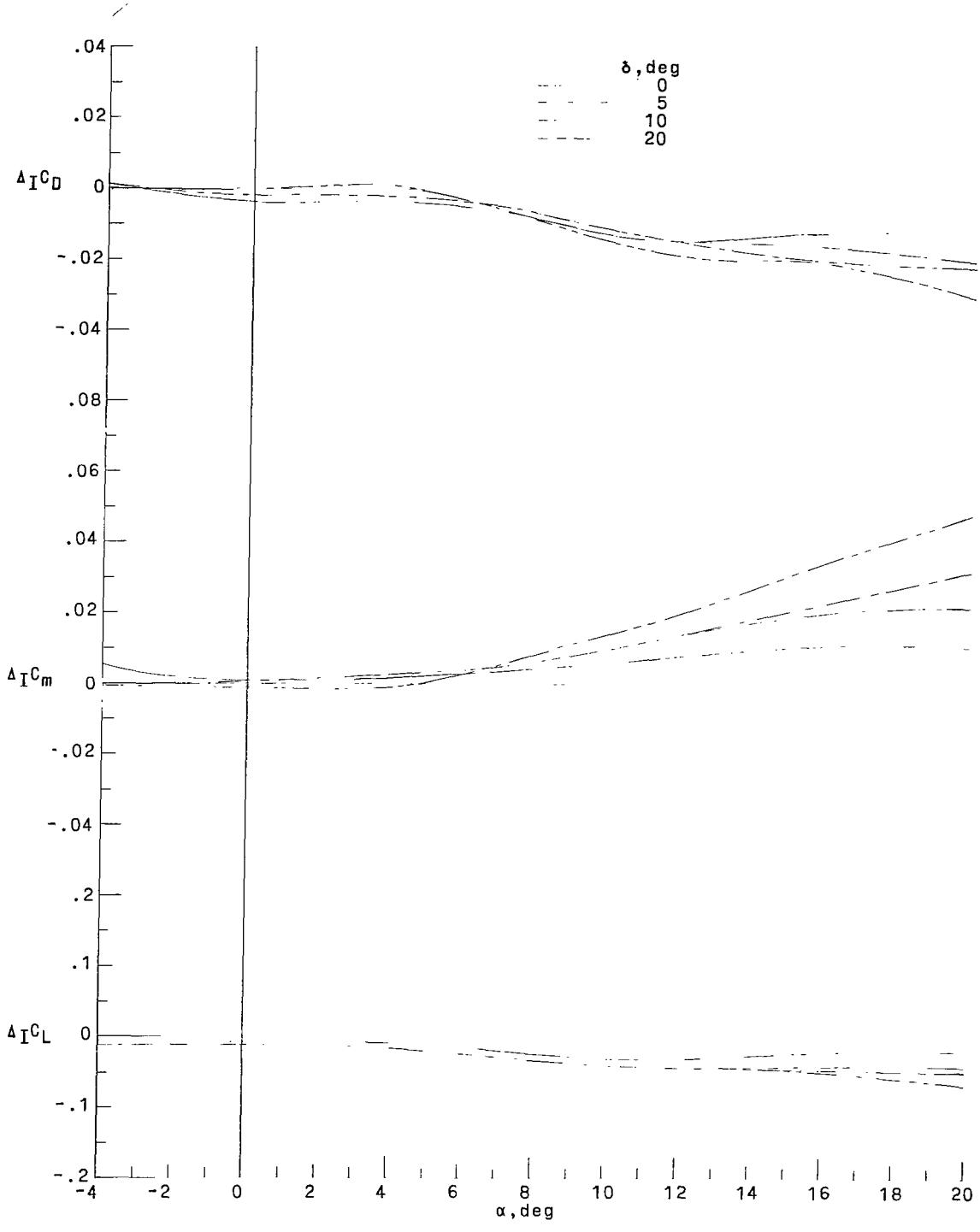

(d) Configuration $DW_1B_2C_3$.

Figure 8.- Continued.

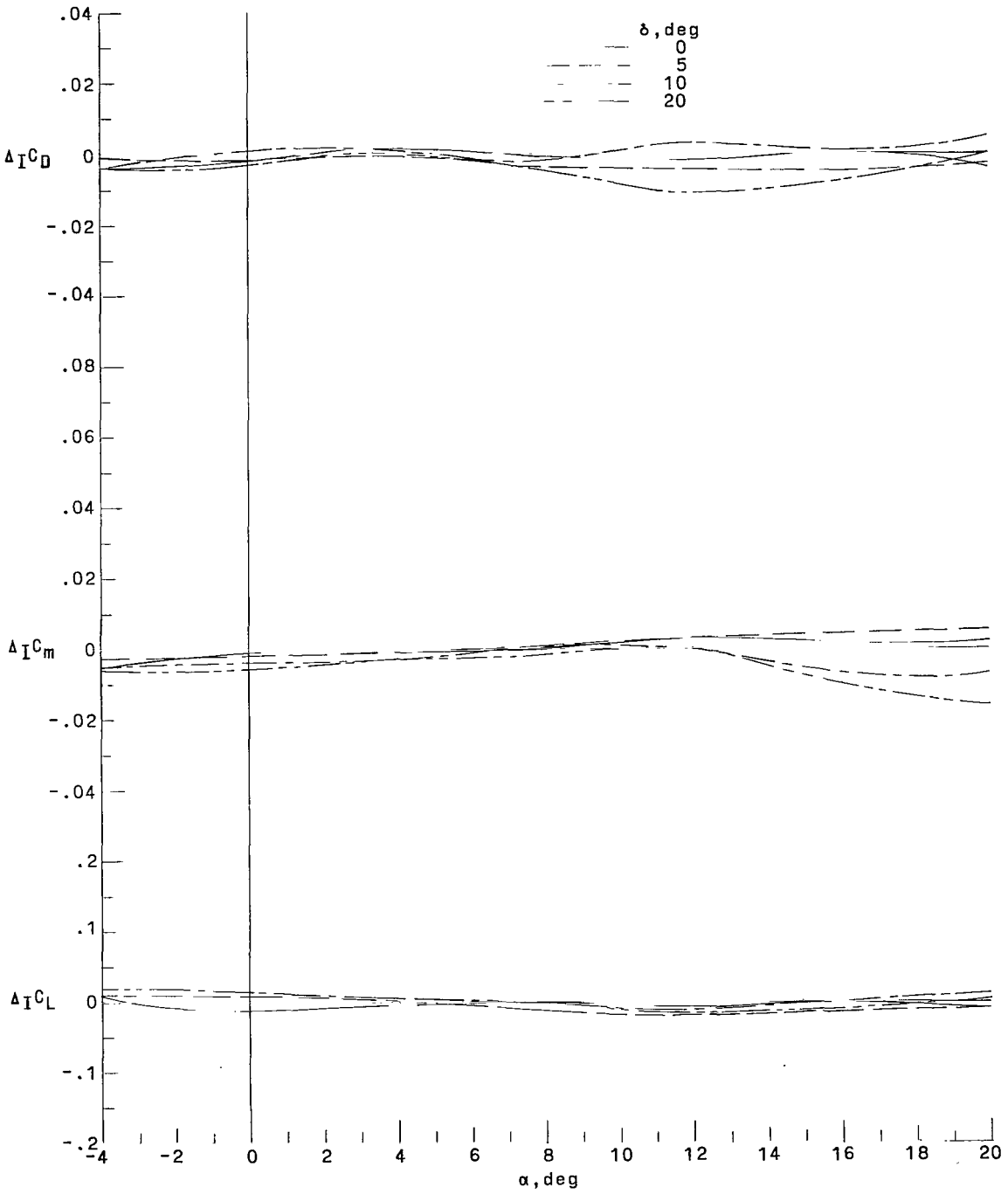

(e) Configuration $DW_2B_1C_1$.

Figure 8.- Continued.

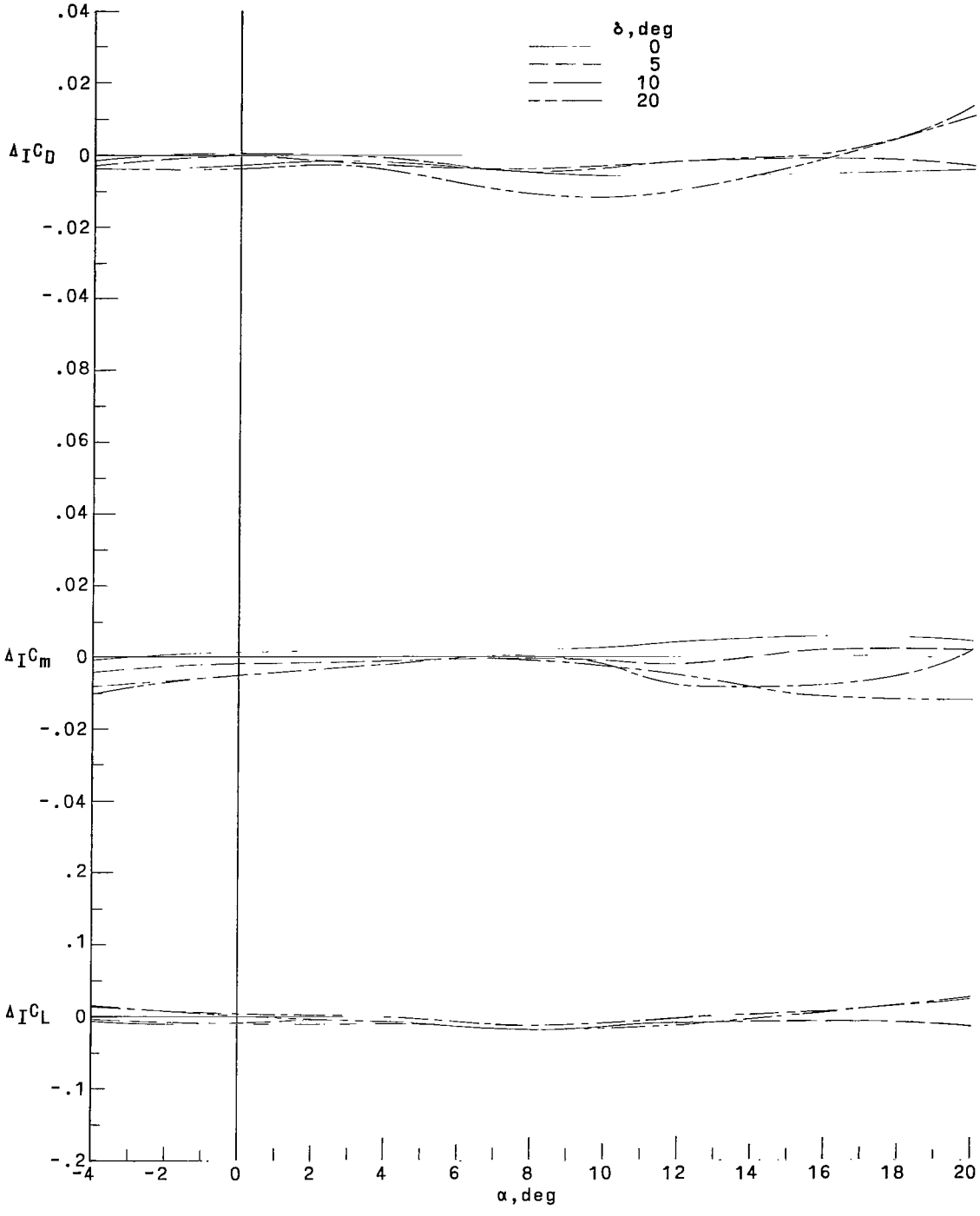

(f) Configuration $DW_2B_2C_1$.

Figure 8.- Continued.

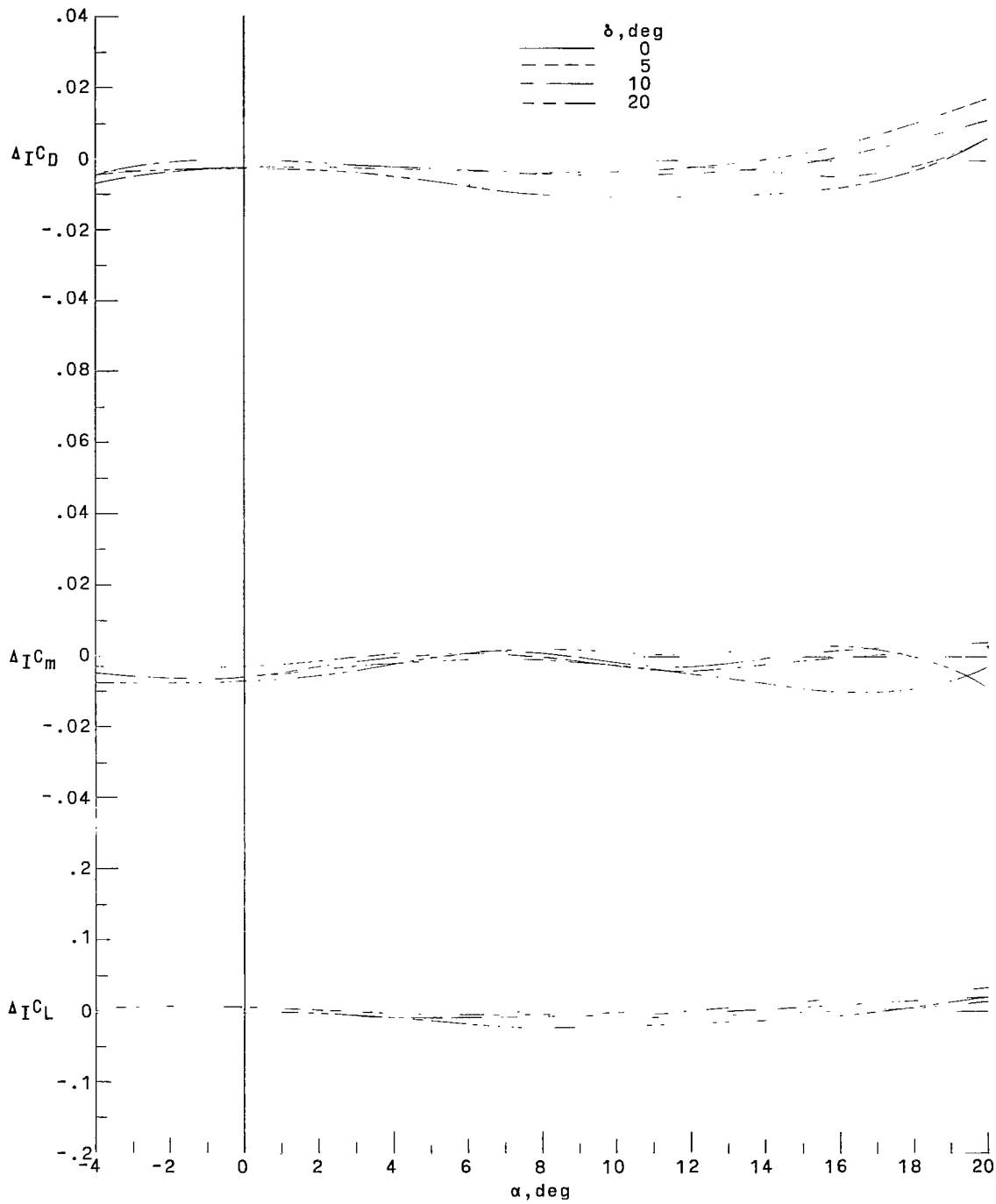

(g) Configuration $DW_2B_2C_2$.

Figure 8.- Continued.

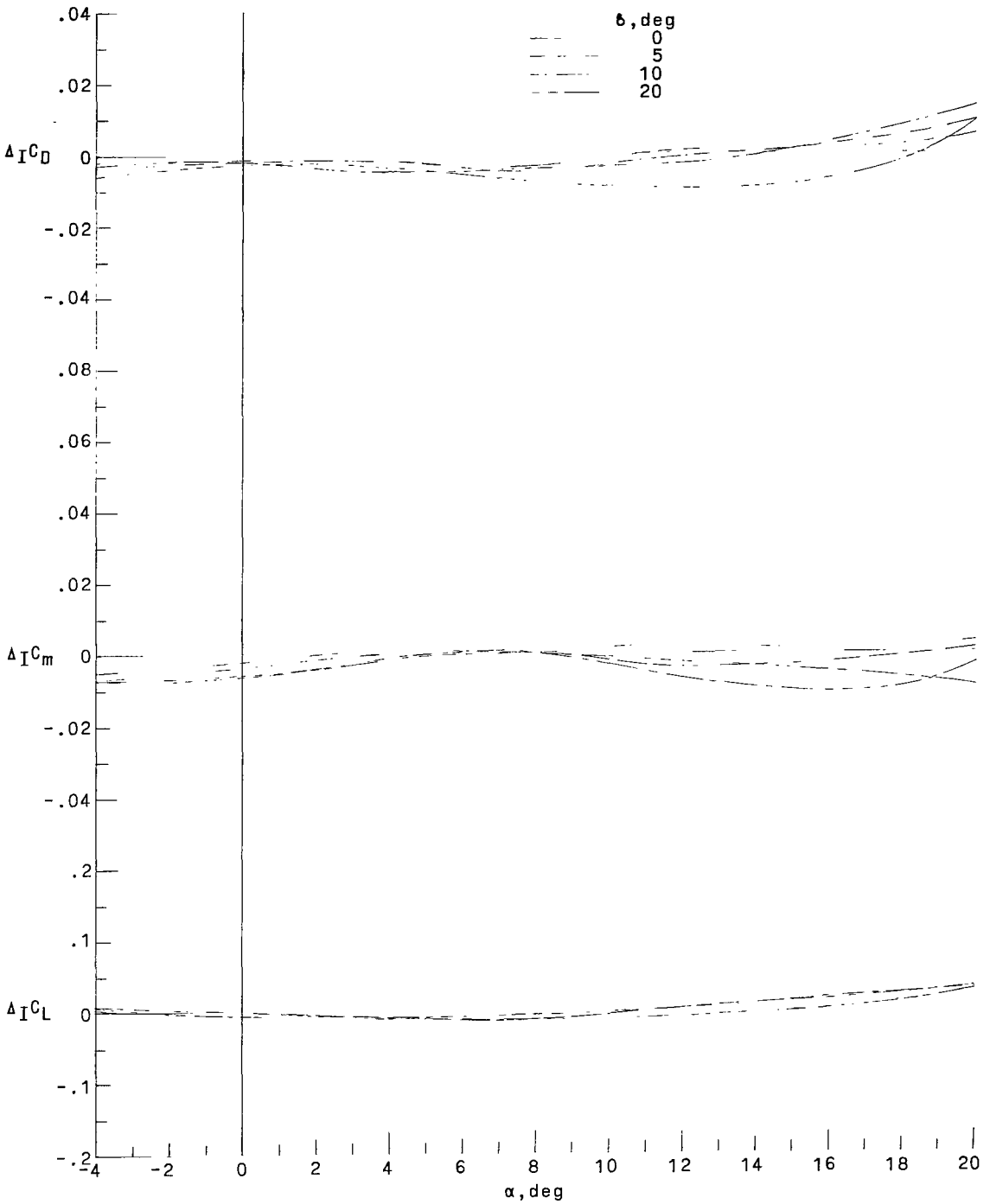

(h) Configuration $DW_2B_2C_3$.

Figure 8.- Continued.

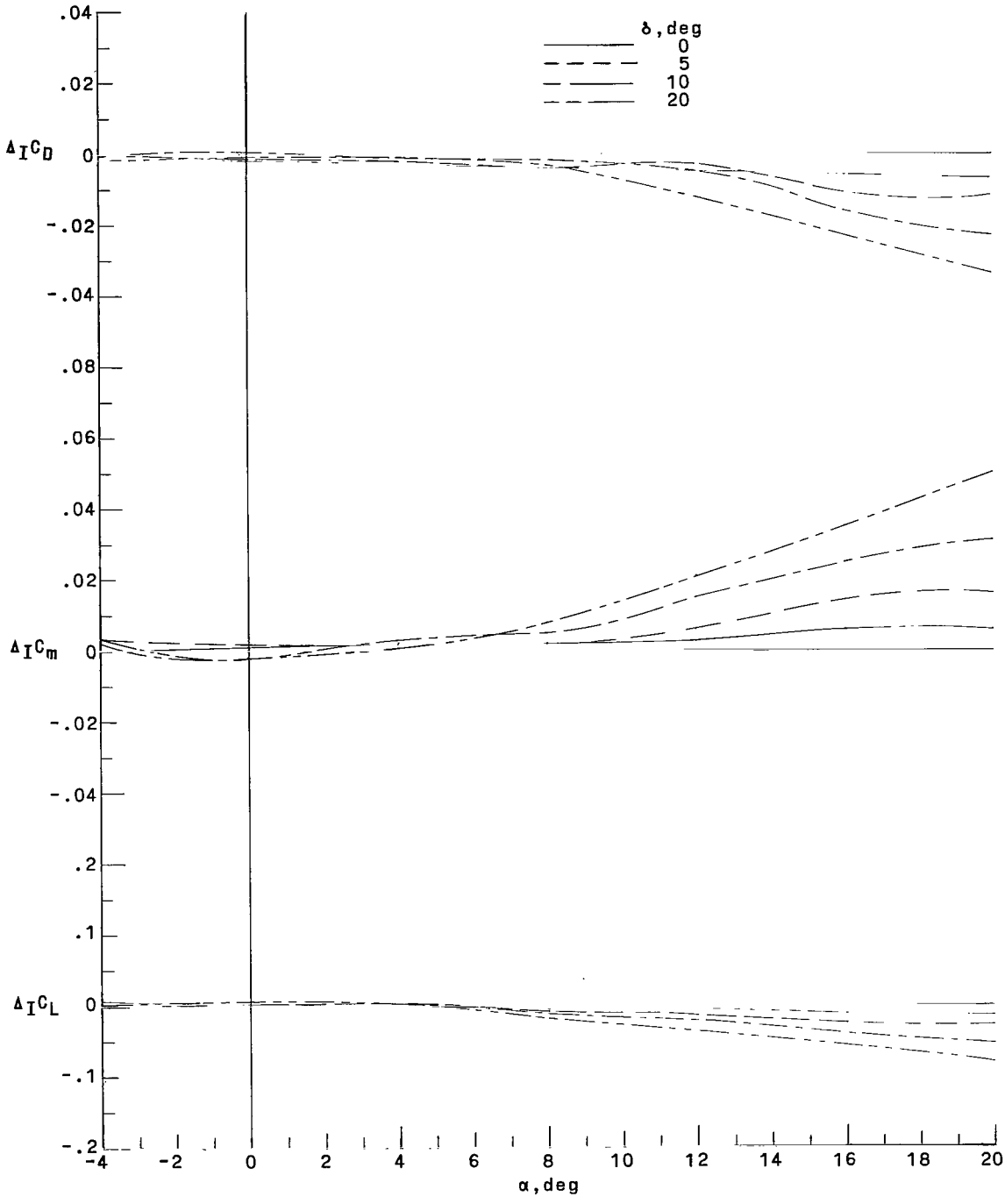

(i) Configuration $TW_1B_1C_1$.

Figure 8.- Continued.

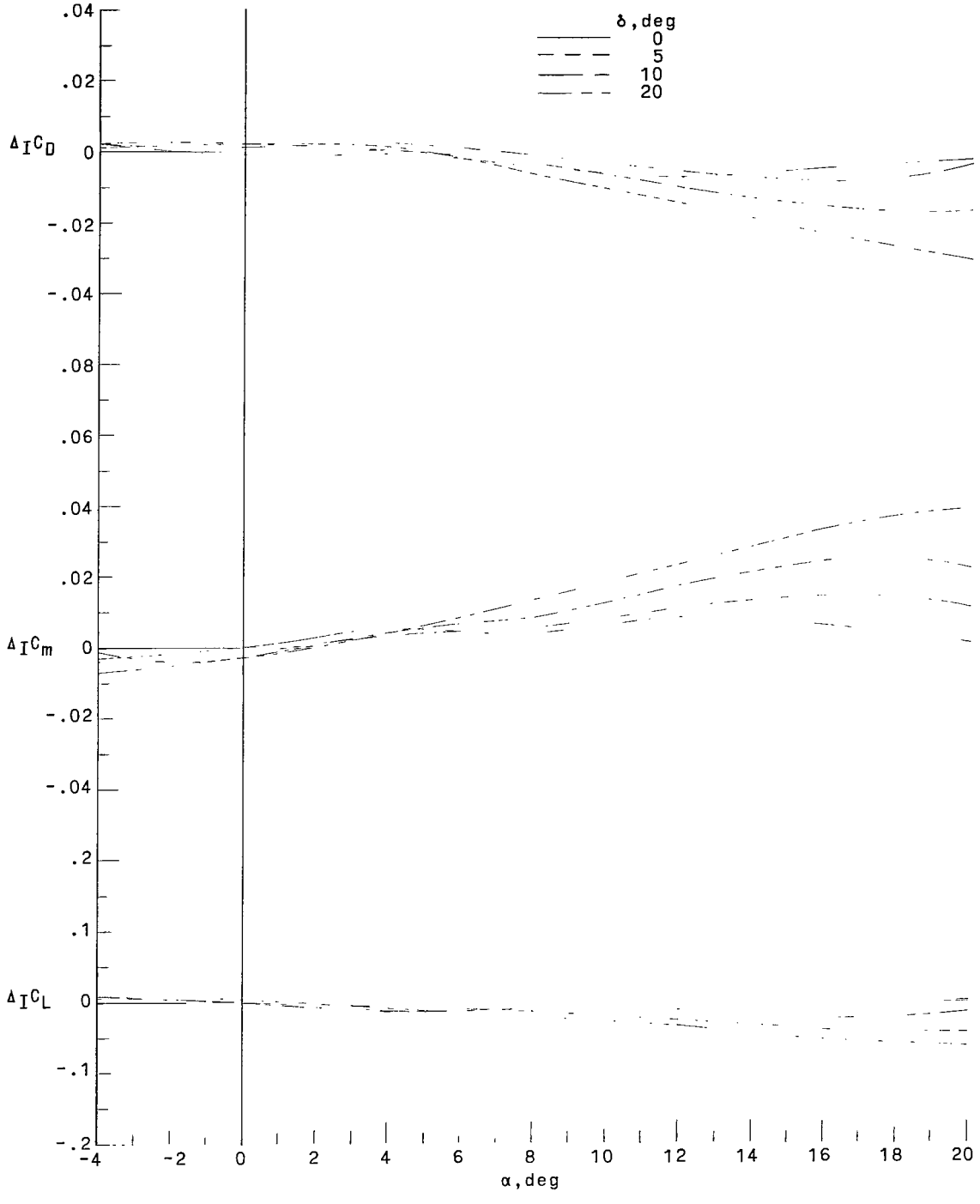

(j) Configuration $TW_1B_2C_1$.

Figure 8.- Continued.

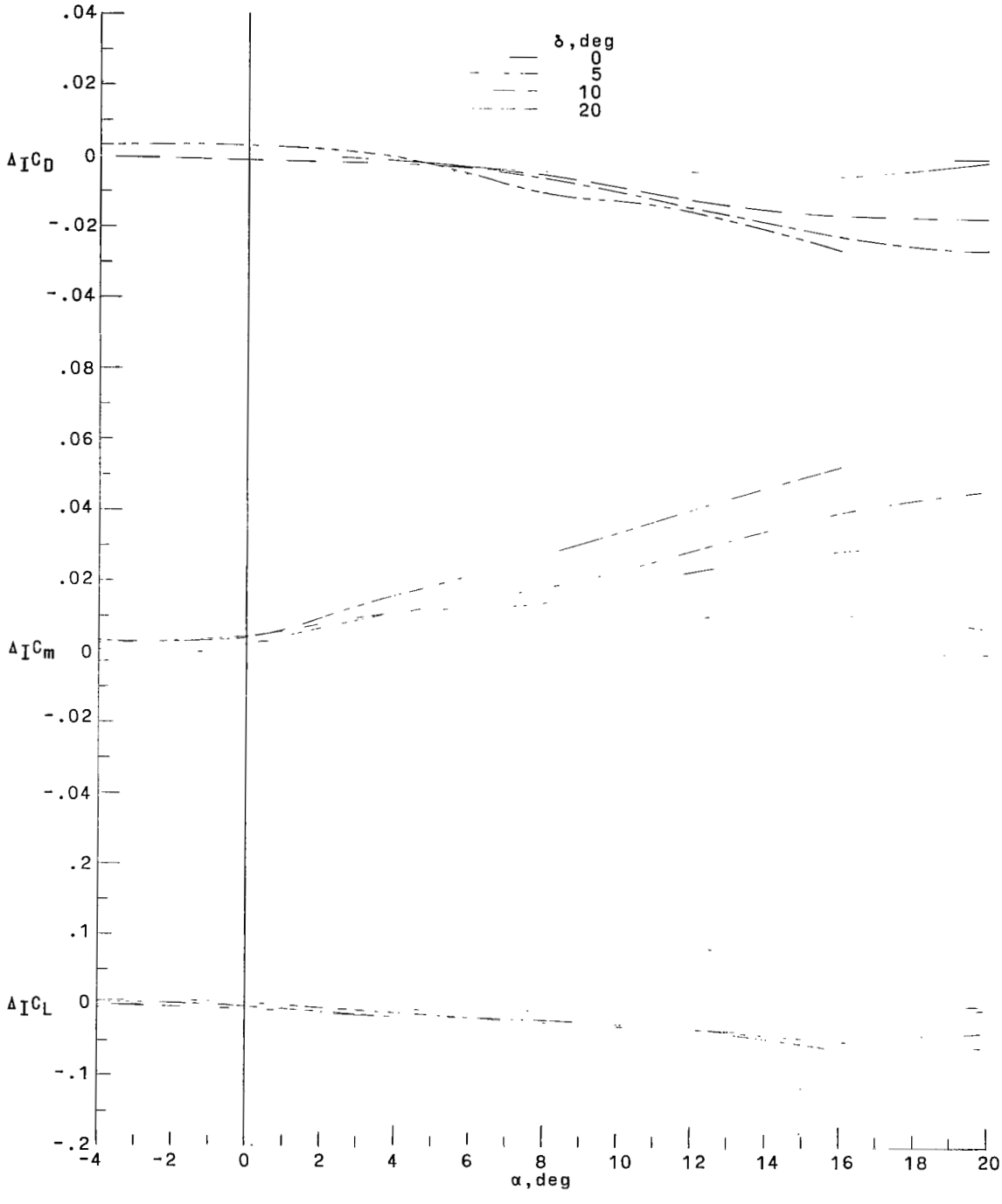

(k) Configuration $TW_1B_2C_2$.

Figure 8.- Continued.

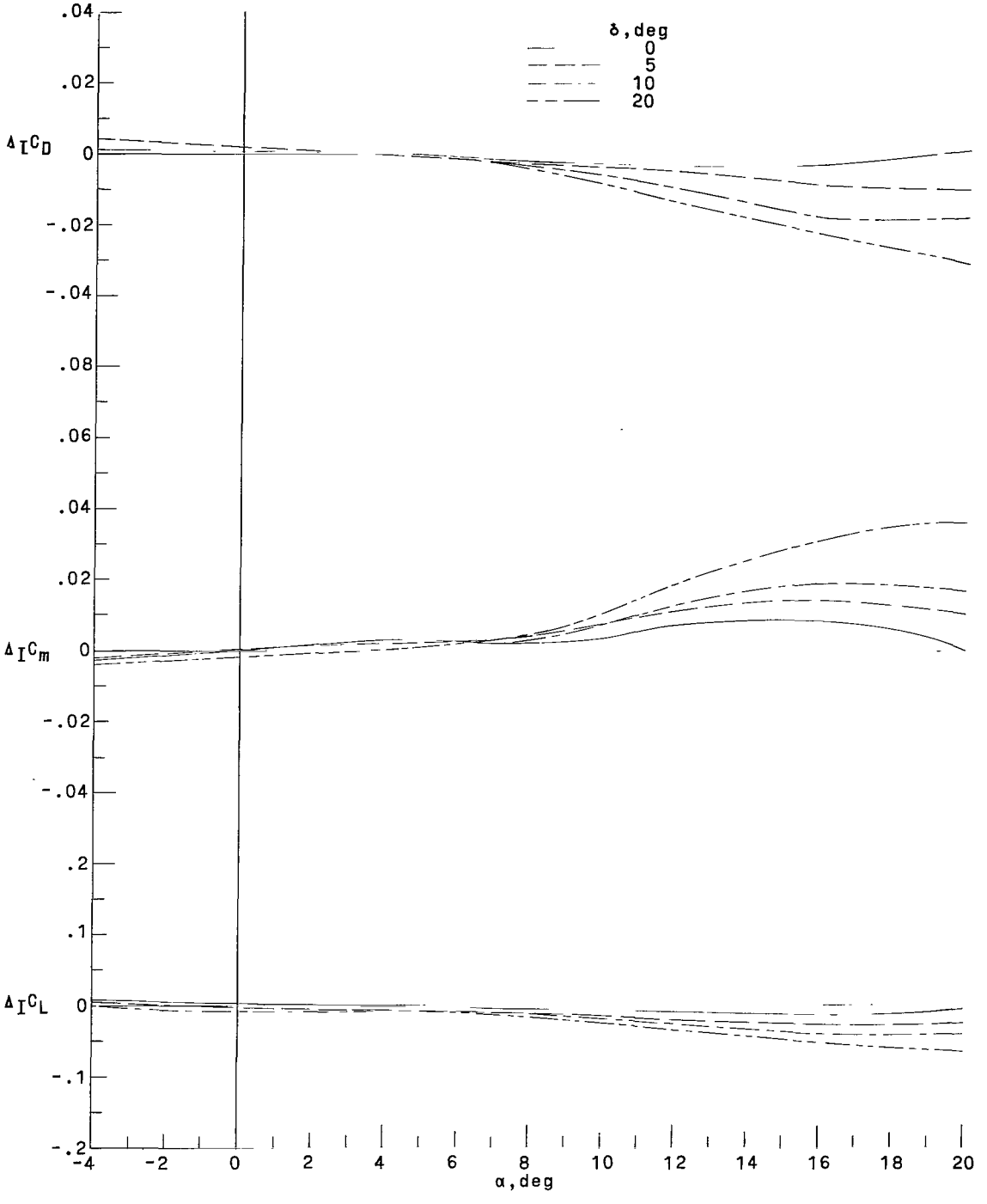

(l) Configuration $TW_1B_1C_3$.

Figure 8.- Continued.

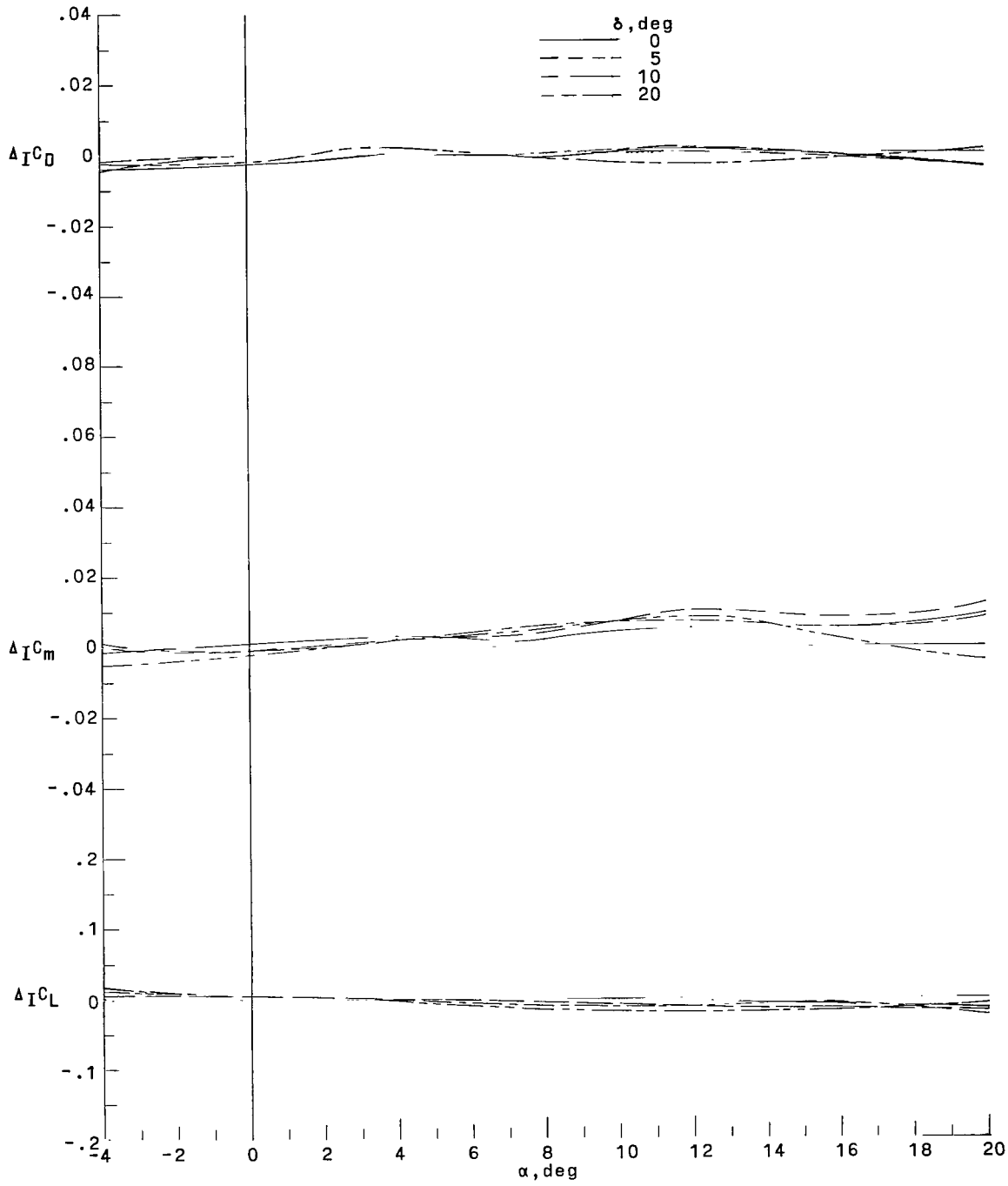

(m) Configuration $TW_2B_1C_1$.

Figure 8.- Continued.

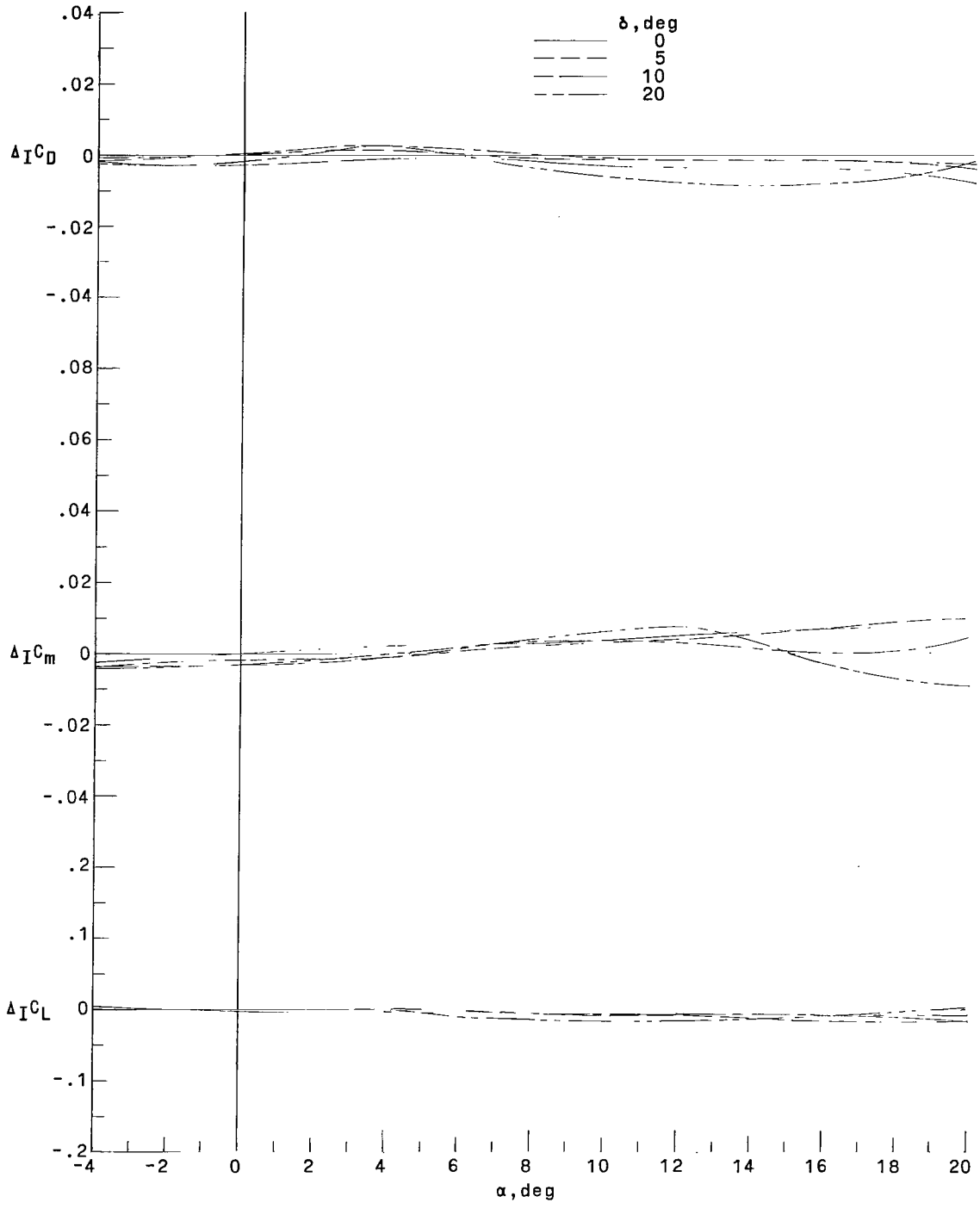

(n) Configuration $TW_2B_2C_1$.

Figure 8.- Continued.

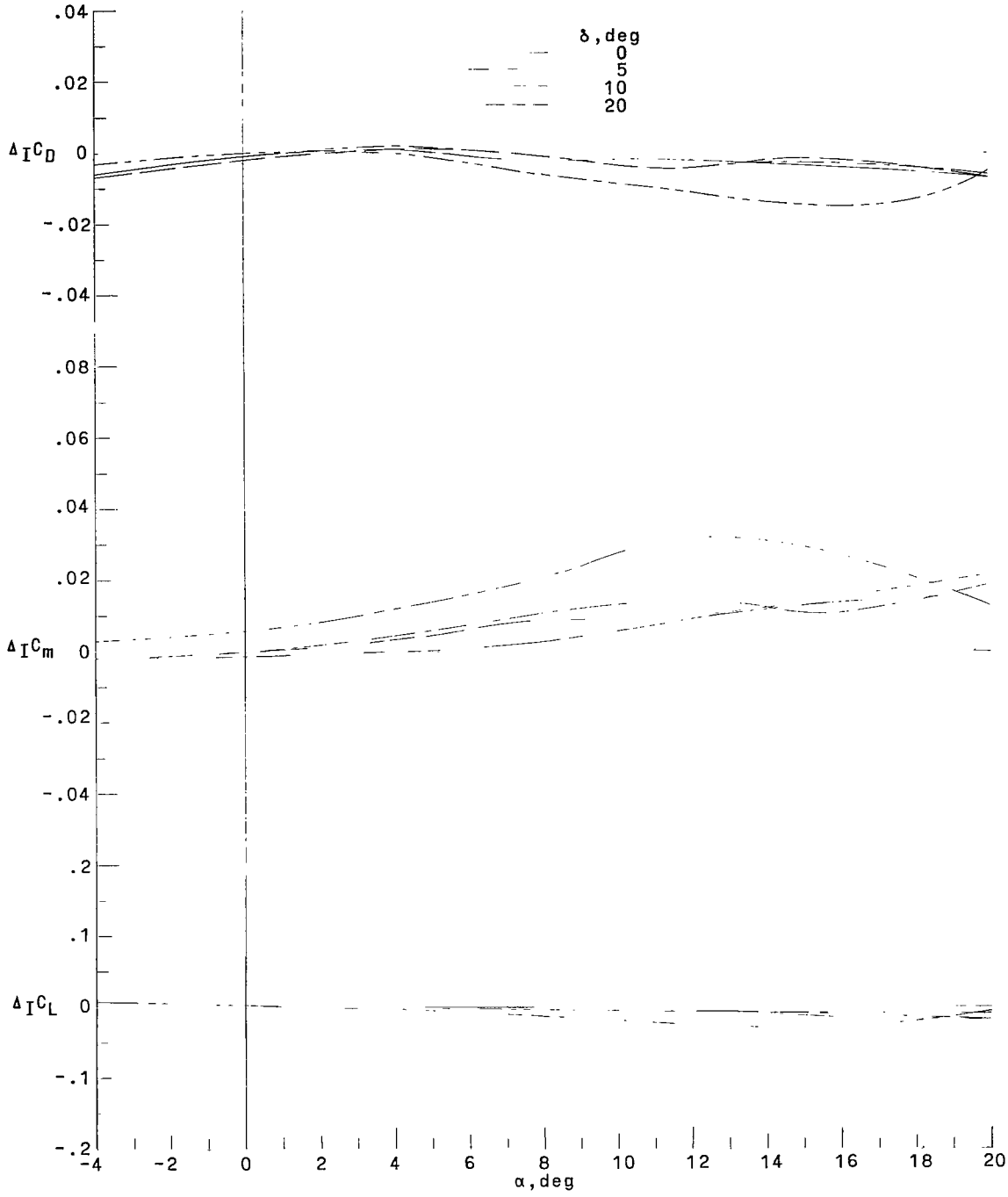

(o) Configuration $TW_2B_2C_2$.

Figure 8.- Continued.

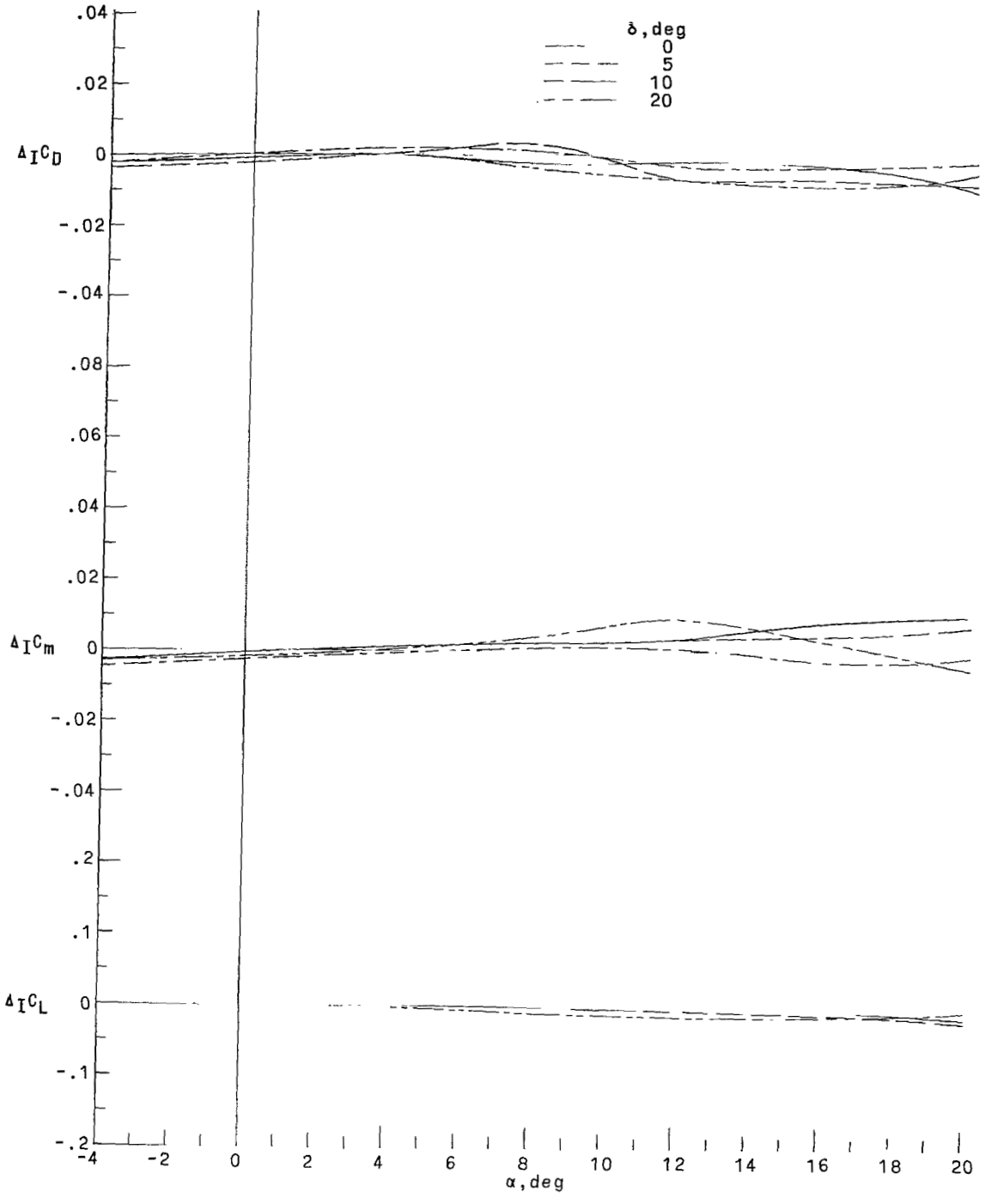

(p) Configuration $TW_2B_2C_3$.

Figure 8.- Concluded.

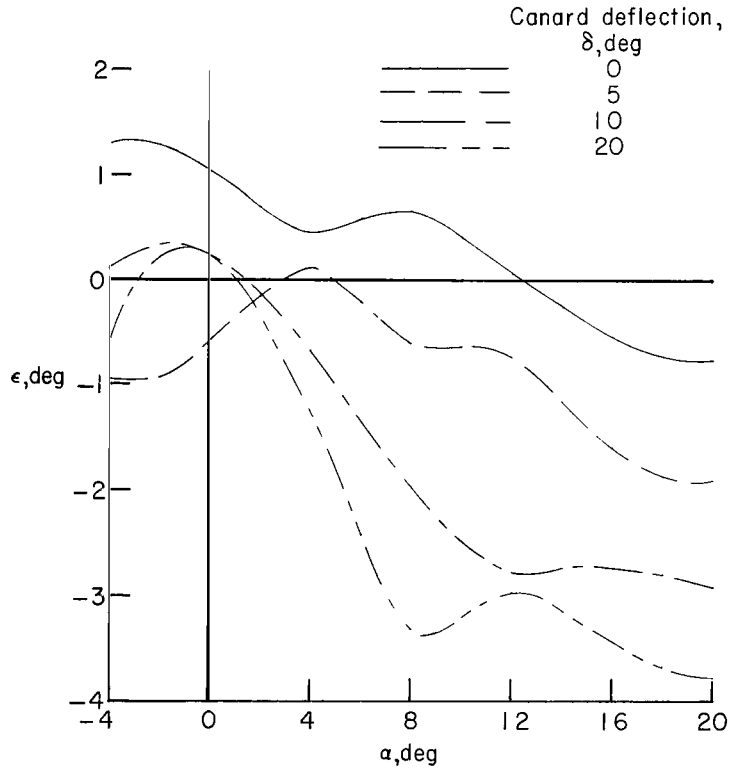

(a) Configuration $DW_1B_1C_1$.

Figure 9.- Effective downwash.

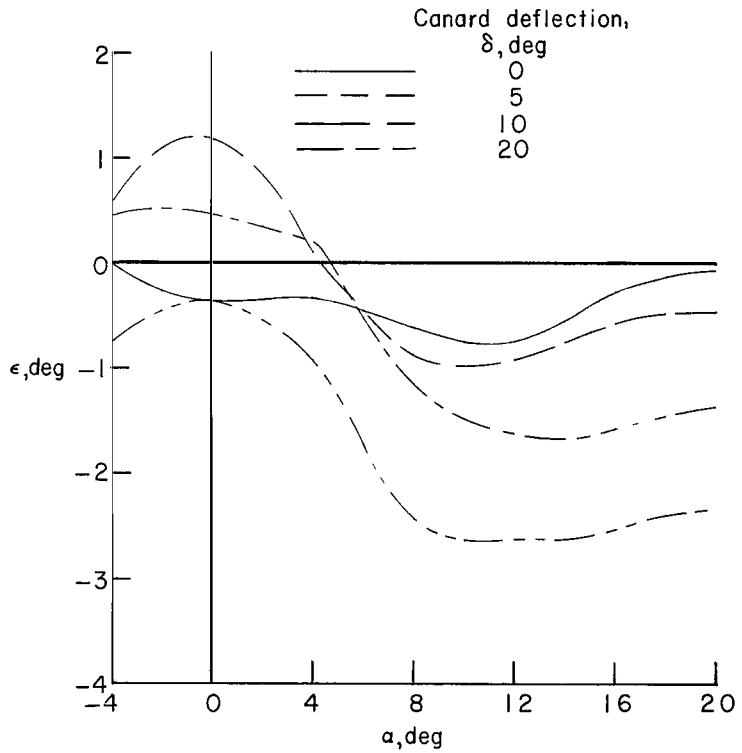

(b) Configuration $DW_1B_2C_1$.

Figure 9.- Continued.

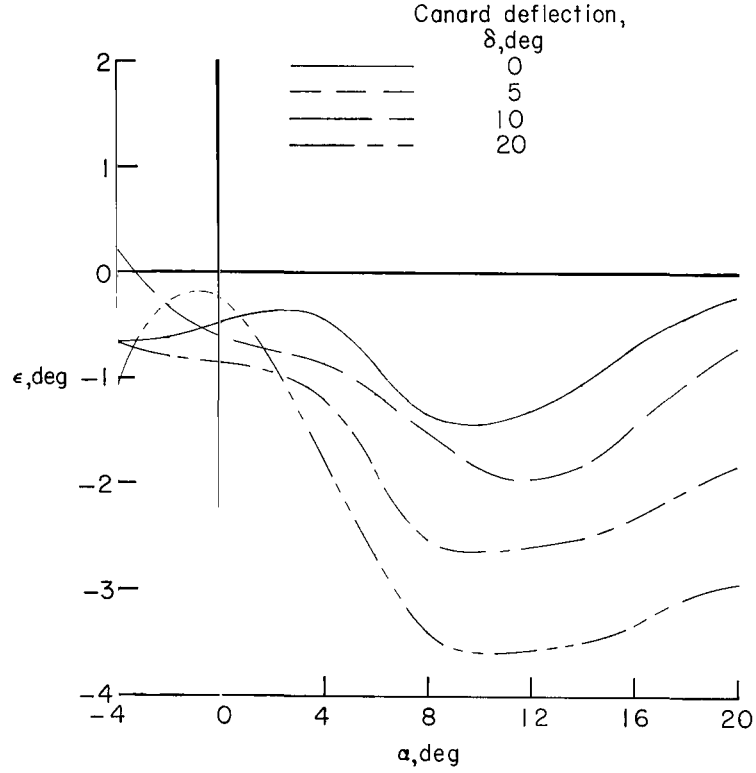

(c) Configuration $DW_1B_2C_2$.

Figure 9.- Continued.

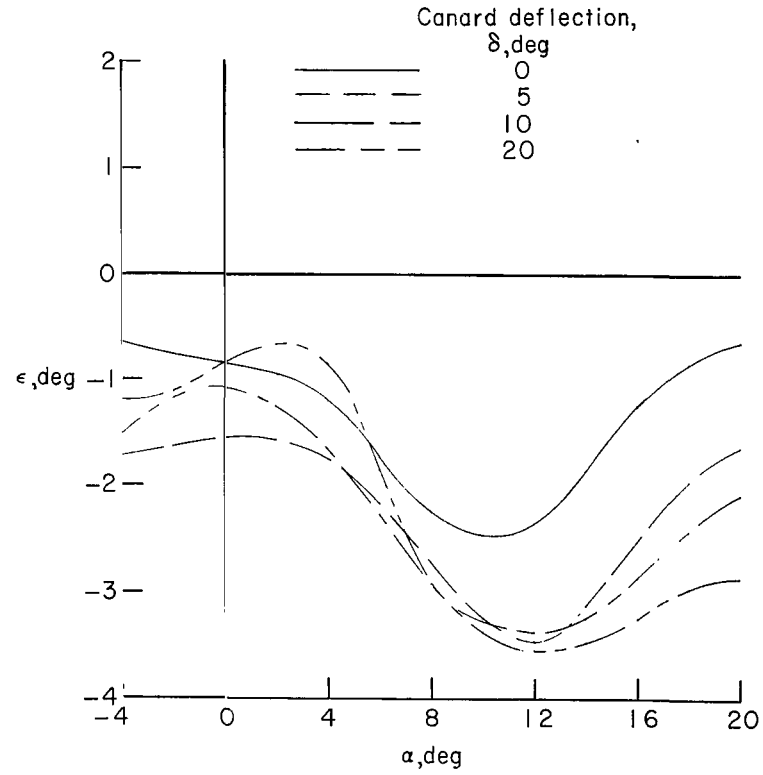

(d) Configuration $DW_1B_2C_3$.

Figure 9.- Continued.

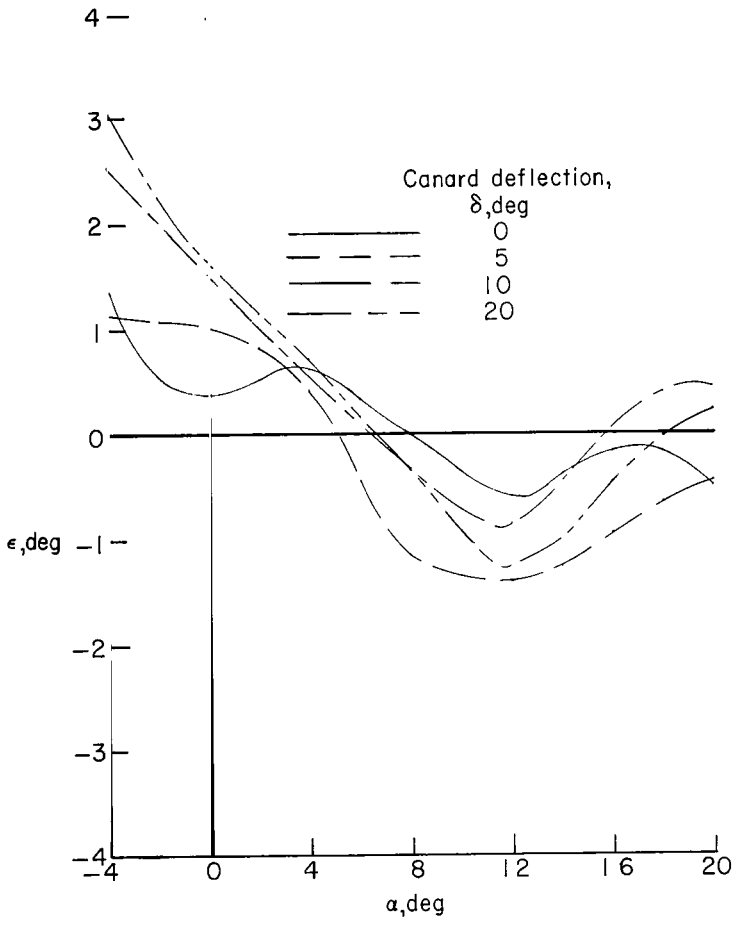

(e) Configuration $DW_2B_1C_1$.

Figure 9.- Continued.

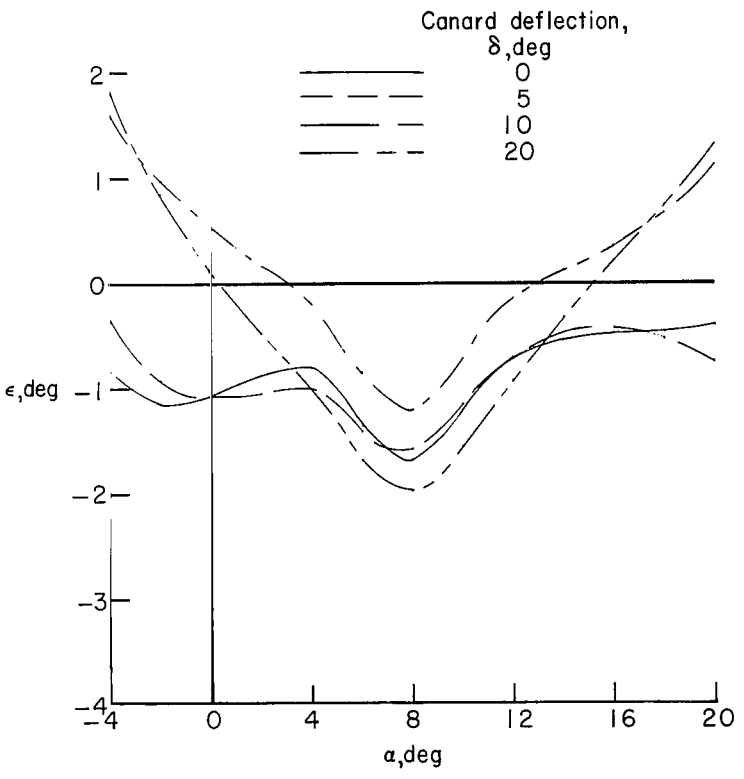

(f) Configuration $DW_2B_2C_1$.

Figure 9.- Continued.

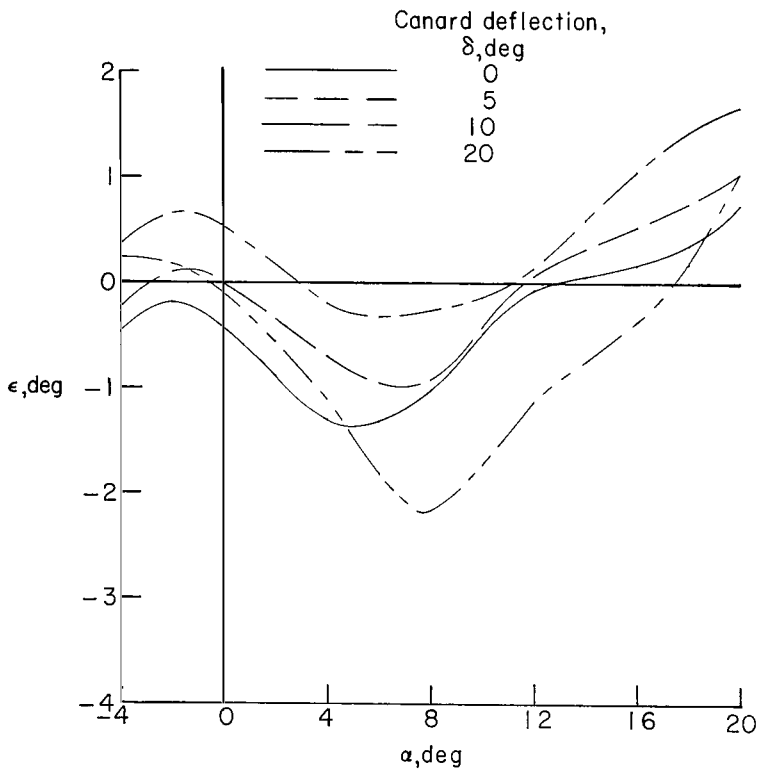

(g) Configuration $DW_2B_2C_2$.

Figure 9.- Continued.

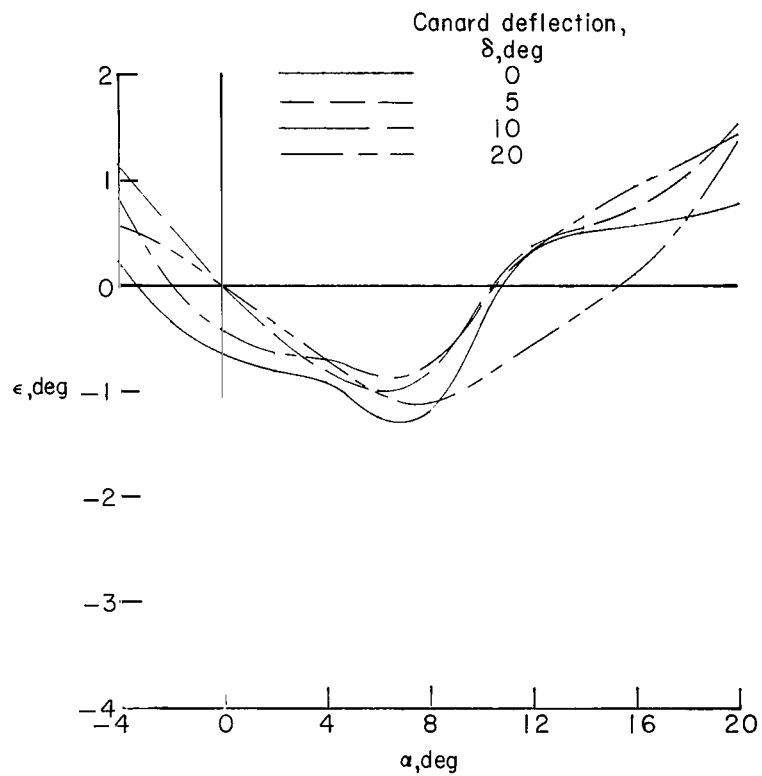

(h) Configuration $DW_2B_2C_3$.

Figure 9.- Continued.

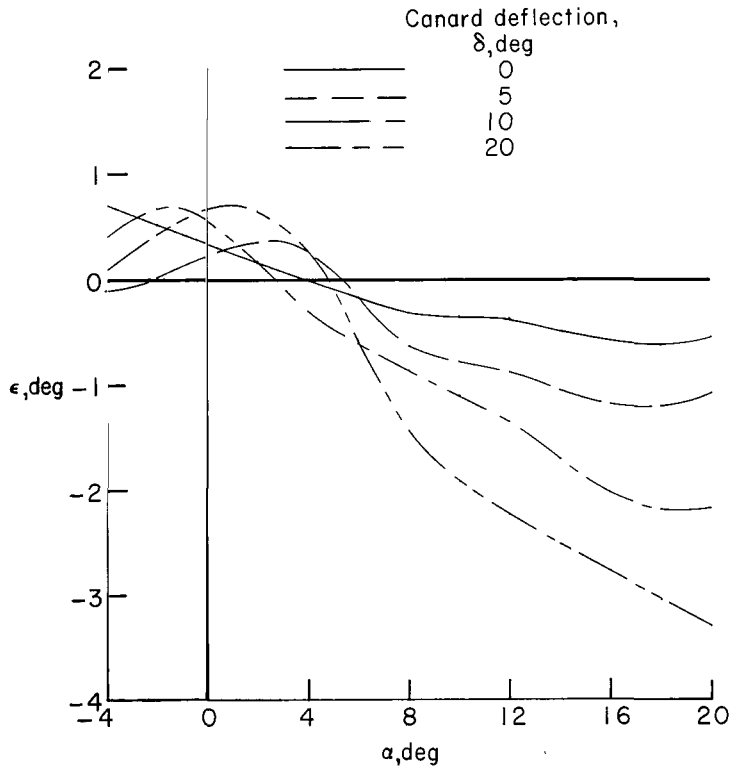

(i) Configuration $TW_1B_1C_1$.

Figure 9.- Continued.

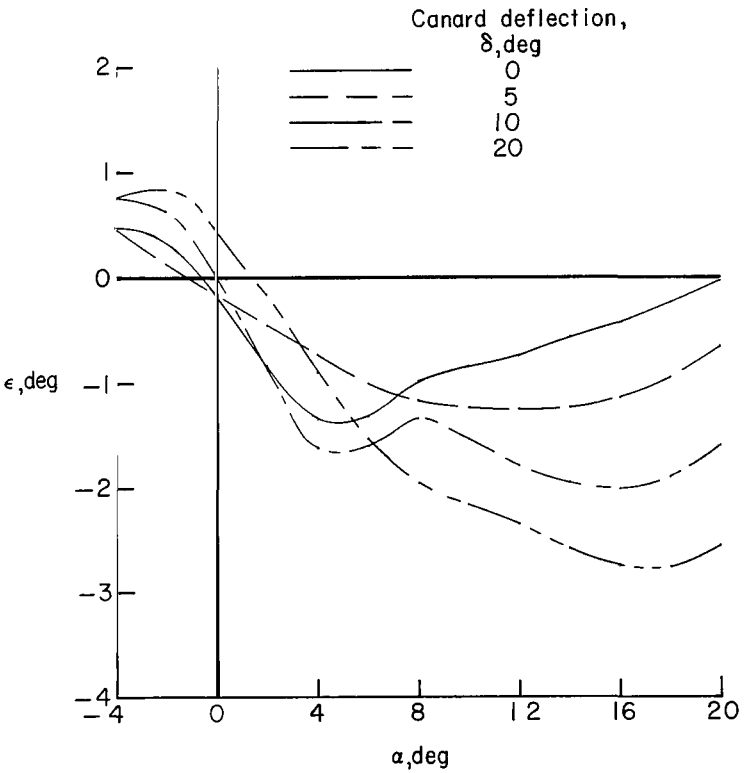

(j) Configuration $TW_1B_2C_1$.

Figure 9.- Continued.

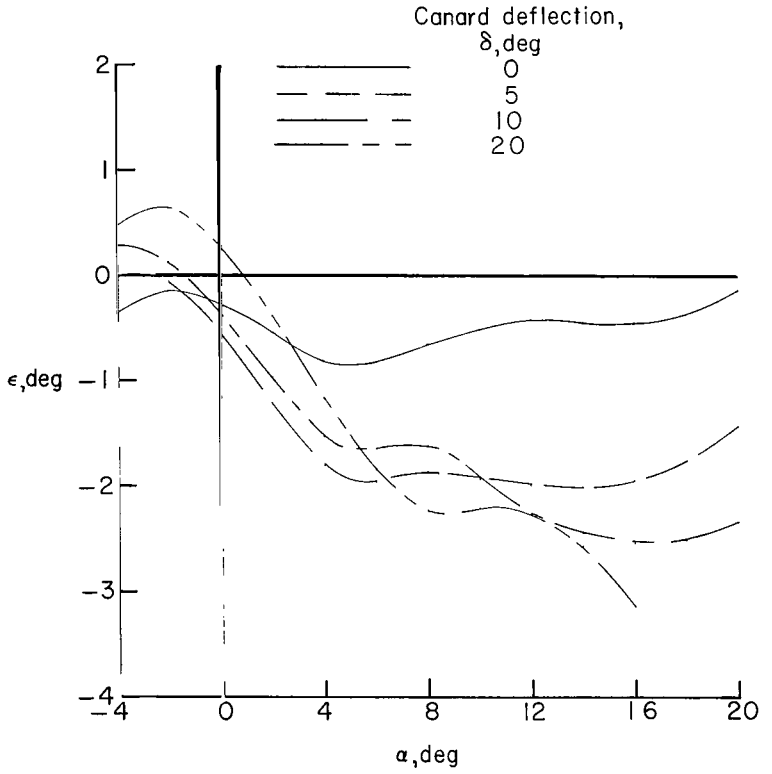

(k) Configuration $TW_1B_2C_2$.

Figure 9.- Continued.

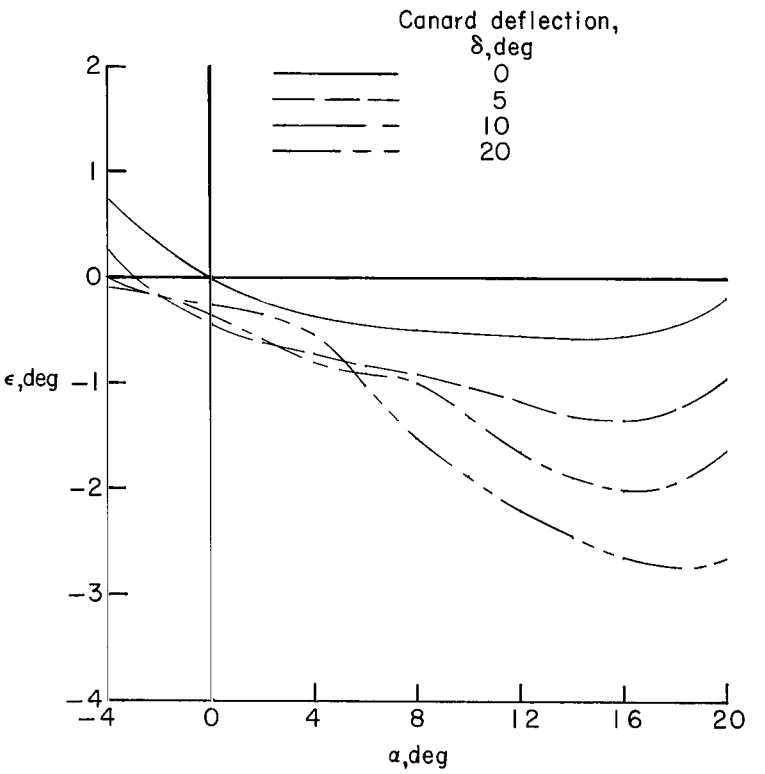

(l) Configuration $TW_1B_2C_3$.

Figure 9.- Continued.

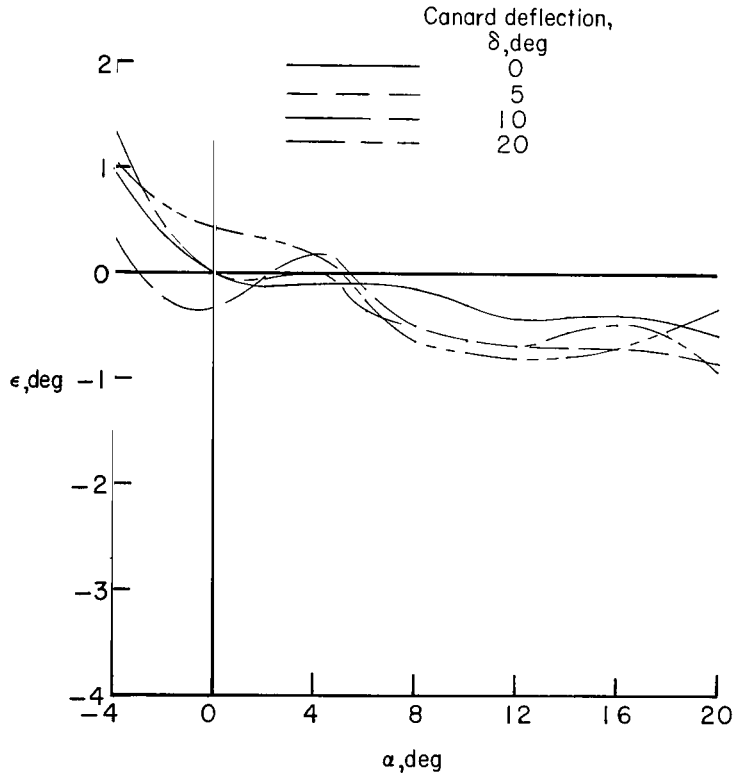

(m) Configuration $TW_2B_1C_1$.

Figure 9.- Continued.

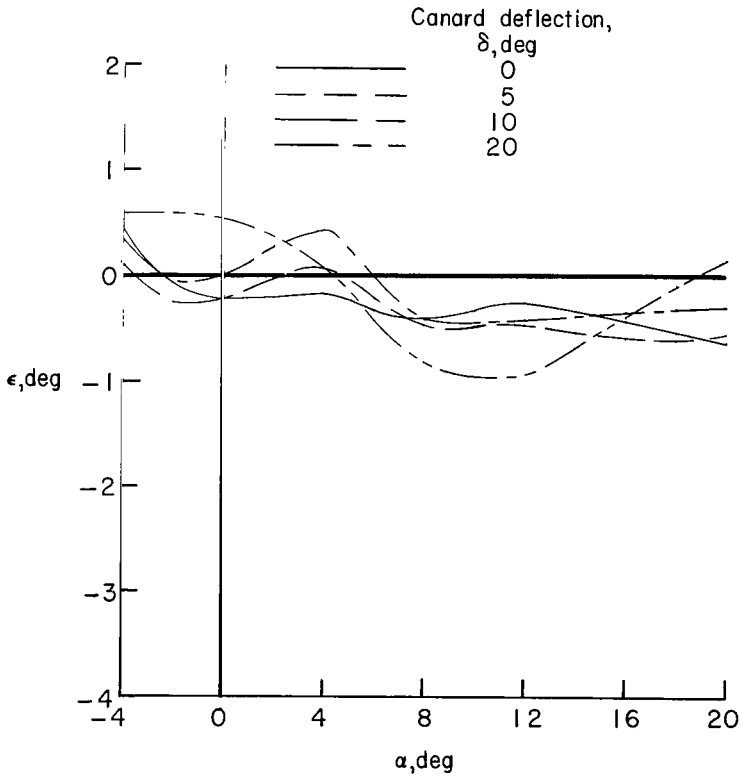

(n) Configuration $TW_2B_2C_1$.

Figure 9.- Continued.

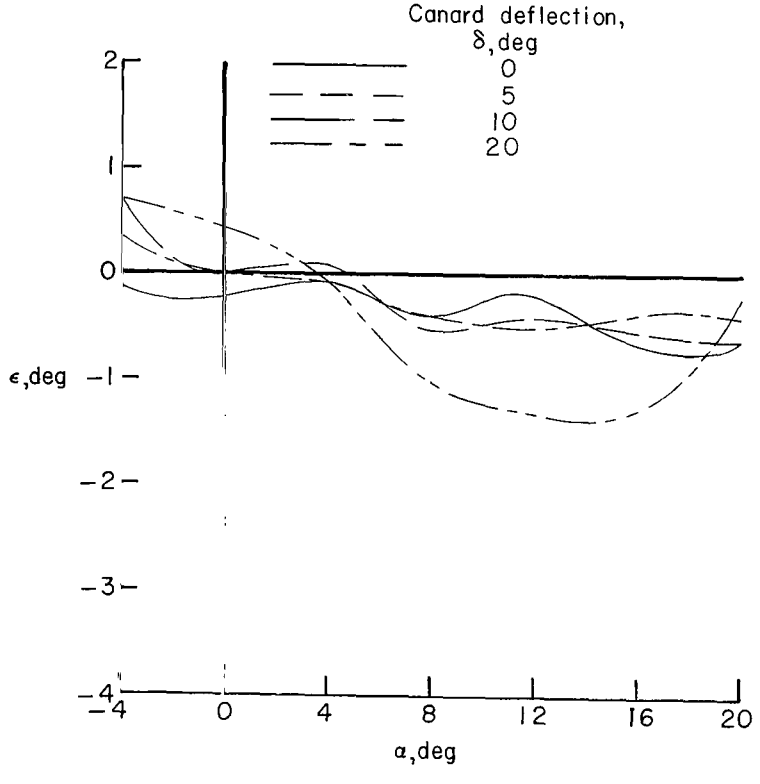

(o) Configuration $TW_2B_2C_2$.

Figure 9.- Continued.

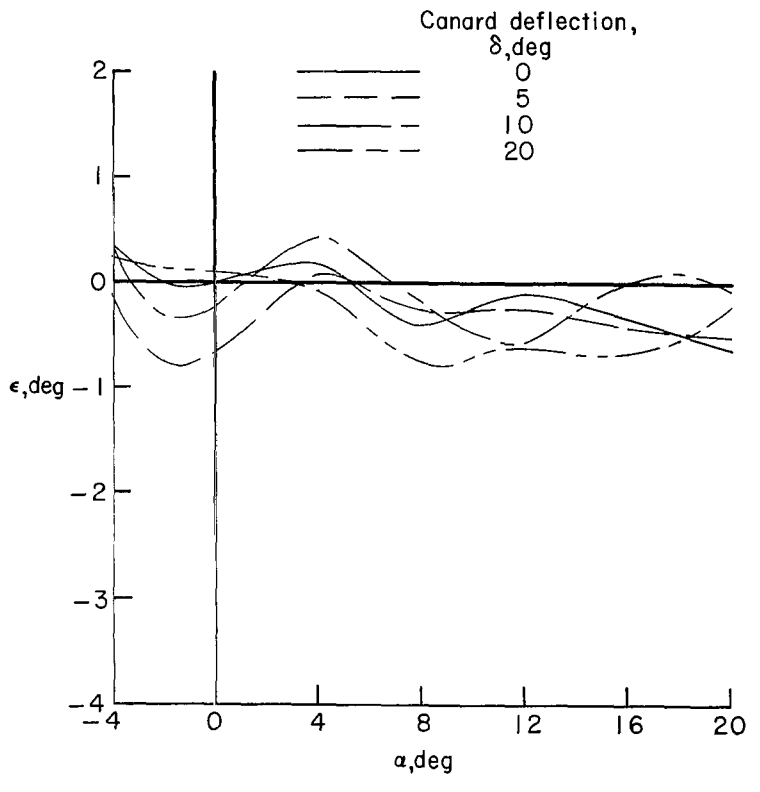

(p) Configuration $TW_2B_2C_3$.

Figure 9.- Concluded.

"The aeronautical and space activities of the United States shall be conducted so as to contribute . . . to the expansion of human knowledge of phenomena in the atmosphere and space. The Administration shall provide for the widest practicable and appropriate dissemination of information concerning its activities and the results thereof."

—NATIONAL AERONAUTICS AND SPACE ACT OF 1958

NASA SCIENTIFIC AND TECHNICAL PUBLICATIONS

TECHNICAL REPORTS: Scientific and technical information considered important, complete, and a lasting contribution to existing knowledge.

TECHNICAL NOTES: Information less broad in scope but nevertheless of importance as a contribution to existing knowledge.

TECHNICAL MEMORANDUMS: Information receiving limited distribution because of preliminary data, security classification, or other reasons.

CONTRACTOR REPORTS: Scientific and technical information generated under a NASA contract or grant and considered an important contribution to existing knowledge.

TECHNICAL TRANSLATIONS: Information published in a foreign language considered to merit NASA distribution in English.

SPECIAL PUBLICATIONS: Information derived from or of value to NASA activities. Publications include conference proceedings, monographs, data compilations, handbooks, sourcebooks, and special bibliographies.

TECHNOLOGY UTILIZATION PUBLICATIONS: Information on technology used by NASA that may be of particular interest in commercial and other non-aerospace applications. Publications include Tech Briefs, Technology Utilization Reports and Notes, and Technology Surveys.

Details on the availability of these publications may be obtained from:

SCIENTIFIC AND TECHNICAL INFORMATION DIVISION

NATIONAL AERONAUTICS AND SPACE ADMINISTRATION

Washington, D.C. 20546